SYNTHESIS AND PHOTOPHYSICAL CHARACTERIZATION OF π-EXTENDED PLATINUM PORPHYRINS FOR APPLICATION IN HIGH EFFICIENCY NEAR-IR LIGHT EMITTING DIODES

By

JONATHAN ROBERT SOMMER

A DISSERTATION PRESENTED TO THE GRADUATE SCHOOL
OF THE UNIVERSITY OF FLORIDA IN PARTIAL FULFILLMENT
OF THE REQUIREMENTS FOR THE DEGREE OF
DOCTOR OF PHILOSOPHY

UNIVERSITY OF FLORIDA

2010

To my parents and to my friends for their unwavering love and support.

ACKNOWLEDGMENTS

I would like to express my gratitude to my advisor, Professor Kirk S. Schanze, whose support and direction have helped me develop and enabled me to complete my studies. His overall knowledge of science, not just chemistry, is extremely impressive. The mentorship I received from him has guided me through my many challenges as a graduate student and for that I will always remain appreciative and thankful for the opportunity to have worked with him. I would especially like to thank, Dr. William Dolbier and Dr. Kenneth Wagener for their time in the class room and also as members of my committee. Their knowledge, advice, and support have been a valuable and cherished resource during my graduate career.

This work would not have been possible with out the hard work of our many collaborators with whom I have interacted: Dr. Ion Ghiviriga for his expertise in NMR and help with characterization of the porphyrins prepared in Chapter 2; Dr. John Reynolds and Dr. Jiangeng Xue for their collaboration and expertise in both chemistry and light emitting diodes; Ken Graham for the fabrication and characterization of PLEDs and our stimulating discussions on aggregation and device efficiency; Yixing Yang for the fabrication and characterization of OLEDs; Dr. Richard Farley and Abby Shelton for their help with the photophysical characterization of the platinum porphyrins synthesized in Chapter 2. I would like to thank all of the present and past members of the Schanze research group. I have made some great friends along the way and enjoyed watching them grow into talented scientists.

TABLE OF CONTENTS

LIST OF TABLES

LIST OF FIGURES

LIST OF ABBREVIATIONS

DBU	1,8-Diazabicyclo[5.4.0]undec-7-ene
DCM	Dichloromethane
DDQ	2,3-dichloro-5,6-dicyanobenzoquinone
EtOH	Ethanol
m-CPBA	3-Chloroperoxybenzoic acid
MeOH	Methanol
ITO	Indium tin oxide
^{t}BuOK	Potassium *tert*-butoxide
OEP	Octaethylporphyrin
PBD	2-(4-biphenylyl)-5-phenyl-1,3,4-oxadiazole
Pc	Phthalocyanine
PEDOT	Poly(3,4-ethylenedioxythiophene)
PhCN	Benzonitrile
PSS	Poly(styrenesulfonate)
PVK	Poly(9-vinylcarbazole)
TAP	Tetraanthroporphyrin
TBP	Tetrabenzoporphyrin
TFA	Trifluoroacetic acid
THF	Tetrahydrofuran
TNP	Tetranaphthoporphyrin
TPP	Tetraphenylporphyrin
TsCl	*m*-Toluenesulfonyl Chloride
TsOH	*p*-Toluenesulfonic acid
ZnTBP	Zinc(II) Tetrabenzoporphyrin

Abstract of Dissertation Presented to the Graduate School
of the University of Florida in Partial Fulfillment of the
Requirements for the Degree of Doctor of Philosophy

SYNTHESIS AND PHOTOPHYSICAL CHARACTERIZATION OF π-EXTENDED PLATINUM PORPHYRINS FOR APPLICATION IN HIGH EFFICIENCY NEAR-IR LIGHT EMITTING DIODES

By

Jonathan Robert Sommer

August of 2010

Chair: Kirk S. Schanze
Major: Chemistry

My research presents the synthesis and photophysical characterization of π-extended platinum porphyrins. These novel near-IR phosphors have emission ranging from 770 to 1000 nm with the highest photoluminescence efficiencies ever reported. Organic light emitting diodes (OLEDs) that feature electroluminescence solely in the near-IR have been fabricated from these materials by two methods: thermal vapor deposition of small molecules (OLEDs) and solution processing with polymers to form thin films (PLEDs).

The synthesis of the platinum complexes for π-extended porphyrins has been retarded due to the difficulty and low yield by current methods. Developed herein is a novel metallation procedure to obtain for the first time platinum complexes for π-extended porphyrins in high yield. This breakthrough has enabled the realization of these materials which would otherwise not be possible.

The goal of the first series of π-extended platinum porphyrins was to extend the conjugation of the porphyrin macrocycle so emission wavelengths could be obtained further in the near-IR. The addition of fused-benzene rings to the β-carbons of the

pyrrole residues effectively extends the conjugation of the porphyrin macrocycle. The platinum tetrabenzoporphyrins in the second series of target compounds were designed in efforts to increase the solution quantum yield. This was achieved by decreasing the non-radiative decay rate through increasing the planarity of the tetrabenzoporphyrin macrocycle by reducing the number of *meso*-aryl substituents. This resulted in the desired higher quantum yield. The third series of platinum tetrabenzoporphyrins examines the effects of a variety of substituents on the photophysical properties and device efficiency. The materials were designed in efforts to create a dye encapsulation effect to prevent self quenching mechanism caused by aggregation.

The most important conclusions from this study are as follows: (i) the use of platinum acetate as the metallation reagent readily affords the desired platinum complexes; (ii) the lifetimes and quantum yields for series 1 π-extended platinum porphyrins follows the energy gap law, were the lifetime and quantum yield decrease with longer emission wavelengths; (iii) increasing the macrocycle planarity decreases the non-radiative decay rate, thus increasing the quantum yield and lifetime; (iv) self quenching mechanisms from aggregation of the π-extended platinum porphyrins in the host material of OLEDs and PLEDs remains a problem seriously limiting the device efficiency despite the high photoluminescence efficiency of the phosphors.

CHAPTER 1
INTRODUCTION TO PORPHYRINS

History and Discovery of Porphyrins- The Pigments of Life

The vast majority of complex animal and plant life that exists on our planet today results from a class of compounds called porphyrins. Photosynthesis and respiration are at the heart of what makes life possible. During the Archean eon life on earth was dominated by bacteria and archaea with the atmosphere void of free oxygen. The evolution of oxygenic photosynthesis from cyanobacteria changed the earth and its atmosphere forever.[1] The process involves the oxidation of water forming molecular oxygen releasing it into the atmosphere. Eventually the earth's atmosphere changed from anaerobic to aerobic leading to a dramatic increase in biodiversity. Life has since evolved using oxygen leading to eukaryotic organisms and plants containing chloroplasts for photosynthesis and eventually hemoglobin in the red blood cells for the respiration of vertebrates (Figure 1-1). It is from the desire of scientist to understand these vital life processes that porphyrins were discovered.

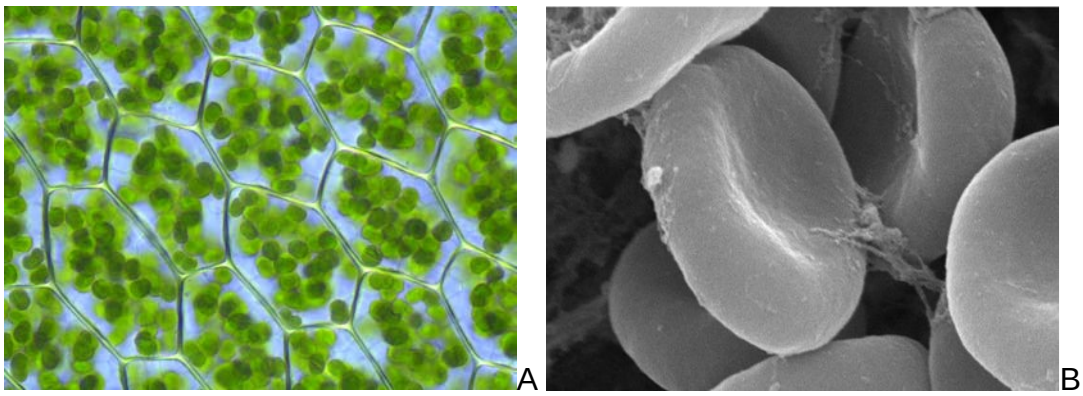

Figure 1-1. Chlorophyll and heme are two naturally occurring porphyrins. A) Microscope image of chloroplasts visible in the cells of *Plagiomnium affine* B) SEM image of human red blood cells which contain the iron porphyrin heme.

The main historical events that led to the discovery of porphyrins has been the subject of many reviews and summarized by Sheldon.[2] The existence of iron in human blood was first reported in 1747 when Menghini burned human blood to ash separating particles of iron with a magnet. Later the experiments by an English chemist named Joseph Priestly in 1774 proved that the oxygen consumed by fire and breathing animals could be restored to the air by plants. This ignited interest in understanding the role of oxygen in respiration. In 1841, treating powdered blood with sulfuric acid Scherer was able to isolate the iron free pigment in blood. A German chemist named Felix Hoppe-Seyler in 1864 was able to isolate the iron-containing oxygen-transport metalloprotein found in red blood cells naming it hemoglobin. Later in 1871 Hoppe-Seyler isolated porphyrins from blood and proved they were pyrrole derivatives and is credited with noting the structural similarities between chlorophyll and heme in 1879. It was not until 1912 that the correct structure for porphyrins was proposed by Küster although at the time not accepted. Milroy published the first general synthesis of porphyrins in 1918.[3] Later the work of Hans Fischer in 1926 who was awarded the Nobel Prize in 1930 for his work in 1929 the de novo synthesis of chlorohemin which proved the structure proposed by Küster almost twenty years earlier.[4]

Structure and Nomenclature of Porphyrins

Fischer also developed the first system of nomenclature outlined in his book *Die Chemie des Pyrrols* published in 1934 for the naming of porphyrin compounds.[5] The general unsubstituted structure of a porphyrin is often referred to as porphine and is outlined in Figure 1-2. Substitution can occur at two positions along the periphery of the macrocycle in the β-carbons of the pyrrole fragments or at the four *meso*-positions which are the methine bridges between the α-carbons of the pyrrole fragments. The

nomenclature developed by Fischer is frequently used today, although another system was developed in effort to name more complicated structures where the Fischer nomenclature failed.

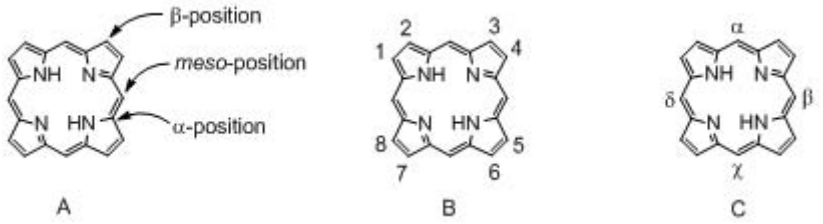

Figure 1-2. Porporphyrin nomenclature developed by Hans Fischer.[5] A) Nomenclature for porphyrin positions B) Numbering for β-positions C) Greek letter notation for *meso*-positions

The nomenclature developed by the International Union of Pure and Applied Chemistry (IUPAC) was adopted in the early 1970's (Figure 1-3).[6] This nomenclature differs from Fischer's in that all the carbon and nitrogens in the porphyrin macrocycle are given a number. Where previously in Fischer's nomenclature α-carbons were not numbered because they could not be substituted and the *meso*-positions were denoted by Greek letters. Looking at the basic porphyrin system (porphine) the β-positions then become 2,3,7,8,12,13,18, and 17 instead of 1-8. The *meso*-positions are numbered 5,10,15,20 in place of the Greek letters Fischer previously assigned.

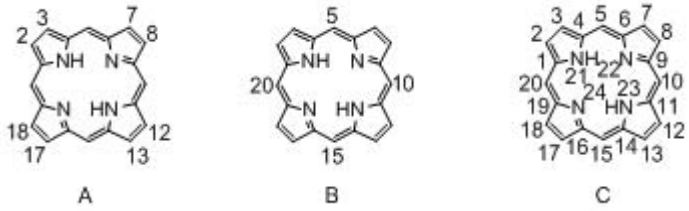

Figure 1-3. The numerical IUPAC nomenclature for porphyrins.[6] A) Numbering for β-positions B) Numbering for *meso*-positions C) Complete IUPAC numbering.

Naming porphyrins is relatively simple when all the substituents around the macrocycle are the same. Two examples would be if all the *meso*-positions were

substituted with phenyl substituents to give tetraphenylporphyrin (H_2TPP) and alternatively if all the β-positions were substituted with ethyl groups to give octaethylporphyrin (H_2OEP). However the naming of porphyrins becomes increasingly difficult with lower symmetries arising from different substituents at either the β- or *meso*-positions.

History of Porphyrin Synthesis

The need for developing practical and efficient synthetic methods for the preparation of porphyrins was born when Fischer confirmed the porphyrin structure in 1929. The significant biological roles and photophysical properties of porphyrins has driven the attention of researchers over the past century. Although at first thorough exploration of these compounds has been severely limited by their synthetic availability. This provided the inspiration for synthetic chemists to develop efficient synthetic methods for their preparation. It is worthwhile to examine the history and synthetic advancements made to completely appreciate the progress that has been made in this field.

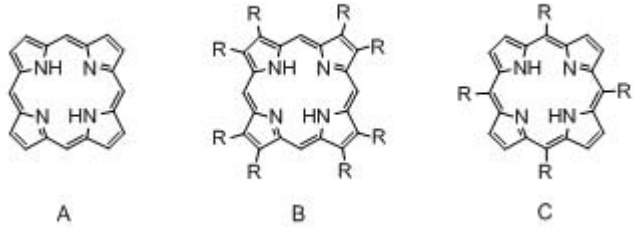

Figure 1-4. Outline of the most common substitution patterns found around the porphyrin macrocycle. A) β- and *meso*-unsubstituted porphine B) β-substituted OAPs C) *meso*-aryl substituted porphyrin.

The synthesis of porphyrins can be divided into three main categories consisting of the β- and *meso*-unsubstituted porphine; β-substituted porphyrins referred to as ocatalkylporphyrins (OAPs) and finally *meso*-aryl substituted porphyrins. These

structures are illustrated in Figure 1-4. Since the focus of this work is on *meso*-aryl substituted porphyrins the initial synthetic strategies developed for the synthesis of porphine and OAPs will not be examined and have already been well reviewed.[7] It is worth noting that both porphine and OAPs closely resemble the porphyrins found in biological systems. This chemistry was developed in order to synthesize naturally occurring porphyrins such as heme and chlorophyll.[4, 8]

Synthesis of *meso*-Substituted Porphyrins

Although *meso*-substituted porphyrins are not naturally occurring compounds they have provided chemists and other scientist with a multitude of applications and fundamental studies. This stems from the simplicity in their preparation where one pot synthesis are normal. On the other hand porphyrins with biological relevance are unsymmetrical and therefore cannot be prepared via simple routes.[7] This is the attraction to *meso*-substituted porphyrins where their symmetry enables their simple preparation from starting materials such as pyrrole and benzaldehyde.[9]

The initial work on *meso*-substituted porphyrins began in 1935 when Rothemund first developed a method for the synthesis of *meso*-tetramethylporphyrin from heating acetaldehyde and pyrrole in methanol at 95°C.[10] Rothemund later expanded the scope of this method to include a variety of aromatic aldehydes in 1936, including benzaldehyde to yield H_2TPP.[11] In 1941 Rothemund described in detail the preparation of H_2TPP in a reported 7-9% yield from heating 10 mL of pyrrole and 20 mL of benzaldehyde in 20 mL of pyridine at 220°C for 48 hours.[12] The Rothemund method can be summarized as using high reactant concentrations at high temperatures in absence of an added oxidant.

Improvement in the synthesis of *meso*-substituted porphyrins came in the mid-1960s from Alder and Longo. The new method utilized lower reactant concentrations compared to the Rothemund method. The reactants were heated in acidic solvents with the reaction vessels open to air. This enabled the preparation of a variety of *meso*-substituted porphyrins in a 30-40% yield.[13, 14] Optimized conditions were obtained by increasing the reactant concentrations and using propionic acid (bp 141°C) rather than other lower boiling acidic solvents like acetic acid. Heating the reaction to reflux open to air and then cooling yielded crystals of the desired porphyrin.[14] This advancement prompted a mechanistic study by Dolphin who examined the condensation of 3,4-dimethylpyrrole with benzaldehyde in refluxing acetic acid under anaerobic conditions. This led to the formation of the porphyrin precursor octamethyltetraphenylporphyrinogen which could then be oxidized to octamethyltetraphenylporphyrin.[15] This result is important as it provides very strong evidence that the precursor porphyrinogen is formed followed by oxidation to the porphyrin.

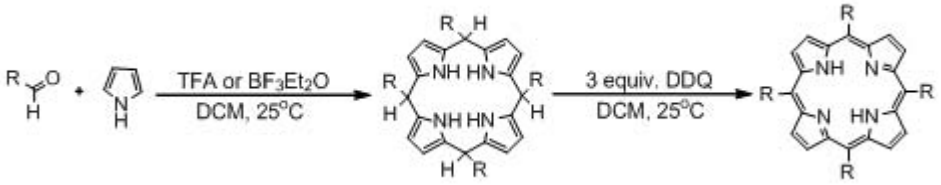

Figure 1-5. Outline of the synthetic conditions for the preparation of *meso*-aryl substituted porphyrins by Lindsey in 1987.[16, 17]

It was not until the late-1980s that Lindsey *et al* reported a new synthetic method that set the standard for *meso*-aryl substituted porphyrin.[16, 17] The methodology allows for a wider variety of substituted aldehydes to be incorporated into the subsequent porphyrins. The reaction can be scaled up to provide gram scale quantities and is reproducible with typical yields in the range of 30-40% for substituted benzaldehydes.

Lindsey *et al* developed this method as a single flask two step reaction based on equilibrium cyclizations and biomimetic studies of porphyrin biosynthesis and is outlined in Figure 1-5. The first step is the acid catalyzed condensation to form the intermediate porphyrinogen, followed by the second step the addition of an external oxidant such as DDQ or chlorinal to form the porphyrin.

The method was developed on the premise that tetraphenylporphyrinogen would be the thermodynamically favored product from the condensation of pyrrole and benzaldehyde under favorable conditions. Also important were to keep the reaction conditions mild utilizing the fact that benzaldehyde and pyrrole are reactive molecules and high temperatures are unnecessary. This enabled new functionalities on substituted benzaldehydes to be compatible with the given reaction conditions. The previous methods used harsh reaction conditions which limited the scope of possible substituents available at the *meso*-position.

Synthesis of π-Extended Porphyrins

Porphyrin systems with β-fused benzene rings represent an interesting class of compounds. The structures for tetrabenzoporphyrin (H_2TBP), tetranaphthoporphyrin (H_2TNP), and the related phthalocyanine (Pc) are outlined in Figure 1-6. The TBP and TNP systems, now commonly referred to as π-extended porphyrins caught the attention of researchers early on for their photophysical properties relative to those of regular porphyrins. The effect on the optical properties of the porphyrin macrocycle from the β-fused benzene rings was studied by the Gouterman in the 1960s.[18-20] These studies provided the data that set forth the motivation to develop efficient synthetic methods to access these compounds for further characterization and use in a multitude of applications.

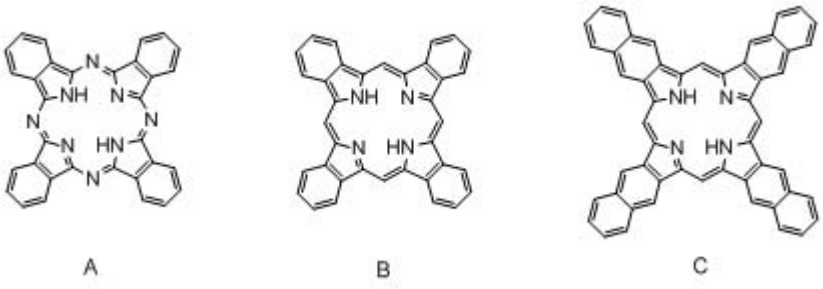

Figure 1-6. General structures for phthalocyanine and *meso*-unsubstituted π-extended porphyrins: A) Phthalocyanine (Pc), B) Tetrabenzoporphyrin (H_2TBP), C) Tetranaphthoporphyrin (H_2TNP).

The initial methods to synthesize TBPs were derived from that of Pc chemistry developed by Linstead in 1934.[21] It was later in 1940 that Tuey and Linstead successfully produced H_2TBP and its aza-substituted derivatives.[22, 23] The method involves heating 3-carboxymethylphthalimide above 300ºC in the presence of zinc or zinc acetate to give the zinc (II) tetrabenzoporphyrin (ZnTBP) in a very low yield (Figure 1-7). Analytically pure samples were obtained by sublimation or crystallization. The authors were able to isolate the free-base (H_2TBP) after treating the zinc complex with acid enabling the synthesis of the respective copper and iron complexes. This method was later refined by Gouterman in 1976 obtaining ZnTBP in a 14.5 % yield,[18] although extensive purification was required. The crude sample was sublimed and then further purified by multiple chromatography columns. The final product was obtained by precipitation into methanol.

Finally a method developed by Kunkely and Volger in 1978 provided ZnTBP and was regarded as the simplest way to synthesize the TBP macrocycle.[24] It requires heating 2-acetylbenzoic acid to high temperature with ammonia and zinc acetate (Figure 1-8). This affords ZnTBP in a moderate 17% yield and until recently was

regarded as the most direct and convenient method for synthesizing the *meso*-unsubstituted TBP.

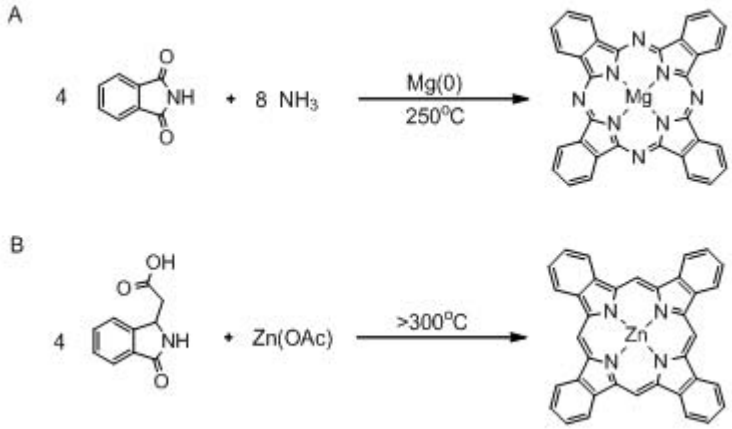

Figure 1-7. Initial synthetic strategy developed by Linstead and Tuey for the preparation of TBP. A) Linstead synthesis of Pc in 1934[21] B) Linstead synthesis of TBP in 1940.[22, 23]

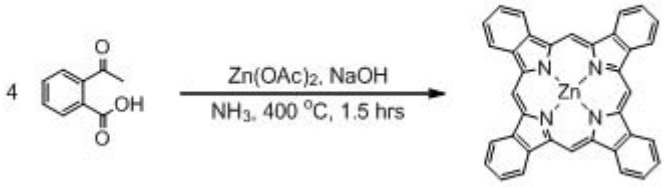

Figure 1-8. Synthetic scheme reported by Kunkely and Volger in 1978 for the preparation of ZnTBP.[24]

Researchers eventually developed synthetic methods for the preparation of tetraaryltetrabenzoporphyrins (H_2Ar_4TBP). The synthesis was motivated by the idea of combining the properties of H_2TPP with the TBP structure. The early reports for the synthesis of H_2TPTBP were developed from strategies analogous to the reported methods for preparing H_2TBP (Figure 1-9). The initial method appeared in 1981 described by Kopranenkov *et al* used 3-benzylidenephthalimide or alternatively the potassium salt of phthalimide and phenylacetic acid with zinc acetate to give ZnTPTBP (Figure 1-9B).[25] Two years later, Remy published a method using the most logical

retro-synthetic precursor of the TBP macrocycle.[26] The high temperature condensation of isoindole with benzaldehyde and zinc acetate also afforded ZnTPTBP (Figure 1-9C). Although earlier in 1972, Bonnet had published a communication describing the instability of isoindole and the rapid decomposition at room temperature.[27] Thus the reproducibility of these methods was scrutinized by other groups that reported mixtures of products identified as TBPs with varying numbers of *meso*-aryl substituents.[28-30] Later in 1991, Ohno *et al* showed that using zinc benzoate in place of zinc acetate with 3-benzylidenephthalimide heating to high temperatures yielded ZnTPTBP without side products (Figure 1-9A).[29]

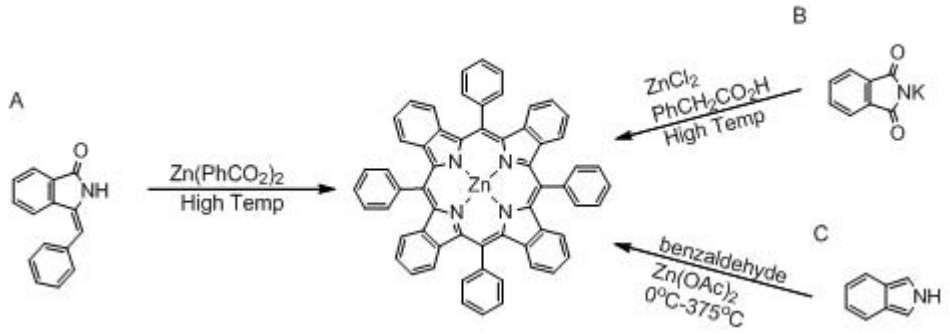

Figure 1-9. Outline of synthetic strategy to prepare H_2TPTBP. A) Ohno *et al* synthesis of H_2TPTBP without side products[29] B) Kopranenkov *et al* synthesis of H_2TPTBP[25] C) Synthesis of H_2TPTBP from isoindole reported by Remy.[26]

Another approach to synthesizing π-extended porphyrins was developed by Ono *et al*.[31, 32] The new method uses a bicyclic pyrrole precursor serving as a protected form of the simplest retro-synthetic precursor isoindole. This enabled the cyclization of the porphyrin macrocycle to occur under mild Lindsey conditions avoiding the high temperature reactions of Pc based related strategies. The key starting material 4,7-dihydro-4,7-ethano-*2H*-isoindole was prepared from a Barton-Zard pyrrole synthesis outlined in Figure 1-10. This synthetic strategy yielded the bicyclic-TPTBP precursor

under Lindsey conditions in a 35% yield. The solid state retro-Diels-Alder (RDA) reaction requires temperatures of 200ºC and produces ZnTPTBP quantitatively with no required purification. This method is powerful in avoiding the major pitfall of the previous methods which required much higher temperatures and extensive purification with lower yields in comparison.

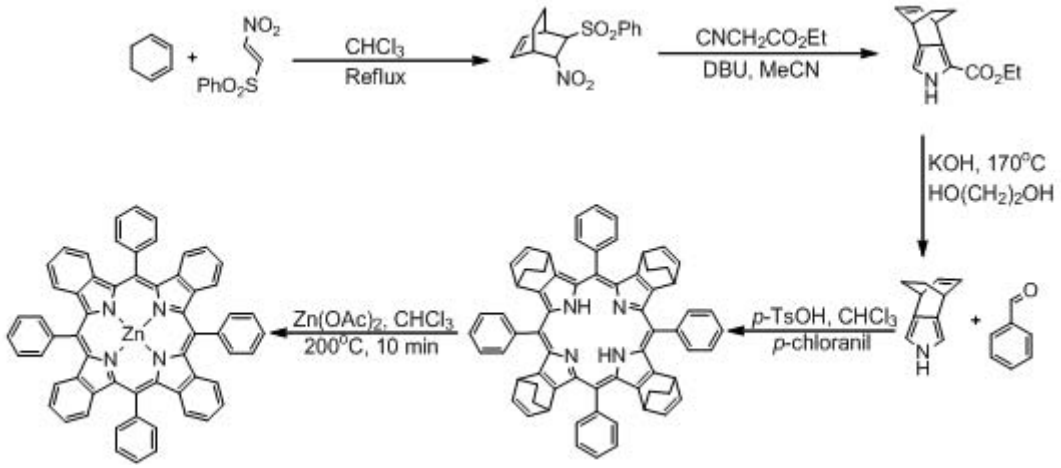

Figure 1-10. The synthesis reported by Ono *et al* for the preparation of H_2Ar_4TBP using Lindsey conditions and a bicyclic-pyrrole as a protected form of isoindole.[31, 32]

Using a similar synthetic strategy to the one developed by Ono, another method for the preparation of π-extended porphyrins was developed by using a different approach to a masked-isoindole derivative. This method was developed by Cheprakov *et al* in 2001 and is based on using tetrahydroisoindoles as the key starting material.[33] The synthetic scheme is depicted in Figure 1-11. The tetrahydroisoindoles are prepared from a modified Barton-Zard synthesis to produce the cyclic pyrrole from vinyl sulfones instead of nitro alkenes.[34, 35] After cleavage of the ester, the deprotected pyrrole is subjected to Lindsey conditions and gives the tetracyclohexenoporphyrin precursor in good yields. Attempts at aromatizing the free-base porphyrin directly by refluxing with DDQ failed to give H_2TPTBP. Alternatively the precursor porphyrin was metallated and

then subjected to oxidizing conditions with excess DDQ in THF to give the metallated TPTBPs in near quantitative yield. This methodology has advantages over Ono's method in that it broadens the scope of *meso*-aryl substituents compatible with the reaction conditions. However despite the improvement over the retro-Diels-Alder approach which requires temperatures at 200ºC, this method still suffered from over oxidation of the TBPs due to the long reaction times required in the oxidative dehydrogenation with DDQ. This drawback led to further improvements to the present oxidative aromatization method for the preparation of π-extended porphyrins.

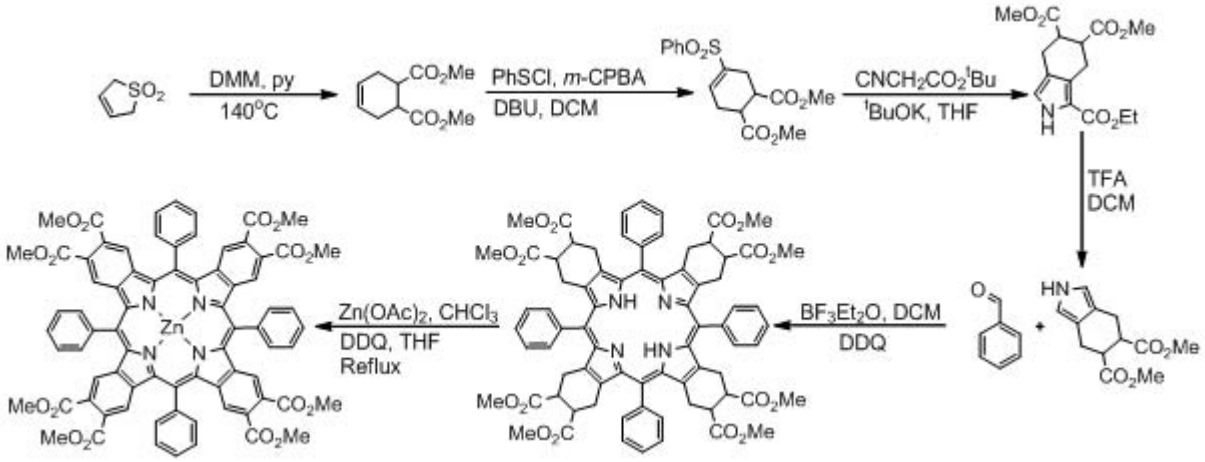

Figure 1-11. Outline of the oxidative aromatization strategy for the preparation H_2Ar_4TBPs reported by Cheprakov *et al*.[33]

A recent paper by Cheprakov and Vingradov in 2005 describes the synthesis of H_2Ar_4TNPs using the oxidative aromatization methodology previously described.[36] The advancement in synthetic strategy is in choosing the pyrrole precursor to resemble isoindole as much as possible. The two key starting materials examined are *cis*-octalin and 1,4-dihydronaphthalene (Figure 1-12). The pyrroles for each strategy were synthesized in a parallel manner to the scheme used for the H_2Ar_4TBP synthesis. The pyrrole from the *cis*-octalin route was condensed with an aromatic aldehyde under

Lindsey conditions and provided the tetra-aryl cycloalkene-fused porphyrin. This precursor to the H_2Ar_4TNP system was metallated and then subjected to oxidative conditions with DDQ under reflux. The highest yield obtained from this route was 40-45% from the palladium complex. The copper complex provided the H_2Ar_4TNP in a 20% yield and efforts to oxidize the zinc complex resulted in demetallation and the formation of a porphyrin dication. In comparison to the analogous H_2Ar_4TBP system the *cis*-octaline scheme to prepare H_2Ar_4TNPs is less efficient.

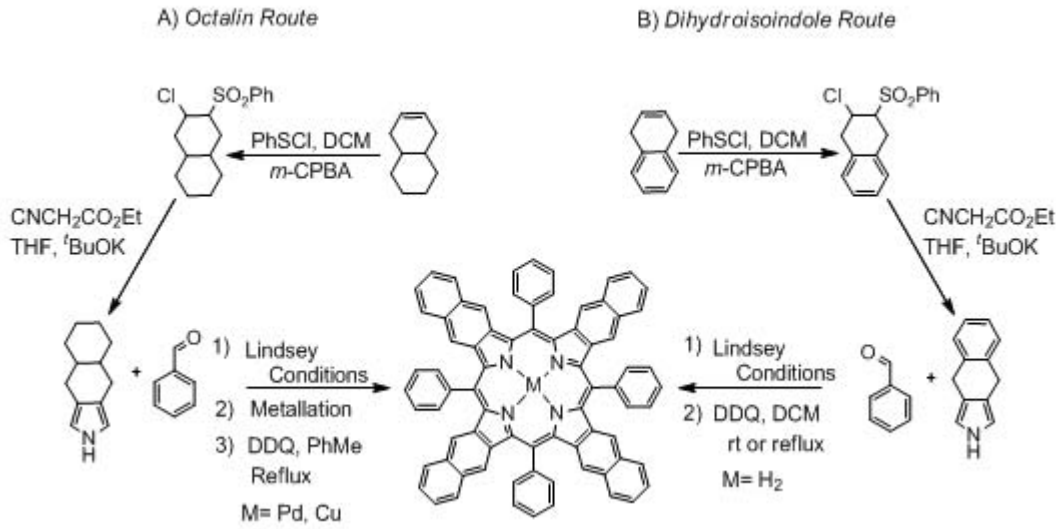

Figure 1-12. Synthetic strategy for H_2Ar_4TNP using the dihydroisoindole method developed by Vinogradov *et al*.[36] A) Octalin strategy towards H_2Ar_4TNP B) Dihydroisoindole strategy towards H_2Ar_4TNP.

Alternatively the route from the key starting material 1,4-dihydronaphthalene smoothly gave 4,9-dihydro-*2H*-benzo[*f*]isoindole which under Lindsey conditions in the presence of an aromatic aldehyde gave the desired H_2Ar_4TNPs after the addition of DDQ. Despite the authors' efforts they were not able to isolate the intermediate porphyrin, which was possible in both the previous octalin and TBP schemes. The overall yield from the Lindsey condensation ranged between 35-50% providing excellent access to the H_2Ar_4TNP system without the requirement of a metallation/demetallation

step. This new strategy was termed the dihydroisoindole method and later applied to the H_2Ar_4TBP and the tetraanthroporphyrin (H_2Ar_4TAP) systems.[37, 38] This strategy represents the most powerful method available for the preparation of π-extended porphyrins. In both the H_2Ar_4TNP and H_2Ar_4TAP systems the oxidative aromatization occurs almost instantly with the intermediate porphyrins to date not isolated. Only in the H_2Ar_4TBP system must the temperature be elevated to 100°C for a short period of time to complete the oxidative aromatization.

Introduction to Photophysics

The interaction of light with matter is something that has caught the interest of scientist since the early 15th century. At the end of the 19th century it was generally accepted that light was a wave and electrons were particles. In the beginning of the 20th century Planck's blackbody experiment concluded that blackbody radiation was limited to finite values of energy. This meant that the energy was quantized and changed the views of light as a wave. Einstein later discovered the photoelectric effect, further cementing the idea of light having wave and particle like properties. Although for most purposes the Maxwell wave equations from 1860 generally explain most of the light-related phenomena. These findings laid the foundation for de Broglie in 1924 to theorize that all particles act as waves. This led to the Schrödinger equation in 1924 which enabled the description of the wave nature of electrons mathematically. The impact of these discoveries has dramatically changed our understanding of atomic and molecular structure.

Absorption of Light

When light interacts with matter it has three possible pathways in that it is either reflected, transmitted or absorbed by the material. The latter pathway often referred to

as absorption can provide important information regarding the electronic molecular structure of a molecule. The absorption of a photon promotes a ground state electron to a higher energy level called an excited state. The difference in energy between these two energy levels is equal to the energy of the absorbed photon. This allows for elucidation of the molecular energy levels of a molecule. The energy of a photon is proportional to the frequency of its electromagnetic wave and is described by the following equation:

$$E = hv = \frac{hc}{\lambda} \tag{1-1}$$

where *E* is the energy of the photon, *h* is Planck's constant, *v* is the frequency, *c* is the speed of light, and *λ* is the wavelength of the photon. Since the electronic energy levels of a molecule are finite the ground state electrons absorb photons of different wavelengths (different energy) with different efficiencies. The efficiency of which a certain wavelength of light is absorbed is described by the molar absorptivity which is described by Equation 1-2.

$$A = \varepsilon bC \tag{1-2}$$

Where *A* is the absorbance, ε is the molar absorptivity (units of M^{-1} cm^{-1}), and *b* is the path length of absorption and *C* representing the molar concentration of the absorbing compound. The molar absorptivity represents the probability of the transition to occur and is directly related to the transition dipole moment between the initial and final states.

Another important principle to understand is the Franck Condon principle. This explains why the absorption bands in molecules appear as broad bands instead of the predicted sharp lines based on the discrete electronic energy levels. This is not the case

because of the difference in time scale between the excited electron (10^{-15} s) and the re-adjustment time of the nuclei (10^{-13} s) and is referred to as the Franck-Condon principle (Figure 1-13).

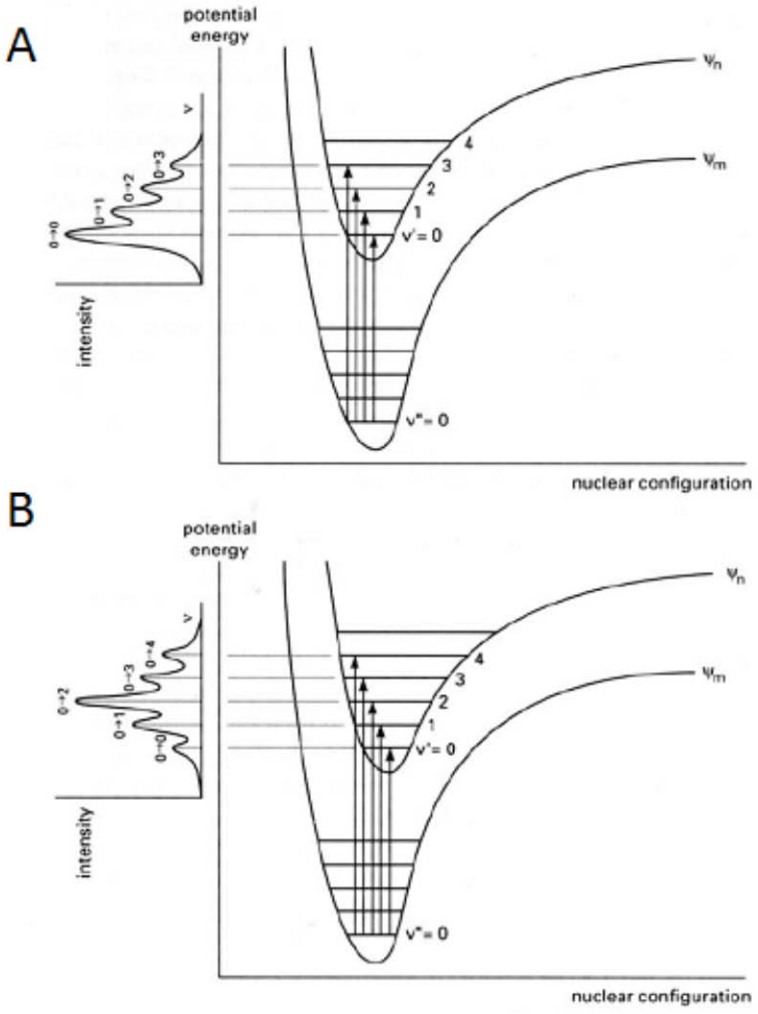

Figure 1-13. Potential energy curves for electronic transitions. A) Electronic transitions between states of similar equilibrium nuclear geometry. B) Electronic transitions between states of different equilibrium nuclear geometry. This figure was adopted from Gilbert and Baggot.[39]

This is illustrated by potential energy curves of the ground and excited states as a function of equilibrium geometry. The electronic transitions are termed “vertical” to illustrate absorption occurring without any changes in the equilibrium geometry. This allows for electrons to be promoted to higher excited states regardless of any

differences in equilibrium geometry between the ground and excited state. After absorption the molecule will relax to the lowest vibrational excited state (v' = 0). This relaxation results in a loss of energy and is the reason why the energy between the ground state (v" = 0) and some vibrational excited state (v' > 0) will always be higher in energy than the 0-0 transition.

Nature of the Excited State

Following absorption of a photon from the ground state (S_0) the electronic excited state (S_1) is created and represented by a vertical arrow (solid) in the Jablonski diagram (Figure 1-14). The molecule will first relax from higher vibrational levels (v > 0) to the lowest energy vibrational level (v = 0). This process occurs through two types of relaxation thermal (loss of heat) and collisional (with other molecules) and is illustrated by the dashed arrow. When the ground state is neutral the electrons in the highest occupied molecular orbital (HOMO) are paired and have opposite spins according to Hund's rule. When the electron is promoted to the excited state the spin is forbidden to change due to spin restrictions imposed by quantum mechanics and is therefore termed a singlet excited state (S_1). It is possible in some cases for the spin of the excited electron to flip; this process is referred to as intersystem crossing (ISC). This creates a situation where both electrons have the same spin. Excited states of this nature are referred to as triplet excited states (T_1). Similar to the singlet excited state the vibrational energy level is greater than zero for the initially formed triplet state and fast relaxation occurs to the lowest energy vibrational level (v = 0). Typically organic molecules have very low rates of ISC therefore the resulting triplet yields are very low. The rate of ISC can be enhanced by the addition of heavy atoms in a process known as the heavy atom effect. The process of ISC involves the conservation of total orbital angular momentum

and in heavy atoms the spin angular momentum and orbital angular momentum are not individually conserved. This facilitates spin-orbit coupling and increases the rate of the electron spin flip to form the triplet excited state. This allows inorganic and organometallic compounds such as platinum porphyrins to have large triplet quantum yields.

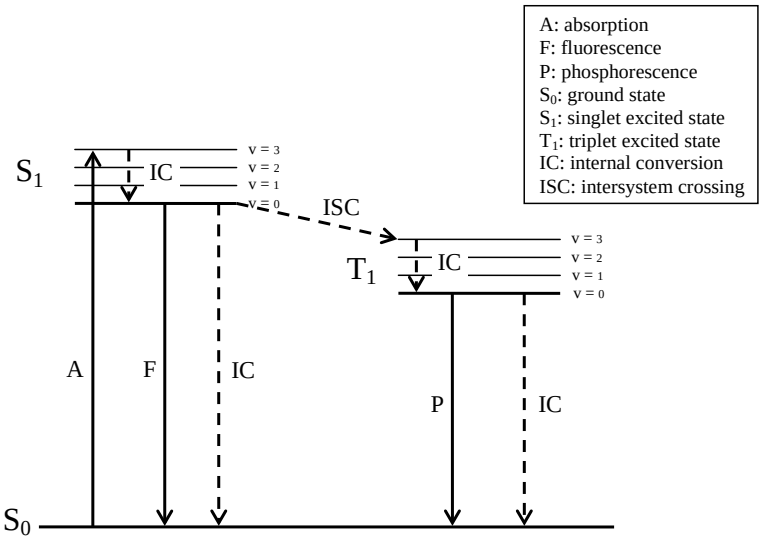

Figure 1-14. Jablonski diagram showing the possible transitions for a singlet excited state after absorption of a photon.

Relaxation of the Excited States

The triplet and singlet excited states are metastable, meaning they are stable and have long lifetimes but are transient in nature and eventually will relax to the ground state. The two pathways by which the self-relaxation mechanisms can occur are radiative and non-radiative decay. The latter represents the return of the excited electron to the ground state without the emission of a photon. Instead the energy is released as heat to the system when non-radiative decay occurs. This process and vibrational relaxation pathways are referred to as internal conversion (IC) on the Jablonski diagram (vertical dashed lines). The rate of non-radiative decay is governed

by the energy gap law. This law states that as the gap (energy difference) between the excited and ground states becomes lower in energy the rate of non-radiative decay will increase exponentially. Simply put one could expect that a fluorophore emitting light at 450 nm would have a smaller non-radiative decay rate than a fluorophore emitting at 700 nm due to the smaller gap in energy between the excited and ground state.

Photophysics of Porphyrins

The aesthetically pleasing purple color of porphyrins is the direct result of their unique absorption. Understanding what gives rise to their fascinating optical absorption and emission spectra has been an intriguing topic for researchers. The 18 π-electrons in the 16-membered porphyrin ring are responsible for the general optical spectra observed. However influences from external substituents and changes in conjugation pathway as well as change in the central substituents all lead to moderate to strong changes in optical absorption and emission spectra. The characterization of porphyrin absorption and emission spectra based on substitution patterns and different central substituents has been well studied and review elsewhere. The focus of this work is on one class of metalloporphyrins, specifically platinum (II) porphyrins.

Absorption of Metalloporphyrins

Metalloporphyrins typically differ very little by optical absorption spectra, but more so in emission from metal to metal. The addition of a metal to the center of the porphyrin changes the overall symmetry to D_{4h} from the lower D_{2h} symmetry of the free-base porphyrin. The absorption spectra for ZnTPP and Pt-TPP in toluene are shown in Figure 1-15. Two visible bands are typically seen between 500-600 nm called the Q-band with molar absorptivity constants in the range of 1.2-2 x 10^4 M^{-1} cm^{-1}. The Q-bands is a quasi-allowed transition. The lower energy band (α) is separated by approximately 1250

cm^{-1} from the higher energy band (β). The α band represents the electronic origin of Q(0,0) of the lowest energy singlet excited state. One mode of vibrational excitation in the singlet excited state is denoted by Q(1,0) and is represented by the β band.

The Soret band, often referred to as the B-band, is an intense band to the blue of the Q-band between 380-420 nm and is strongly allowed. Typical molar absorptivity constants for this band are in the range of 2-4 x 10^5 M^{-1} cm^{-1}. The electronic origin of the Soret band is B(0,0) of the second singlet excited state additionally with better resolved spectra another band appears to the blue (~1250 cm^{-1}) representing one mode of vibrational excitation B(1,0).

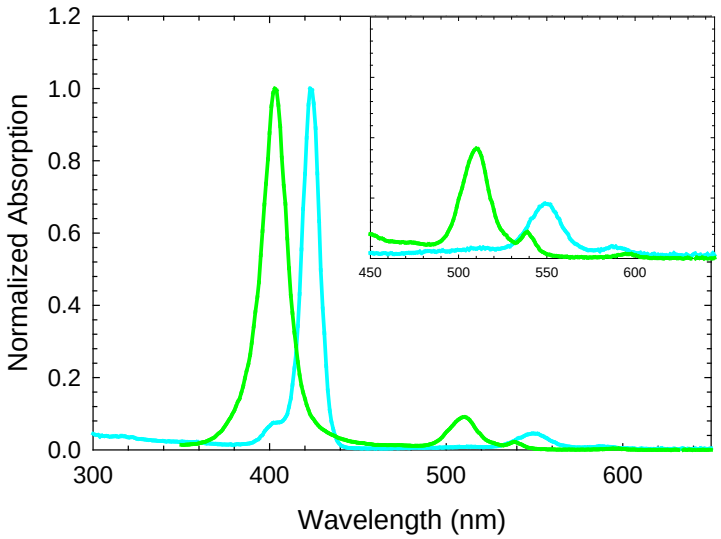

Figure 1-15. Examples of metalloporphyrin absorption spectra for ZnTPP (blue) and Pt-TPP (green) in toluene with the Q-band region magnified in the inset.

The metalloporphyrins are classified into two classes called "*regular*" and "*irregular*". This is based on whether or not the coordinated metal has a closed or open shell of valence electrons. The metalloporphyrins classified as "*regular*" give *normal* optical absorption and emission spectra. The *normal* absorption spectra are primarily

based on the porphyrin's π-electrons with the atomic orbitals of the coordinated metal having little interaction with the π-molecular orbitals of the porphyrin ring.

The irregular metalloporphyrins show spectra that are classified into three main types called *normal*, *hypso*, and *hyper*. The orbitals of the coordinated metal have a much stronger effect on optical spectra due to stronger mixing with the porphyrins π-electrons. The metals from the d- or f-block where the metal electrons are lower in energy and do not sufficiently interact with the porphyrins π-electrons give *normal*-type absorption spectra. An example of this would be zinc tetraphenylporphyrin (ZnTPP).

The *hypso*-type spectra also resemble the normal spectra but the Soret and Q bands are blue shifted relative to the free-base porphyrins absorption spectra. This results from metals in the d-block with unfilled d-orbitals (d^6-d^9). The d-electrons from the metal may be donated into the π*-orbitals of the porphyrin resulting in metal-to-ring charge transfer. This has the effect of increasing the energy of the porphyrins π-π* transition and thus blue shifting the absorption spectra. The blue shift increases with atomic number of the transition metal for example in series of Ni(II), Pd(II), and Pt(II).

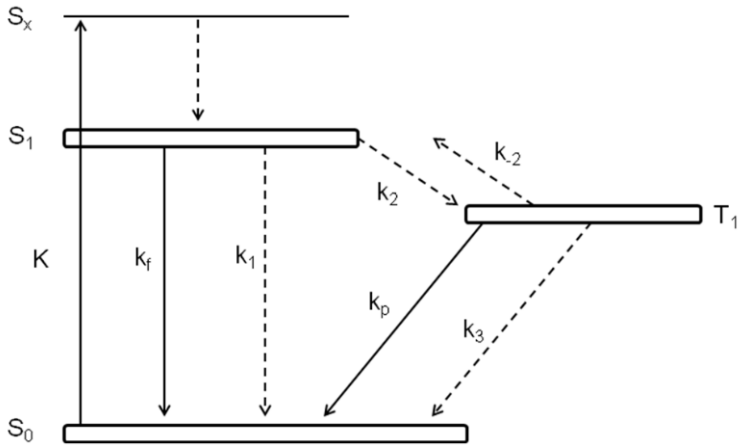

Figure 1-16. Jablonski diagram showing the decay schemes for singlet and triplet relaxation after absorption of a photon. The radiation processes depicted as solid lines and radiationless processes as dashed lines.

Introduction to Porphyrin Emission

One of the first reports of emission observed from a porphyrin was from the reduced porphyrin chlorophyll in 1834. The energy level diagram in Figure 1-16 illustrates the possible pathways of the singlet excited state (S_1) after absorption of a photon from the singlet ground state (S_0). Excitation of the ground state S_0 to any singlet excited state S_x leads to the population of the lowest singlet excited state S_1 by very fast radiationless decay (~10^{-12} -10^{-13} sec). The excited state S_1 can radiatively decay (fluorescence) $S_1 \rightarrow S_0$ with a rate k_f. From S_1 there are two possible non-radiative decay path ways the first being relaxation back to S_0 with a rate k_1 and the second intersystem crossing to the lowest energy triplet state T_1 with a rate k_2. The triplet state (T_1) can then radiatively decay to S_0 (phosphorescence) with a rate k_p. The first non-radiative decay path way is back to the singlet ground state S_0 with a rate k_3. Alternatively through thermal repopulation or triplet-triplet collisions repopulation of the singlet excited state (S_1) may occur resulting in another non-radiative decay pathway followed by delayed fluorescence.

Emission from Metalloporphyrins

The insertion of a heavy metal to form a metalloporphyrin causes a decrease in the fluorescence quantum yield from the expected increase in the rate of intersystem crossing from the heavy atom effect. The emission properties for *regular* metalloporphyrins are described by fluorescent quantum yields in the range 10^{-3}- 0.2 and phosphorescence quantum yields in the 10^{-4}- 0.2 range. Emission from the excited states for *regular* porphyrins occurs from the π-π* state of the porphyrin ring. The metal contributes small electronic perturbations resulting in small spectral changes or spin-orbit perturbations which lead to larger variations in both fluorescent and

phosphorescent quantum yields and triplet lifetimes. Like free-base porphyrins the *regular* metalloporphyrins give *normal* fluorescence spectra with two bands labeled Q(0,0) and Q(1,0). An example of this type of porphyrin and emission is depicted in Figure 1-17 by ZnTPP.

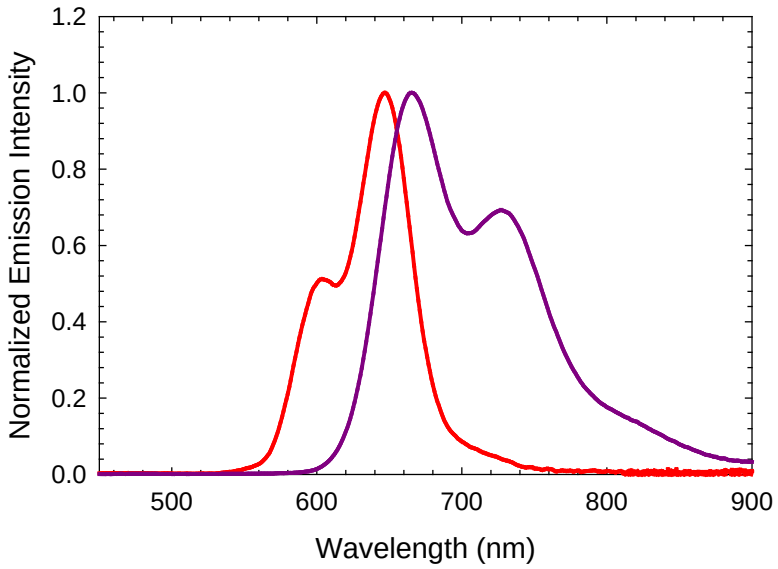

Figure 1-17. Examples of metalloporphyrin emission in toluene for ZnTPP (red) and Pt-TPP (purple) excited at the Soret band.

Platinum porphyrins are an example of an *irregular* metalloporphyrin giving *hypso*-type absorption spectra. The insertion of platinum increases the rate of ISC such that phosphorescence (radiative decay) is the dominant decay pathway. These phosphors are defined in many cases of having no observable fluorescence or quantum yields of fluorescence that are < 10^{-3}. This is a result of very high rates of intersystem crossing and leads to the phosphorescent quantum yields being much higher in the range between 10^{-4}-0.2 with the triplet lifetimes usually < 3 msec. The phosphorescence for Pt-TPP which represents an *irregular* metalloporphyrin is shown in Figure 1-17. The emission spectrum is red shifted relative to the fluorescence emission from ZnTPP due to the lower energy of the triplet state. The intensity of Q(0,0) is higher in Pt-TPP than in

ZnTPP, whereas the intensity of the lower energy band corresponding to Q(1,0) is higher in intensity relative to Q(0,0) in ZnTPP than in Pt-TPP.

Near-IR Light Emitting Diodes: State-of-the-Art

The three major roles of porphyrins in nature were accurately defined by Gouterman as electron transfer, oxygen transfer, and photosynthesis.[40] However, the research area which encompasses porphyrins has since broaden with scientists finding new applications in different scientific disciplines and is well reviewed elsewhere.[41] One such application for platinum porphyrins is in light emitting diodes (LEDs) which are devices fabricated from inorganic or organic materials sandwiched between two electrodes. Upon application of an electric field these devices emit light. This process is known as electroluminescence (EL) and discussed further in more detail along with other aspects of LEDs in the introduction section of Chapter 3.

Pt-OEP was first reported and incorporated into an OLED by Thompson *et al*.[42, 43] The use of Pt-OEP produced deep red emitting OLEDs with record high efficiencies at the time. The increase in overall device efficiency was attributed to the use of a phosphor over a fluorophore which is discussed in greater detail in Chapter 3.

The development of LED devices that exhibit electroluminescence solely in the near-infrared (NIR) has continued to be a rapidly growing field over the past decade. The realization of devices with high efficiencies will enable new technology to be commercialized for use in infrared signaling and displays, telecommunications, and wound healing.[44-47]

The earliest reports of near-IR LEDs date back to the early 1970's fabricated from inorganic materials which yielded low overall device efficiencies. Today over a hundred publications in the field exist with less than twenty percent reported prior to 2000. The

use of organic materials for electroluminescence was first reported in 1987 by Tang and Van Slyke.[55] This eventually led to the first deep red and near-IR organic LED report using buckminsterfullerene in 1991 by Katsumi *et al*.[56] Today a variety of materials are reported for use in near-IR LEDs, but in general the devices still suffer from low efficiencies. Much work is still needed in the design and synthesis of highly efficient emitters in the near-IR spectral region for device applications. The majority of reports for near-IR LED devices have reported external quantum efficiencies (EQE) of less than one percent. The EQE data and the peak electroluminescence wavelengths for some recent literature reports representing the highest efficiency devices to date for near-IR LEDs is summarized in Table 1-1.

Table 1-1. Recent literature reports of near-IR LED devices demonstrating the state-of-the-art in terms of emission wavelength and device efficiency.[48-54]

Year	Molecule	λ_{max} (nm)	Power	Efficiency (EQE)	Ref.
2001	Ln-TPP (Ln = Yb^{3+} or Er^{3+})	977, 1560	--	0.015%, 0.1%	48
2003	DDD (Zn porphyrin Trimer)	820		0.1%	49
2005	PPyrPyrPV (Copolymer)	800	60 nW/cm^2	Low	50
2005	PMOPV-TBSV30 (Copolymer)	800	--	0.01%	51
2005	PFO-SeBSe 10 (Copolymer)	759	--	0.20%	52
2007	Pt-TPTBP (Pt-porphyrin)	773	750 μW/cm^2 at 12 V	6.3%	53
2008	PtPc (Pt-Phthalocyanine)	966	80 μW/cm^2 at 140 ma/cm^2	0.3% at approx. 1 mA/cm^2	54

Previous work in our group focused on the synthesis and characterization of lanthanide monoporphyrinate complexes as near-IR emitters for LED applications.[48] The lanthanide monoporphyrinate complexes were fabricated into near-IR LEDs by blending them into conjugated polymers (Figure 1-18). The TPP ligand served as an

antenna to sensitize the narrow near-IR emission from the coordinated lanthanide metal. However these transitions are weak with photoluminescence quantum yields generally well below one percent leading to device efficiencies well below half a percent.

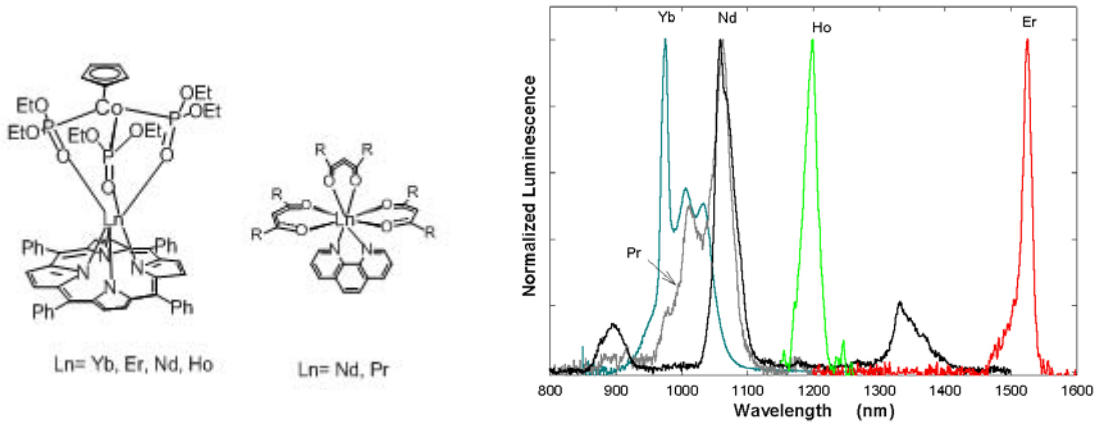

Figure 1-18. Lanthanide based near-IR emission from lanthanide monoporphyrinate complexes towards near-IR LED applications.[48]

Therien and Bazan in 2003 reported near-IR PLEDs using ethyne-bridged zinc porphyrin fluorophores.[49] A zinc porphyrin trimer (DDD) was doped into polymer host materials and electroluminescence observed at 820 nm. The overall performance of the device was rather low with an EQE of 0.1%. PLEDs fabricated from near-IR emitting polymers have been reported.[50-52] Conjugated polymers in general usually have lower PL efficiencies and broad emission profiles. The use of these materials for LED applications is less than ideal and results in lower device efficiencies.

An alternative to the Lanthanide porphyrin complexes are the π-extended porphyrins which have been initially investigated since the 1940's. However use of these materials towards material science applications has been limited due to the difficulty in their preparation. The recent advances in the synthesis of π-extended porphyrins made by Finikova *et al* have allowed access to these ideal targets for use in

near-IR LED device applications. The success in fabricating deep red emitting LED devices using Pt-OEP cements the promise of these materials in this field. Recently Thompson *et al* demonstrated the use of a platinum π-extended porphyrin as a near-IR phosphor for use in a near-IR LED (Figure 1-19) by incorporating platinum tetraphenyltetrabenzoporphyrin (Pt-TPTBP) in an Alq_3 host matrix. The optimized device displays an electroluminescence peak in the near-IR region at 772 nm with a record EQE for this wavelength region of 8.5%. Similarly a near-IR LED based on a platinum phthalocyanine (Pt-Pc) has also been reported with electroluminescence centered at 966 nm with an EQE of ~0.3%.[54]

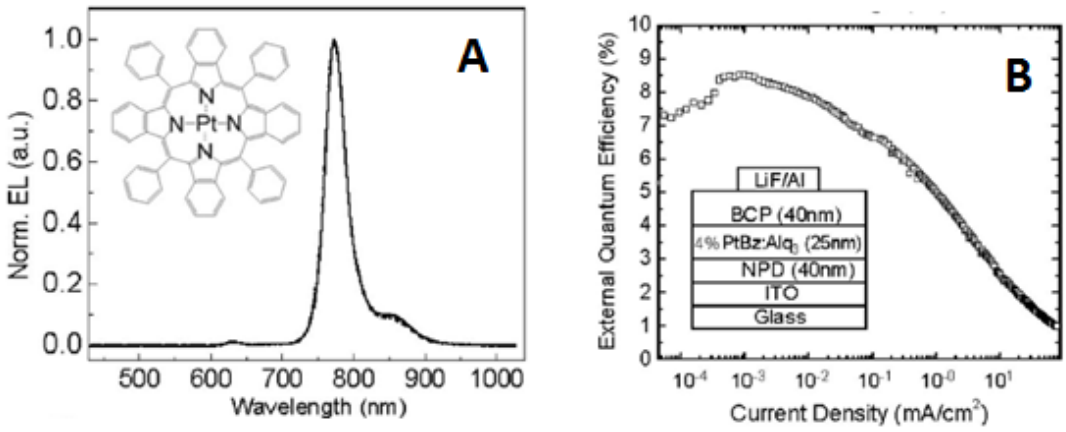

Figure 1-19. Near-IR OLED device data for Pt-TPTBP doped in to Alq_3 reported by Thompson *et al*.[53] A) Electroluminescence at 772 nm from Pt-TPTBP doped in Alq_3 B) External quantum efficiency of 8.5% and optimized device structure.

π-Extended Platinum Porphyrins as Near-IR Phosphors

Platinum complexes of π-extended porphyrins have been demonstrated by Thompson *et al* to be ideal targets for application in near-IR LEDs. To the best of our knowledge only five platinum TBP derivatives have been reported, while no reports exist for the TNP and TAP systems.[53, 57, 58] This is largely due to the difficulty in the preparation of the platinum complexes in good yield from the free-base porphyrins.

Therefore the development of metallation conditions to provide access to the platinum complexes of π-extended porphyrins is imperative and described in Chapter 2. The novel reaction conditions have allowed access to platinum TNP and TAP systems for the first time, where this work would otherwise not be possible.

Figure 1-20 outlines the nearly all the known structures for free-base and metallo-TBPs, where **Pt-1a** and **Pt-4b** represent two of the known platinum complexes for π-extended porphyrins.[32, 33, 58-62] The other three platinum complexes are derivatives of Pt-TPTBP were the *meso*-aryl groups are fluorinated to different degrees.[57] The PL spectra for **Pt-1a** and **Pt-4b** have maximum emission wavelengths reported at 765 and 745 nm respectively. The quantum yields of **Pt-1a** and **Pt-4b** are the highest reported for this wavelength region of 0.70 and 0.51 respectively. The previously reported free-base and metallo-TNPs are shown in Figure 1-21.[36, 58, 63-65] Completely absent is the report of a platinum complex, although quite a few palladium complexes have been reported.

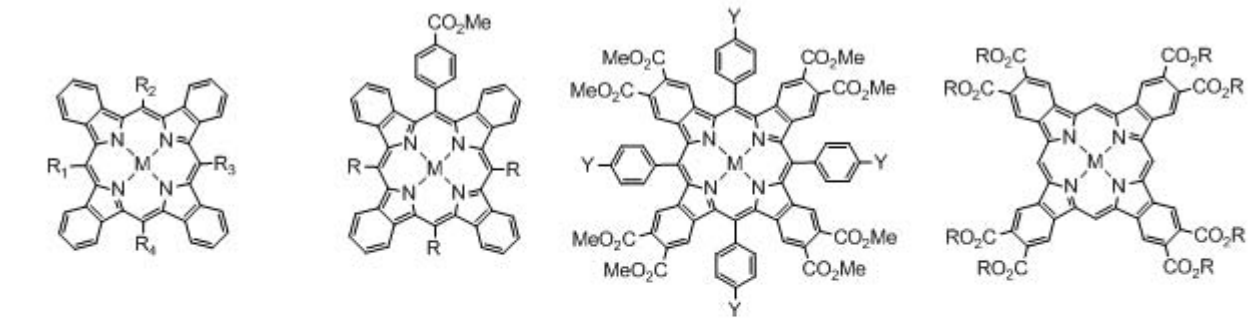

1a: R_{1-4}= Ph; M= H_2, Zn, Pd, Pt
1b: R_{1-4}= thiophene; M= Zn
1c: R_{1-4}= H; M= H_2, Pd
1d: $R_{1,3}$= H_2; $R_{2,4}$= Ph; M= H_2, Pd
1e: $R_{1,3}$= H_2; $R_{2,4}$= 4-$NO_2C_6H_4$; M= H_2
1f: $R_{1,3}$= H_2; $R_{2,4}$= 4-BrC_6H_4; M= H_2
1g: $R_{1,3}$= H_2; $R_{2,4}$= 4-MeO_2C-C_6H_4; M= H_2
1h: $R_{1,3}$= H_2; $R_{2,4}$= 3,5-^{t}BuPh; M= H_2

2a: R= Ph; M= H_2, Zn
2b: R= H; M= H_2, Zn, Mg

3a: Y= H
3b: Y= CO_2Me
3c: Y= Br
3d: Y= OMe
3e: Y= NO_2
M= H_2, Cu, Ni, Zn, Pd

4a: R= Me
4b: R= Bu
M= H_2, Zn, Pd, Pt, Fe

Figure 1-20. Current literature reports for free-base and metallo-TBPs.

The PL spectra reported in the literature for Pd-TNPs are shown to have maximum wavelengths ranging from 920 -950 nm depending on substitution of the TNP. This is over a 100 nm red shift compared to the emission of Pd-TBPs. The PL spectra from Pt-TNPs will likely be blue shifted relative to the Pd-TNPs, following the same trend in platinum and palladium complexes for porphyrins and TBPs. The quantum yields range from 2-5% and are lower than the 6.7% reported for a Pd-Ar_4TBP derivative. The quantum yields for Pt-TNPs should be expected to be higher than the Pd-TNPs based on the observed trend in the Pd-TBP (0.067) and Pt-TBP (0.51) derivatives. This data suggest that a Pt-TNP derivative will likely have a high PL efficiency for this wavelength region making it an ideal candidate for near-IR LED applications.

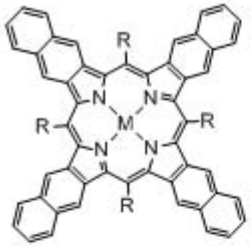

5a: R= H; M= H_2, Zn
5b: R= 3,5-^{t}BuPh; M= H_2, Zn

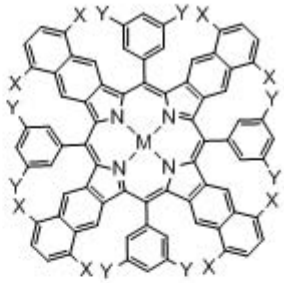

6a: X=H, Y= CO_2Bu; M= H_2, Pd
6b: X= OMe, Y= CO_2Bu; M= H_2, Pd

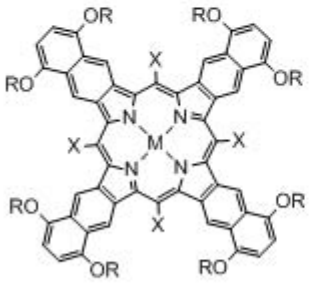

7a: X= H, R= Me; M= H_2, Zn, Pd
7b: X= H, R= -$(CH_2)_3CO_2Et$; M= H_2, Zn, Pd
7b: X= Ph, R= Me; M= H_2, Zn, Pd
7c: X= mesityl, R= Me; M= H_2

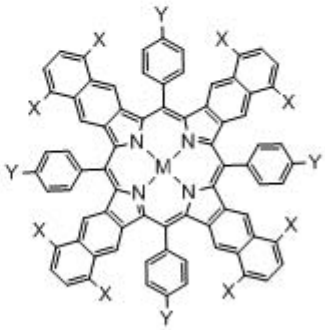

8a: X= H, Y=H; M= H_2, Zn, Cu, Pd
8b: X= H, Y= 4-MeO_2C; M= H_2, Zn, Pd
8c: X= OMe, Y= H; M= H_2, Zn, Pd
8d: X= OMe, Y= 4-MeO_2C; M= H_2, Zn, Pd

Figure 1-21. Current literature reports for free-base and metallo-TNPs.

Recent literature reports for TAPs suggest that PL from a Pt-TAP should be centered beyond a 1000 nm. To date there are only a couple reports on PL from TAPs.[38, 66] Ono *et al* report the fluorescence and quantum yield data for ZnTAP derivatives. The reported emission maxima are ~820 nm. There is only one known report of a phosphorescent TAP reported by Cheprakov *et al*. They report a Pd-TAP porphyrin with the PL centered at 1107 nm and a phosphorescence quantum yield of less than 0.5%. There are no reports for a Pt-TAP and the photophysical properties remain unknown. However, the preparation of a Pt-TAP derivative will allow access to a new wavelength region in the near-IR.

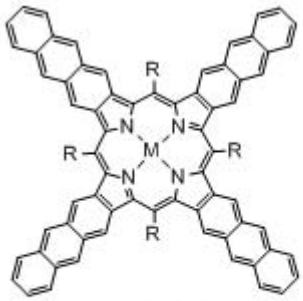

9a: R= H_2; M= Zn
9b: R= Ph; M= Zn
9c: R= 3,5-^{t}BuPh; M= Zn
9d: R= 4-MeO_2C-Ph; M= H_2, Zn, Pd

Figure 1-22. Current literature reports for free-base and metallo-TAPs.

Objective of Present Study

The objective of the present study is to expand the known series of π-extended platinum porphyrins beyond the TBP system to the TNP and TAP systems. A novel metallation procedure is reported herein providing access to the platinum complexes in high yield for the first time. The photophysics of these materials will be reported for the first time in both solution and in thin films. The present study will also aim to optimize

the porphyrin macrocycle through chemical modification by looking at the effects on solution and film photophysical and device properties of different substituents and substitution pattern of the π-extended platinum porphyrins in an attempt to increase the device efficiencies. This optimization should lead to higher phosphorescence quantum yields and reduced aggregation in a solid state matrix. Devices will be fabricated by two methods the first being from materials that are vapor deposited (sublimation) onto a substrate termed organic light emitting diodes (OLED) devices. The second methodology uses solution processing to form thin films of conjugated polymers doped with the platinum π-extended porphyrins by spin coating the materials onto the device substrate referred to as PLED devices. The overall goals for device efficiencies (EQE) are to produce an OLED device with electroluminescence solely in the near-IR spectral region operating at external quantum efficiency greater than 10%. The efficiency goals for a PLED device are to fabricate a device that operates at an overall efficiency greater than 1% with electroluminescence solely in the near-IR.

CHAPTER 2
SYNTHESIS OF π-EXTENDED PLATINUM PORPHYRINS

Introduction

The advances in synthetic methodology from the recently developed dihydroisoindole technique for preparing π-extended porphyrins has provided researchers with access to materials once thought inaccessible. Thompson's group recently demonstrated a highly efficient near-IR OLED device using Pt-TPTBP as the near-IR phosphor.[53, 67] This work along with the recent reports of the synthesis of TNP and TAP systems are encouraging for further development of new π-extended platinum porphyrins as NIR phosphors. While the free-base porphyrins and a few metal complexes have been reported for each of these systems, the platinum complexes are still unknown.[36, 38] The published absorption and emission data for TBP, TNP and TAP systems (Figure 2-1) was reviewed in Chapter 1. The increase in conjugation to the porphyrin macrocycle via additional fused-benzene rings systematically red shifts the absorption and emission spectra.[58]

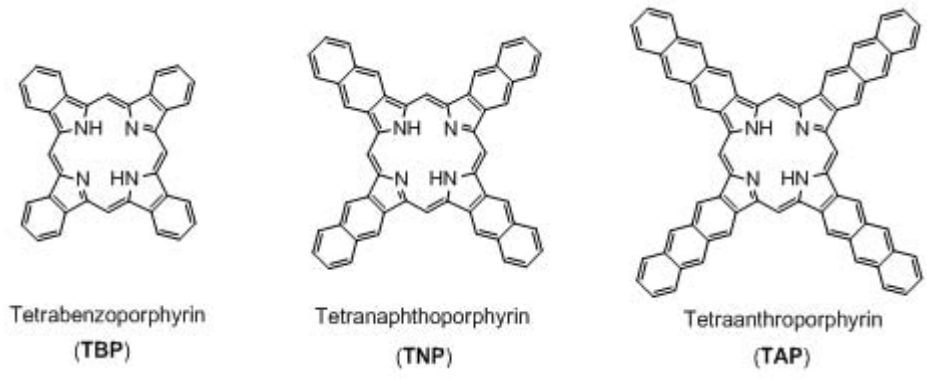

Figure 2-1. General structures for *meso*-unsubstituted π-extended porphyrins.

The present study presents three novel series of π-extended platinum porphyrins. The goal of the first series is aimed at pushing device emission further into the near-IR by the addition of fused-aromatic rings to the porphyrin macrocycle. The second series

of target TBPs focuses on increasing the solution quantum yield of platinum TBPs by varying the number of *meso*-aryl substituents around the porphyrin macrocycle in attempts to understand the factors that control the emission yield. The third series presents platinum TBPs designed to increase device efficiencies by chemical modification to the porphyrin macrocycle incorporating new substituents to either enhance mixing with the host or by preventing the porphyrin from aggregating. The target π-extended platinum porphyrins are outlined in Figure 2-2. Only four of the free-base porphyrins have been previously reported in the literature (H_2TPTBP, H_2TPTNP, H_2DPTBP, and H_2Ar_2TBP).

More importantly only one of the ten subsequent platinum complexes has been previously reported and studied (Pt-TPTBP). Demonstrating the degree of which the platinum complexes for π-extended porphyrins have been under studied. The recent synthetic methodology has allowed the preparation of the free-base porphyrins while the synthesis and characterization of the platinum complexes has been absent from the literature due to the difficulty in their preparation. The following series of target π-extended platinum porphyrins has been prepared in efforts to characterize the photophysical properties of these novel phosphors in most cases for the first time.

The first series of target π-extended platinum porphyrins are outlined in Figure 2-2. The series is aimed at the preparation of platinum porphyrins with longer emission wavelengths across the series from Pt-TPTBP to Pt-Ar_4TAP. The solution phosphorescence of Pt-TPTBP has been reported at 773 nm. The emission wavelength can be further shifted by the preparation of Pt-TPTNP. Recently Finikova *et al* reported the phosphorescence of Pd-Ar_4TNPs beyond 900 nm and noted that substitution with

eight methoxy-substituents further red shifted the emission to 957 nm.[36] This makes Pt-TPTNP and Pt-Ar_4TNP$(OMe)_8$ attractive candidates for NIR LEDs with expected emission wavelengths beyond 900 nm. Later Yakutkin *et al* reported the synthesis of Pd-Ar_4TAP derivative and measured the phosphorescence at 1107 nm. The synthesis of Pt-Ar_4TAP would likely provide access to emission beyond 1000 nm. The platinum complexes for TNP and TAP systems have not been reported in the literature and thus the photophysical properties remain unknown to date.

The second series of target platinum TBPs is aimed at increasing the solution quantum yield across the series from Pt-TPTBP to Pt-Ar_2TBP. The solution quantum yields of Pt-TPP (0.07) and Pt-OEP (0.45) have been well studied.[43, 68] The large difference in quantum yields is attributed to the increased planarity of Pt-OEP. The effects of the number of *meso*-aryl substituents on the structural and photophysical properties in the TBP system was recently studied for a series of free-base and Pd-TBPs.[61] The quantum yield for Pd-Ph_2TBP is reported to be twice that of Pd-Ph_4TBP due to increased planarity of the TBP macrocycle. The proposed series of tetra-aryl and 5,15-diaryl platinum TBPs are outlined in Figure 2-2. It is expected that the solution quantum yields for Pt-DPTBP and Pt-Ar_2TBP should follow the reported trend for Pd-TBPs likely leading to significantly higher quantum yields and device efficiencies.

The past decade has seen a surge in the complexity of the fluorophores and phosphors synthesized for use in LEDs. The early work was focused on finding materials that displayed electroluminescence at specific regions in the visible (blue, green, and red) with high quantum yields. However despite the advances made in the

field quenching of the emitting species from intermolecular interactions or poor carrier mobility within the device matrix remains a problem.[69]

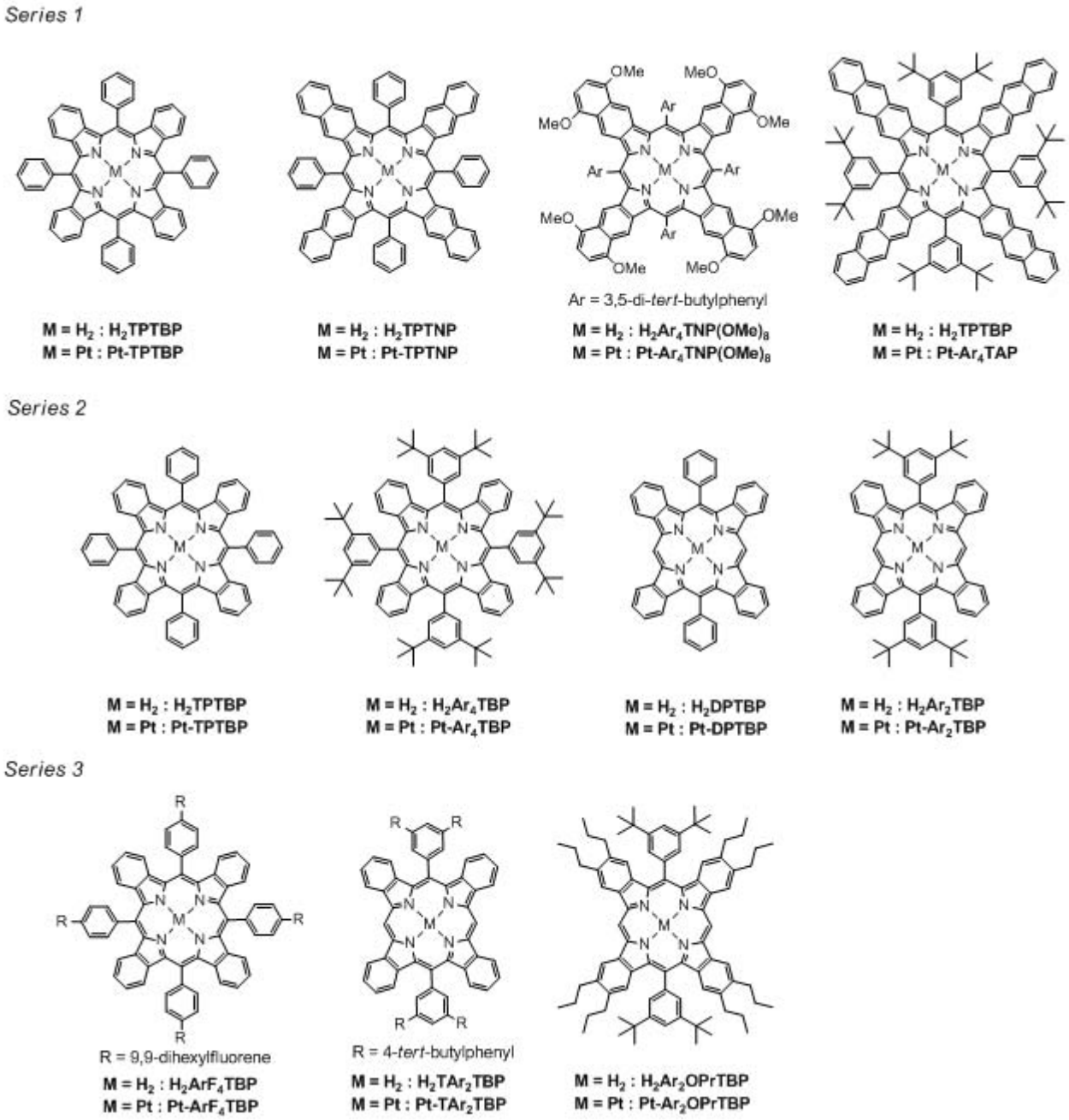

Figure 2-2. Target free-base and platinum porphyrins towards new near-IR phosphors.

The use of dendrimer encapsulated phosphors has proven effective in reducing aggregation problems.[70-73] The area of porphyrin dendrimers is a growing field with the

new materials being applied to a variety of applications.[74] Fluorescent porphyrin dendrimer systems have been reported for use in LED device applications with improvements reported in device efficiencies over other fluorescent porphyrin systems.[75] Only one platinum porphyrin based dendrimer system has been reported for LED applications displaying higher device efficiencies than those reported for pure Pt-OEP or PVK: Pt-OEP devices.[76] Unfortunately the synthesis of dendrimers is lengthy and often accompanied by difficult purification making targets of this nature impractical. Recently porphyrins have been reported with bulky *meso*-aryl substituents that in effect create the desired dye encapsulation obtained by a porphyrin dendrimer system noted by an increase in the solution quantum yield.[77] The fluorescence quantum yields for some reported TPP derivatives are reported to be twice that of TPP from the reduction in porphyrin aggregation in solution. The target Pt-TBP structures in series 3 are aimed at reducing aggregation effects or increasing host compatibility in the device matrix (Figure 2-2). The structures are based on recent literature reports for similar porphyrin systems.[77-79]

In the work described in the present chapter, we report the design and synthesis of three novel series of π-extended platinum porphyrins. The free-base porphyrins have been prepared using the dihydroisoindole method. The platinum porphyrins have been prepared from a novel metallation procedure developed herein. The materials have been characterized by ^{1}H and ^{13}C NMR and HRMS. The photophysical properties for each series have been studied and are reported in Chapter 3 along with the performance for each material as near-IR phosphors in near-IR LEDs.

Synthesis of Aromatic Aldehydes for π-Extended Porphyrins

The synthetic scheme for the target aromatic aldehydes is outlined below in Figure 2-3 along with commercially available benzaldehyde (**1**). Aldehyde **3** was prepared starting from commercially available **2** which was brominated with NBS and then subjected to oxidation/hydrolysis with hexamine to produce **3** in moderate yield following a previously reported method.[80]

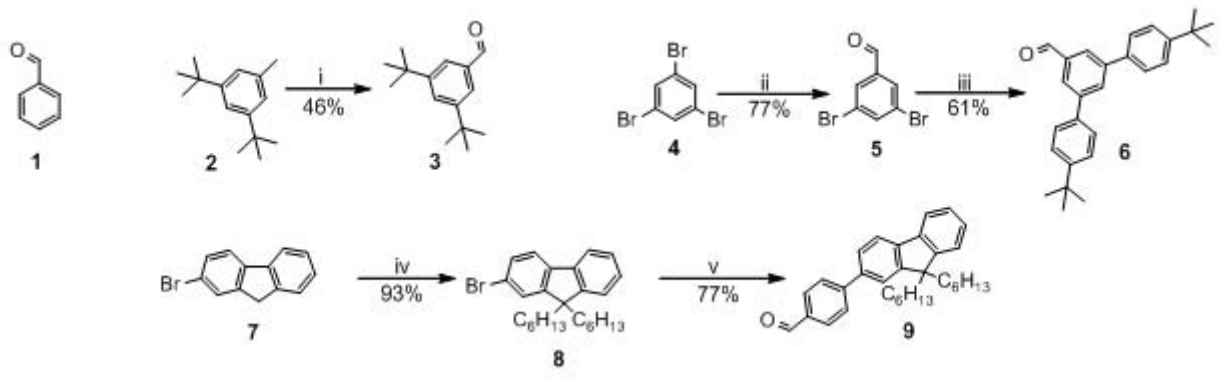

Figure 2-3. Synthetic scheme for aromatic aldehydes towards *meso*-aryl substituted π-extended porphyrins. *Reagents and conditions*: i) NBS, CCl_4, 12 h reflux, hexamine, MeOH, H_2O, reflux 4 h; ii) *n*-BuLi, DMF, ether, -78°C, 30 min; iii) $Pd(PPh_3)_4$, Na_2CO_3,4-^{t}BuPhB$(OH)_2$, PhMe, THF, H_2O, 100°C, 120 h; iv) Br-Hexyl, NaOH, DMSO, H_2O, 80°C overnight; v) $Pd(PPh_3)_4$, Na_2CO_3,4-formylPhB$(OH)_2$, THF, H_2O, 80°C, overnight

Aldehyde **6** was prepared in analogous manner to the reported 3,5-diphenylbenzaldhyde.[77] Treating 1,3,5-tribromobenzene (**4**) with one equivalent of *n*-BuLi followed by the addition of DMF gave **5** in good yield.[81] Compound **5** was then introduced to Suzuki coupling with 4-*tert*-butylphenylboronic acid yielding aldehyde **6** in good yield.[77] The preparation of **9** followed a previously reported method.[82] The alkylation of 2-bromo-fluorene was performed by a previously reported method to give **8** in excellent yield.[83] Compound **8** was introduced to a Suzuki coupling with 4-formylbenzeneboronic acid to give aldehyde **9** in good yield.

Synthesis of Pyrroles for π-Extended Porphyrins

The synthesis of six of the eight free base TBPs share a common intermediate in 2-ethoxycarbonyl-4,7-dihydro-2H-isoindole (**18a**) which was prepared according to a previously reported method (Figure 2-4).[37] The other two TBP derivatives required a substituted butadiene to access the desired pyrroles.

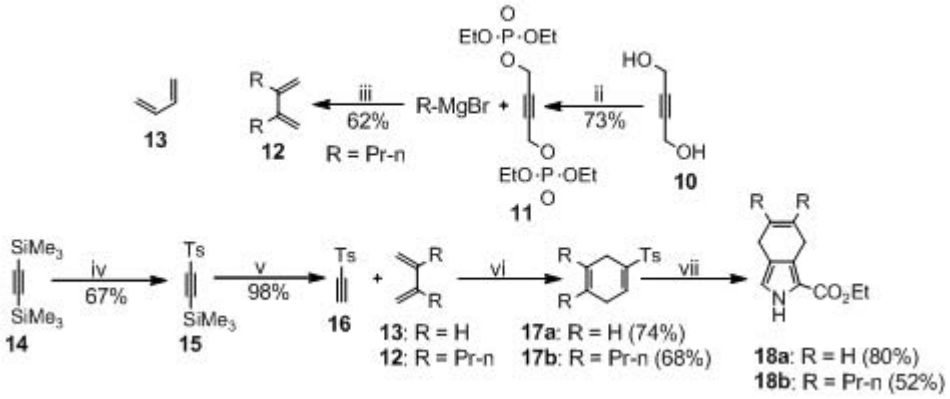

Figure 2-4. Synthetic scheme for benzopyrroles **18a-b** towards TBPs. *Reagents and conditions*: i) HCl, 25ºC, 1h; ii) $(EtO)_2P(O)Cl$, pyridine, 0°C, 2 h; iii) THF, CuI, 0°C-25°C, overnight; iv) DCM, $AlCl_3$, TsCl, 24 h, 25 °C; v) MeOH, NaF in H_2O, 0°C-25°C, 1.5 h; vi) **13** neat 25ºC, **12** PhMe 130ºC, 48 h; vii) THF, ^tBuOK , $CNCH_2CO_2Et$, 0°C-25°C, 4 h.

The 2,3-substituted butadiene **12** was prepared according to a previously reported method. Following a published procedure compound **11** was prepared by treating commercially available **10** with diethyl chlorophosphate in the presence of pyridine to give **11** in good yield. The addition of an alkyl Grignard reagent to **11** gave the desired 2,3-substituted butadiene **12** in moderate yield. The Diels-Alder adducts **17a-b** where prepared from butadienes **12** and **13**. Starting from commercially available **14** treated with a solution of $AlCl_3$ and TsCl in dry DCM to afford the alkylation adduct **15** in good yield.[84, 85] Compound **15** was converted to ethynyl p-tolyl sulfone (**16**) following a published procedure by deprotecting **15** with aqueous sodium fluoride in methanol to give **16** nearly quantitatively.[86] The Diels-Alder adduct **17a** was obtained by reacting **16**

in neat 1,3-butadiene (**13**) to give **17a** in good yield following a previously reported method. Similarly **17b** was prepared from **16** and **12** from a modified literature method to give **17b** in good yield. Dropwise addition of the vinylic sulfones **17a-b** to a one equivalent ^{t}BuOK and ethyl isocyanoacetate mixture in dry THF in a modified Barton-Zard synthesis gave benzopyrroles **18a-b** in good yield.

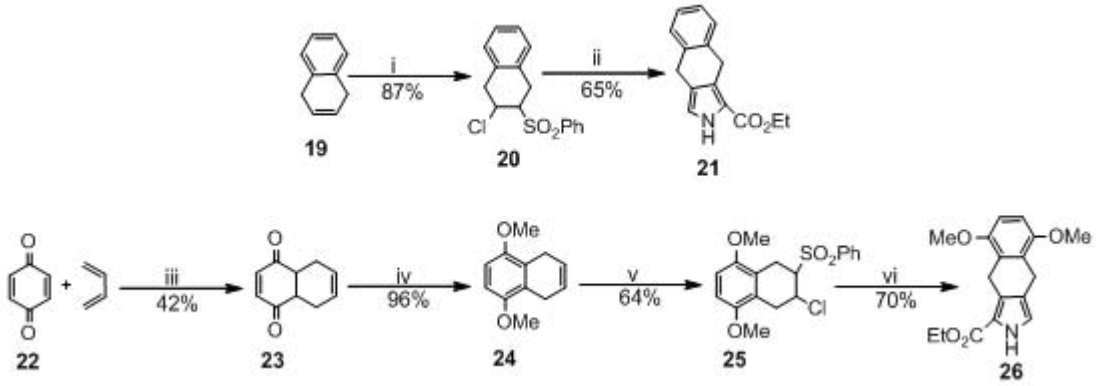

Figure 2-5. Synthetic scheme for naphthopyrroles **21** and **26** towards TNPs. *Reagents and conditions:* i) PhSCl, DCM, 0°C, 1 h, *m*-CPBA, 0°C-25°C, 1 h; ii) THF, ^{t}BuOK , $CNCH_2CO_2Et$, 0°C-reflux, 1 h; iii) AcOH, 25°C, 24 h; iv) Me_2SO_4, K_2CO_3, acetone, reflux 40 h; v) PhSCl, DCM, 0°C-25°C, 2 h, *m*-CPBA, 0°C-25°C, 1 h; vi) THF, ^{t}BuOK , $CNCH_2CO_2Et$, 0°C-reflux, 1 h.

The synthesis of naphthopyrroles **21** and **26** have been previously reported and is outlined in Figure 2-5.[36] Pyrroles **21** and **26** were similarly prepared from commercially available 1,4-dihydronaphthalene (**19**) and 5,8-dimethoxy-derivative **23**. Starting from commercially available 1,3-butadiene and 1,4-benzoquione (**22**) in acetic acid at room temperature gave the Diels-Alder adduct **23** in a moderate yield.[87] Compound **23** was treated with potassium carbonate and dimethyl sulfate in refluxing acetone to give **24** in an excellent yield.[87] The α-chlorosulfones **20** and **24** were prepared from the dropwise addition of phenylsulfenyl chloride (PhSCl) in dry DCM to **19** and **23** followed by oxidation with *m*-CPBA which gave the α-chlorosulfones **20** and **24** in good yield. The pyrrole esters **21** and **26** were obtained in good yields and prepared analogously to **18a**

from a modified Barton-Zard synthesis requiring an extra equivalent of base to form the vinylic sulfone in situ from the protected α-chlorosulfone.

The anthropyrrole precursors **32** and **38** that provide access to the TAP system were prepared from previously reported literature methods.[38, 66] The key intermediates for the pyrrole synthesis are 1,4-dihydroanthracene (**35**) and bicyclic-precusor **30**. Compound **30** was prepared starting from 1,4-naphthoquione (**27**) and 1,3-cyclohexadiene in refluxing ethanol to give the Diels-Alder adduct **28** in a good yield.[88] The reduction of dione **28** in anhydrous methanol with sodium borohydride smoothly gave the diol **29** in excellent yield.[89]

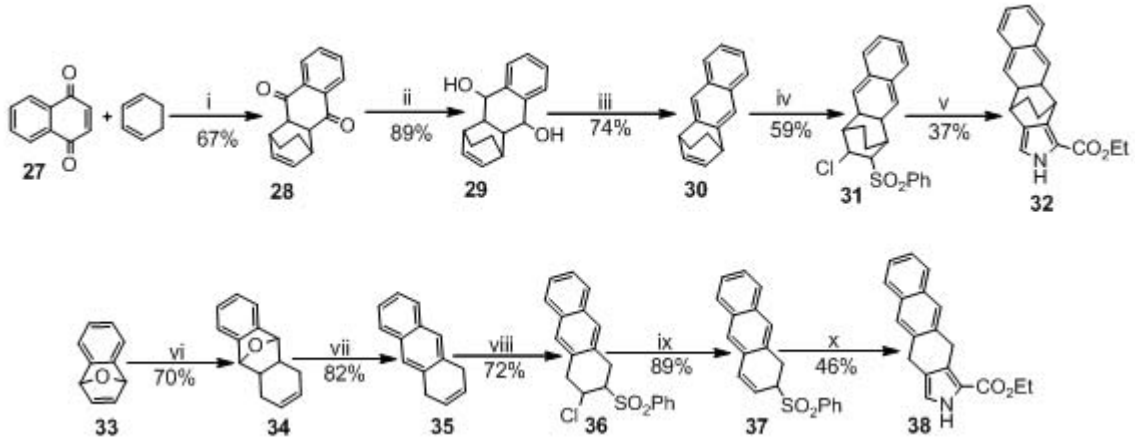

Figure 2-6. Synthetic scheme for anthropyrroles **32** and **38** towards TAPs. *Reagents and conditions:* i) EtOH, 3 h, reflux; ii) MeOH, $NaBH_4$, 0°C, 2h; iii) Pyridine, TsCl, 48 h, 25°C; iv) PhSCl, DCM, -78°C-25°C, 4 h, *m*-CPBA, 0°C-25°C, 18 h; v) THF, ^{t}BuOK , $CNCH_2CO_2Et$, 0°C-25°C, 18 h; vi) Pyridine, 3-sulfolene, $NaHCO_3$, 120°C, 70 h; vii) EtOH, HCl, reflux, 24 h; viii) PhSCl, DCM, -78°C-25°C, overnight, m-CPBA, 0°C-25°C, 48 h; ix) DCM, DBU, 25°C, 1 h; x) THF, ^{t}BuOK , $CNCH_2CO_2Et$, 0°C-25°C, overnight.

The dehydration of **29** with excess tosyl chloride in dry pyridine yielded **30** in good yield.[90, 91] Key intermediate **35** was obtained starting from **33** which was prepared from a literature procedure from benzyne and furan.[92, 93] Compound **33** was treated with 3-sulfolene while heating in pyridine to yield the Diels-Alder adduct **34** in good yield.

Compound **34** was then introduced to refluxing ethanol and HCl to give **35** in a good yield. The reported method of preparing **36** using Oxone as the oxidant failed. The α-chlorosulfones **31** and **36** were obtained from a modified procedure for **20**.[66] The dropwise addition of PhSCl in dry DCM to **30** and **35** at -78°C followed by oxidation with *m*-CPBA for 18 to 48 hours gave **31** and **36** in good yields.

Pyrrole esters **32** and **38** could be prepared directly from α-chlorosulfones **31** and **36** forming the vinylic sulfone in situ to give the anthropyrroles in moderate yield. Alternatively **38** could also be prepared in a similar yield from the deprotection of **36** to allylic sulfone **37** with DBU. Allylic sulfones have previously been demonstrated as suitable substrates in the modified Barton-Zard synthesis over vinylic sulfones.[36] The modification requires a small excess of strong base to induce the allylic-vinylic sulfone isomerization.

Synthesis of Symmetrical π-Extended Porphyrins

Deprotection of Pyrrole Esters

The major advantage of the dihydroisoindole method is that the desired π-extended porphyrins are prepared under Lindsey conditions. This requires cleavage of the ester from the pyrrole-esters obtained from the modified Barton-Zard reaction. Two methods have been reported for the ester-cleavage of the pyrroles. Pyrrole esters prepared from *tert*-butyl isocyanoacetate can be deprotected from TFA at room temperature.[59]

However pyrrole-esters obtained from ethyl isocyanoacetate are heated in ethylene glycol in the presence of excess KOH to provide the unprotected pyrroles.[37] The latter method was used to smoothly yield all the precursor pyrroles in good yields and is outlined in Figure 2-7. Due to instability of the unprotected pyrroles, they are not

subjected to purification to analytical standards and are subjected to minimal purification prior to immediate use in a porphyrin synthesis.

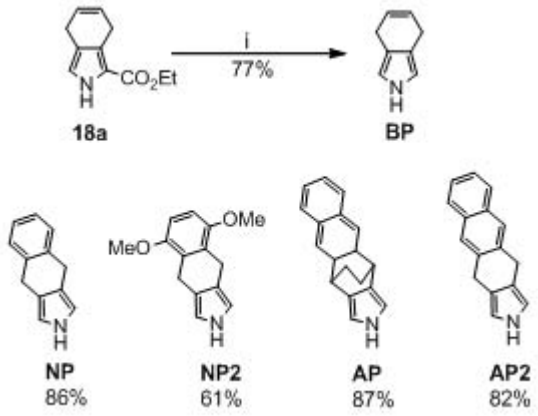

Figure 2-7. Synthetic scheme for the deprotection of pyrrole esters. *Reagents and conditions:* i) Ethylene glycol, KOH, 170°C, 1 h.

Synthesis of Tetraaryltetrabenzoporphyrins

Tetraaryltetrabenzoporphyrins **39a-c** were prepared from pyrrole **BP** and the respective aromatic aldehydes (**1,3,9**) following the reported method for **39a** and as outlined in Figure 2-8.[37] Pyrrole **BP** with one equivalent of aromatic aldehyde (**1,3,9**) in DCM in the presence of Lewis acid catalyst yielded the H_2Ar_4octahydroTBPs which were not isolated and further oxidized to the target TBPs by refluxing in toluene with DDQ in good yields.

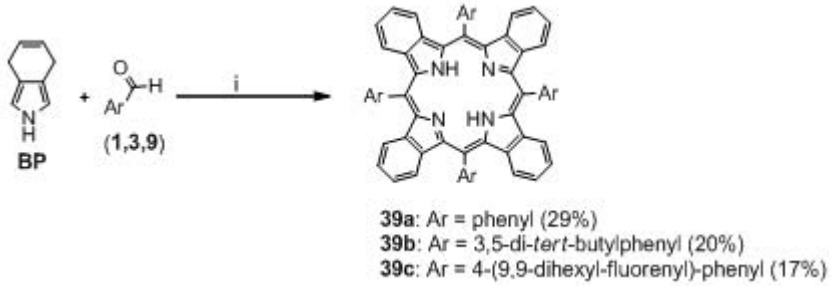

Figure 2-8. Synthetic scheme for H_2Ar_4TBPs. *Reagents and conditions*: i) DCM, $BF_3{\cdot}O(Et)_2$, DDQ, 4 h, PhMe, DDQ, reflux 1 h.

The target TBPs were purified via column chromatography and exhibited good solubility in common organic solvents (DCM, $CHCl_3$, THF). The materials were further purified by multiple precipitations from a good solvent (DCM, $CHCl_3$) into excess methanol under vigorous stirring. Compounds **39a-c** were characterized by ^{1}H and ^{13}C NMR and mass spectrometry.

Synthesis of Tetraaryltetranaphthoporphyrins

The synthesis of TNPs **40a** and **40b** from the respective naphthopyrroles **NP** and **NP2** followed the reported method for **39a** as outlined in Figure 2-9.[36] Under Lindsey conditions pyrroles **NP** and **NP2** were reacted with one equivalent of aromatic aldehydes (**1,3**) gave the target TNPs **40a** and **40b** in good yields. In the synthesis of H_2Ar_4TBP a tetraaryloctahydrotetrabenzoporphyrin could be isolated and then oxidized with DDQ. However in the present synthesis of H_2Ar_4TNPs an analogous intermediate was not isolated. The H_2Ar_4TNPs formed after the addition of DDQ and stirring at room temperature overnight or a one hour reflux in DCM. The target compounds were purified by chromatography and precipitation into methanol. Compounds **40a** and **40b** were both characterized by ^{1}H and ^{13}C NMR and mass spectrometry and exhibited good solubility in common organic solvents (DCM, $CHCl_3$, THF).

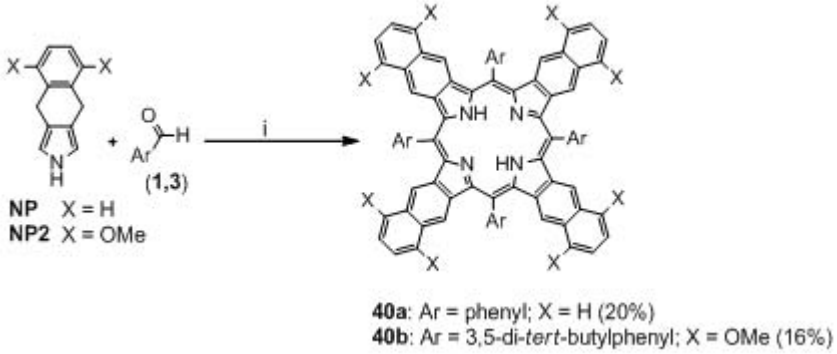

Figure 2-9. Synthetic scheme for H_2Ar_4TNPs. *Reagents and conditions*: i) Dry DCM, $BF_3{\cdot}O(Et)_2$, 1.5 h, DDQ, reflux 1 h.

Synthesis of Tetraryltetraanthroporphyrins

Recently two methods have been reported for the preparation of H_2Ar_4TAPs as outlined in Figure 2-10.[38, 66] The methods differ in that the one reported by Ono *et al* from **AP** uses a solid state high temperature retro-Diels-Alder reaction to quantitatively yield **42** after intermediate porphyrin **41** has been isolated. Initial attempts to reproduce this method failed leading to incomplete reaction mixtures. However, small milligram quanities of **42** can be obtained from **41**.The method was abandoned due to this difficulty and the unlikely hood of being able to scale the reaction up beyond 10-20 milligrams.

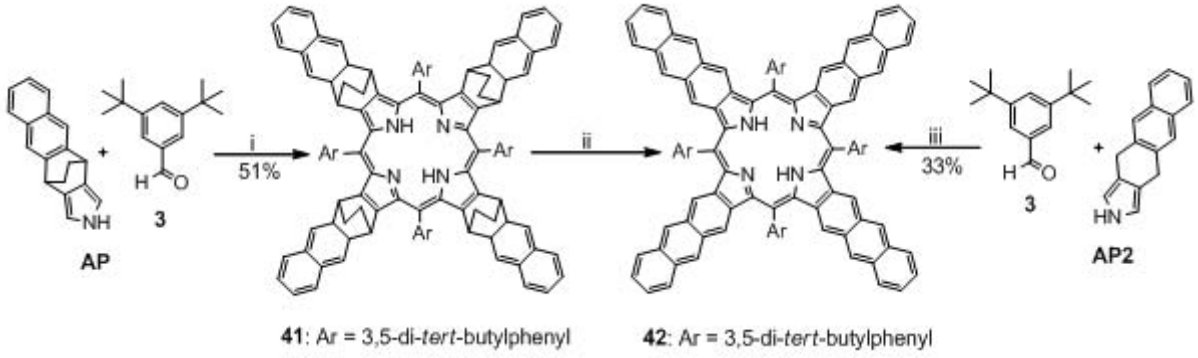

Figure 2-10. Synthetic scheme for H_2Ar_4TAP. *Reagents and conditions*: i) DCM, $BF_3{\cdot}O(Et)_2$, 18 h, DDQ, r.t., 1 h; ii) High vacuum, 290°C, 2 h; iii) DCM, $BF_3{\cdot}O(Et)_2$, 1 h, DDQ, r.t., 1 h.

Alternatively the use of the dihydroisoindole method provides access to the Ar_4TAPs at room temperature forming **42** almost instantly after the addition of DDQ to the reaction mixture. However as noted by both literature reports, the free-base and metal complexes of the TAPs are unstable towards oxygen in the presence of room light. Extreme caution must be taken in the handling and synthesis of these materials by either protecting the material from light or working under inert atmospheres. TAP (**42)**

was prepared from pyrrole **AP2** as reported in the literature in a good yield (Figure 2-10). The material was purified by column chromatography and then stored under inert atmosphere and further characterized by ^{1}H and ^{13}C NMR and mass spectrometry.

Synthesis of 5,15-Diaryltetrabenzoporphyrins

The interest in 5,15-diaryltetrabenzoporphyrins was outlined in the beginning of this chapter. The synthesis of 5,15-diarylporphyrins from *meso*-unsubstituted dipyrromethanes were reported by Treibs *et al* in 1968.[94] Other methodologies were reported by MacDonald and Baldwin *et al* from *meso*-aryl substituted dipyrromethanes for the preparation of 5,15-diarylporphyrins.[95-97] Recently the synthesis of 5,15-diaryltetrabenzoporphyrins was reported by Filatov *et al* from *meso*-unsubstituted dipyrromethane **44a** and aromatic aldehydes.[59] The synthesis is outlined in Figure 2-11, starting from pyrrole-esters **18a-b** with one half equivalent of dimethoxy methane in the presence of acid catalyst *meso*-unsubstituted dipyrromethanes **43a-b** were obtained in good yield from the previously reported method.

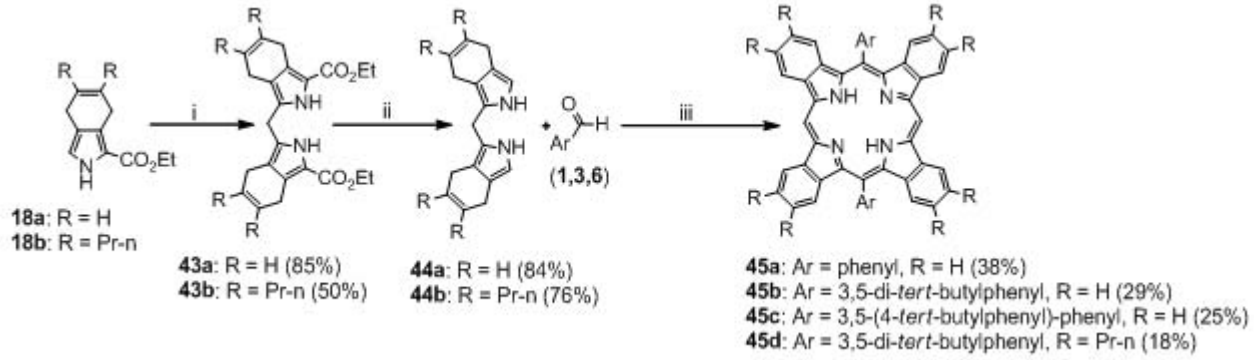

Figure 2-11. Synthetic scheme for H_2Ar_2TBPs. *Reagents and conditions*: i) AcOH, TsOH, $CH_2(OMe)_2$, 25°C, 24 h; ii) Ethylene glycol, KOH, 170°C, 1 h; iii) DCM, TFA, 25°C, 18 h, DDQ, PhMe, DDQ, reflux, 1 h.

Compounds **44a-b** was prepared in a parallel manner to pyrrole **BP** by heating in ethylene glycol with KOH. Similar to **BP**, compounds **44a-b** were not subjected to

extensive purification and used immediately in a porphyrins synthesis. The 5,15-diaryltetrabenzoporphyrins were obtained by condensing **44a-b** with one equivalent of aromatic aldehyde (**1,3,6**) in the presence of a catalytic amount of TFA followed by the addition of DDQ. The H_2Ar_2TBPs (**45a-d**) were obtained in good yields after adding the required additional equivalents of DDQ in refluxing toluene to complete the oxidative aromatization. Compounds **45a-d** were purified by column chromatography and from multiple precipitations into methanol from a good solvent. The overall the solubility of compounds **45b-d** was good in common organic solvents, except for **45a** which exhibited low solubility. The materials were characterized by ^{1}H and ^{13}C NMR and mass spectrometry with **45a-b** having identical data to the previous literature reports.[37, 59]

Synthesis of π-Extended Platinum Porphyrins

The classical conditions for the preparation of platinum (II) porphyrins involves excess molar equivalents of $PtCl_2$ in refluxing benzonitrile (> 190°C) with the free base porphyrin. The benzonitrile and $PtCl_2$ form a complex that increases the solubility of the platinum reagent. However despite the increase in solubility the reaction often precedes slowly requiring long reaction times. The addition of the metal to the porphyrin center increases the symmetry of the porphyrin changing the absorption spectra. Therefore the metallation reaction is often followed by UV-vis spectroscopy by the disappearance of the Soret and Q-band for the free-base porphyrin.

Thompson *et al* recently reported Pt-TPTBP and prepared the platinum complex from $PtCl_2$ and benzonitrile prior to oxidation with DDQ to form the TBP ring.[53] This represents one of the few reports for a platinum π-extended porphyrin report to date. The oxidation step with the precursor platinum porphyrin gave Pt-TPTBP in a low yield (30%). The initial attempts to prepare Pt-TPTNP (**Pt-40a**) from $PtCl_2$ and benzonitrile

(200°C) were followed by UV-Vis spectroscopy (Figure 2-12A). The reaction was followed over five hours with no detectable amounts of **Pt-40a** in the UV-vis spectrum for the reaction mixture represented by the black, red and blue traces in Figure 2-12A. Additionally small amounts of **Pt-40a** could be detected in the UV-Vis spectrum after heating at higher temperatures (>230ºC) for prolonged periods of time making these conditions unpractical due to the decomposition of **40a**.

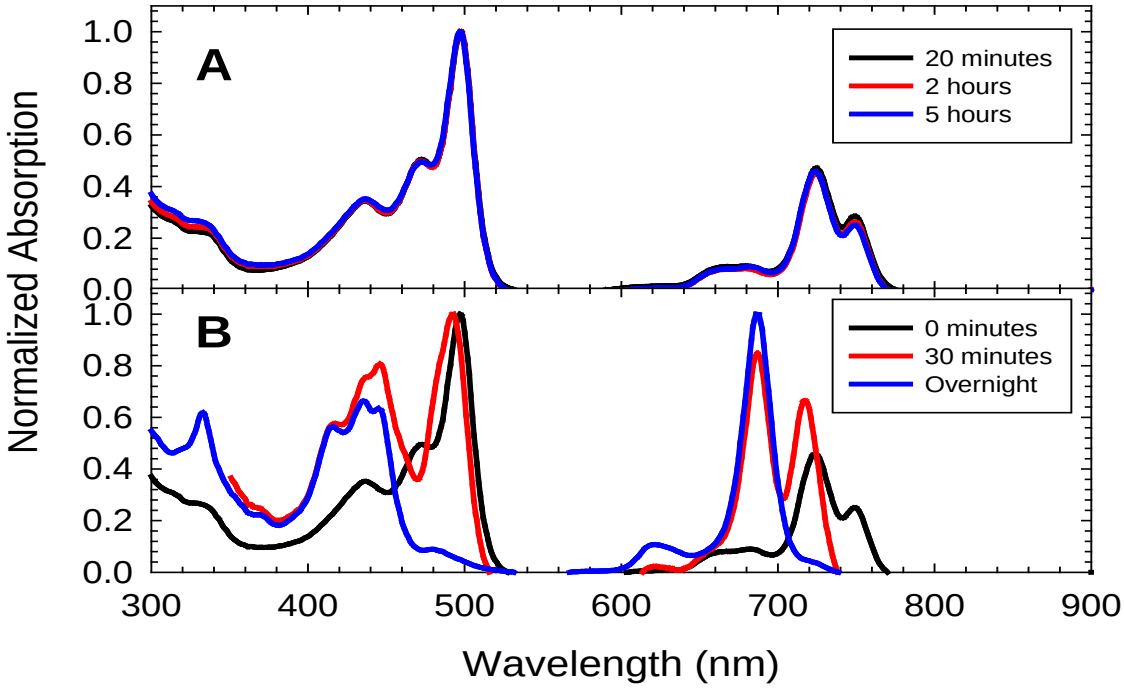

Figure 2-12. Platinum metallation reaction for Pt-TPTNP (**Pt-40a**) followed by UV-vis spectroscopy. A) H_2TPTNP and $PtCl_2$ in PhCN at 200ºC followed over 5 h by UV-vis spectroscopy. B) H_2TPTNP and $[Pt_4(OAc)_8]\cdot 2HOAc$ in PhCN at 180ºC followed overnight by UV-vis spectroscopy.

However, it is known that metal(II) acetates are more reactive than the respective metal(II) halogen species. Platinum(II) acetate is not commercially available and only two reports exist for its preparation but is readily prepared from silver acetate in refluxing acetic acid under and inert atmosphere.[98] The reaction of platinum(II) acetate with **40a** in benzonitrile (180°C) immediately shows the formation of the **Pt-40a** after 30

minutes (red trace) from the appearance of a new blue shifted Soret and Q-band. The UV-vis spectrum of the reaction mixture after heating overnight or five hours (blue trace) shows the complete disappearance of the free-base Soret and Q-band (Figure 2-12B). This represents a unique method for preparing π-extended platinum porphyrins at lower temperatures and shorter reaction times in higher yields. The novel reaction conditions have allowed the preparation of platinum complexes for the TNP and TAP systems for the first time, while also providing an improved yield in the synthesis of platinum TBPs over previous literature methods. The target π-extended platinum porphyrins (Figure 2-13) were all prepared in an analogous manner to **Pt-40a**. The materials were subjected to vacuum distillation to remove the high boiling solvent followed by chromatography and multiple precipitations to remove small amounts of free-base porphyrins prior to characterization by ^{1}H and ^{13}C NMR and HRMS.

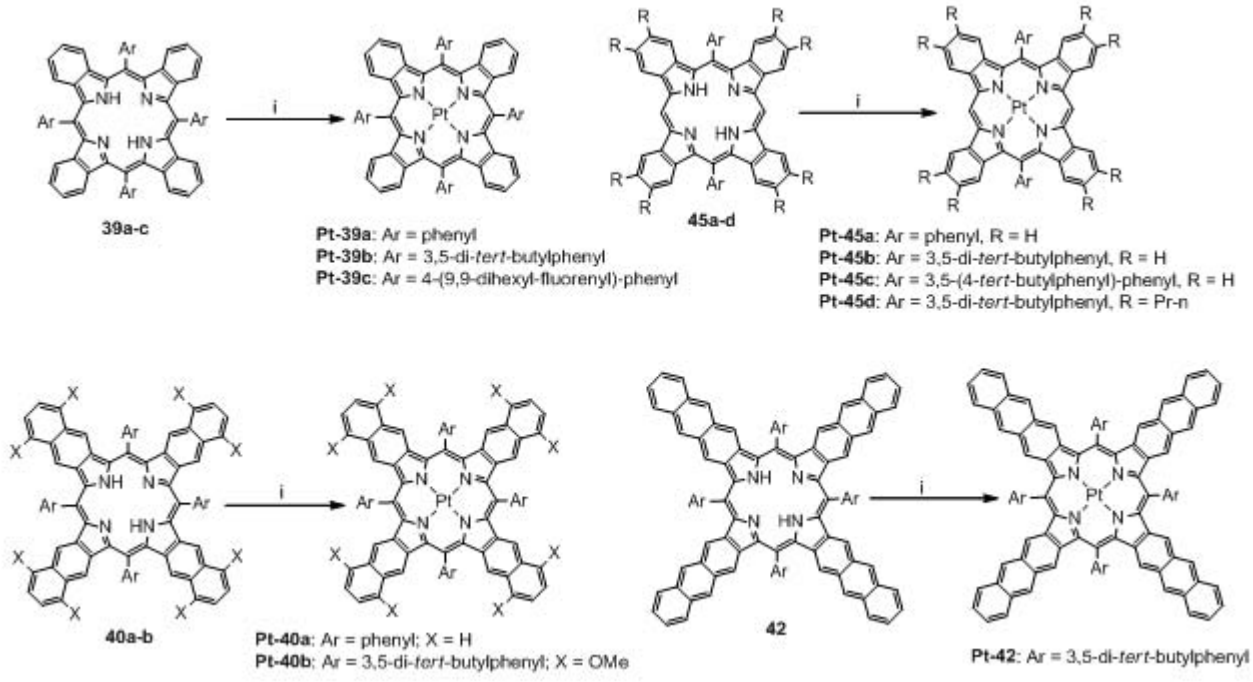

Figure 2-13. Synthetic scheme for π-extended platinum porphyrins. *Reagents and conditions*: i) $[Pt_4(OAc)_8]\cdot 2HOAc$, PhCN, 180ºC, under anaerobic conditions.

Conclusions

The desired goal of developing 3 series of π-extended platinum porphyrins was realized. The free-base π-extended porphyrins were prepared following previously reported literature methods. The platinum complexes were prepared from the novel metallation conditions with platinum acetate developed herein allowing the platinum complexes for TNPs and TAP to be reported for the first time. Also reported for the first time are platinum complexes for unsymmetrical 5,15-diaryl TBPs. The synthesis of π-extended platinum porphyrins overall are reported in higher yield than previous literature methods. Access to these new materials has finally allowed for complete characterization followed by investigation of these materials as near-IR phosphors in light emitting diode applications.

Experimental

Materials and General Procedures. All chemicals used for synthesis were of reagent grade and used without further purification unless noted otherwise. Reactions were carried out under inert atmospheres of argon or nitrogen. Dry solvents were obtained from a solvent purification system or from standard distillation methods unless otherwise noted. All glassware was flame or oven dried prior to use unless otherwise noted. NMR spectra were recorded on a Varian Gemini 300, VXR 300, Mercury 300 or Varian Inova 500 spectrometer and chemical shifts are reported in ppm relative to $CDCl_3$ unless otherwise noted. Ethyl isocyanoacetate was purchased from Sigma Aldrich and vacuum distilled each time prior to use. Solutions of PhSCl were prepared according to literature methods from *N*-chlorosuccinimide and thiophenol.[34] Platinum acetate was prepared from a previously reported method.[98] Purification by column chromatography was performed on SiliaFlash silica-gel (mesh 230-400).

3,5-Di-*tert*-butylbenzaldehyde (**3**). The title compound was prepared following a modified literature procedure.[80] A solution of **2** (10.00 g, 48.9 mmol) and NBS (18.00 g, 101 mmol) in CCl_4 (160 mL) with benzoyl peroxide (80 mg, 0.33 mmol) was refluxed overnight. The formed precipitated was removed by filtration through celite and the solvent removed to yield an oil. The crude material was dissolved in mixture of water (15 mL) and EtOH (15 mL) with hexamethylenetetramine (19.90 g, 142 mmol) and then heated to reflux for 4 hours. The reaction was diluted with a toluene/ether (1:1, 200 mL) mixture and then washed with brine (100 ml x 3). The organic layer was dried over $MgSO_4$ and the solvent removed. The crude material was recrystallized twice from MeOH to give 4.94 g of the title compound (46%). The material gave identical spectral data to that previously reported in the literature.[80] ^{1}H NMR ($CDCl_3$, 300 MHz): δ = 10.01 (s, 1H), 7.73 (m, 3H), 1.36 (t, 18H).

3,5-Dibromo-benzaldehyde (**5**). The title compound was prepared following a modified literature method.[81] Compound **4** (3.01 g, 9.6 mmol) in diethyl ether (80 mL) was cooled to -78°C followed by the addition of one equivalent of *n*-BuLi dropwise (2.5 M, 3.8 mL). The reaction was stirred for 30 minutes then DMF (740 µL, 9.6 mmol) was added dropwise to the reaction and stirred at -78°C for one hour. The vessel was then placed in an ice bath and stirred for 30 minutes. A 10% HCl solution (100 mL) was added to quench the reaction followed by $CHCl_3$ (150 mL). The organic layer was collected and the aqueous layer washed with $CHCl_3$ (80 mL). The organic layers where combined and dried over $MgSO_4$ and the solvent removed. The crude product was purified by column chromatography eluting with 10% EtOAc in hexanes to give 1.93 g of the title compound (77%). Spectral data for the title compound was not reported in the

literature reference.[81] ^{1}H NMR ($CDCl_3$, 300 MHz): δ = 9.90 (s, 1H), 7.92 (d, 2H), 7.60 (s, 1H); ^{13}C NMR ($CDCl_3$, 75 MHz) δ = 189.3, 139.7, 139.0, 131.37, 124.1; GC-MS $[M+H]^+$ 262.8709, calcd 262.8707.

3,5-Di(4-*tert*-butylphenyl)benzaldehyde (**6**). The title compound was prepared following a modified literature method.[77] Compound **5** (1.02 g, 3.9 mmol) and 4-*tert*-butylphenyl boronic acid (1.47 g, 8.3 mmol) were dissolved in toluene (75 mL) and THF (60 mL) with Na_2CO_3 (1.12 g) and water (9 mL). The solution was purged with argon for 15 minutes followed by the addition of $Pd(PPh_3)_4$ (200 mg, 0.2 mmol). The reaction was stirred and purged with argon for 20 minutes and then heated at 100°C for 120 hours. The solvent was removed and the crude material loaded on silica eluting with a hexane/DCM mixture (70/30). The fractions were combined and the solvent removed. The material was dissolved in minimum of DCM and diluted with MeOH precipitating 865 mg of the title compound (61%). The title compound is reported in the literature with no experimental or spectral data.[99] ^{1}H NMR ($CDCl_3$, 300 MHz): δ = 10.14 (s, 1H), 8.05 (m, 3H), 7.63 (d, 4H), 7.53 (d, 4H); ^{13}C NMR ($CDCl_3$, 75 MHz) δ = 192.7, 151.4, 142.7, 137.6, 137.1, 131.7, 127.1, 127.0, 126.2, 34.8, 31.5; DART-MS $[M+H]^+$ 371.2369, calcd 371.2369.

2-Bromo-9,9-dihexylfluorene (**8**). The title compound was prepared following a modified literature method.[83] A mixture of **7** (2.00 g, 8.2 mmol) and bromohexane (10 mL, 70.8 mmol) with NaOH (2.8 g, 70 mmol) and Bu_4NCl in DMSO (20 mL) and water (3 mL) was stirred. The reaction was heated at 80°C overnight and then poured into excess ethyl acetate (200 mL). The precipitated NaOH was filtered off and the organic layer washed with 2N HCl solution (100 mL) and brine (100 mL). The organic layer was

collected and dried over $MgSO_4$. The solvent was removed and the crude product purified by column chromatography eluting with hexane to yield 3.14 g of the title compound (93%). The material gave identical spectral data to that previously reported in the literature.[83] ^{1}H NMR ($CDCl_3$, 300 MHz): δ = 7.68-7.64 (m, 1H), 7.57-7.54 (m, 1H), 7.46-7.43 (m, 2H), 7.33-7.31 (m, 3H), 1.97-1.90 (m, 4H), 1.15-1.03 (m, 12H), 0.79 (t, 6H), 0.62-0.58 (m, 4H).

4-(9,9-dihexyl-fluorenyl)-benzaldehyde (**9**). The title compound was prepared following a modified literature method.[82] A solution of **8** (1.10 g, 2.7 mmol) and 4-formylbenzene boronic acid (438 mg, 2.9 mmol) with Na_2CO_3 (2.96 g) in THF (20 mL) and water (15 mL) mixture was purged with argon for 30 minutes. Then $Pd(PPh_3)_4$ (15 mg, 12.9 μmol) was added and the solution stirred and purged with argon for 15 minutes prior to heating at 80°C overnight. The reaction was cooled to room temperature and then diluted with DCM (100 mL). The organic layer was washed with saturated aqueous NH_4Cl solution (100 mL) and then dried over $MgSO_4$. The solvent was removed and the crude material purified by column chromatography eluting with 45% hexane in DCM to give 900 mg of the title compound (77%). The material gave identical spectral data to that previously reported in the literature.[82] ^{1}H NMR ($CDCl_3$, 300 MHz): δ = 10.1 (s, 1H), 7.98 (d, 2H), 7.84 (d, 2H), 7.80-7.77 (m, 1H), 7.57-7.72 (m, 1H), 7.64-7.61 (m, 1H), 7.59 (m, 1H), 7.35 (m, 3H), 2.01 (m, 4H), 1.05 (m, 12H), 0.75 (t, 6H), 0.68-0.62 (m, 4H).

2-Butyne-1,4-diyl tetraethyl ester phosphoric acid (11). The title compound was prepared following a modified literature method.[100] In dry pyridine (25 mL) compound **10** (5.76 g, 66.9 mmol) under an argon atmosphere was cooled to 0°C

followed by the dropwise addition of diethyl chlorophosphate (25 g, 144.9 mmol). The reaction was stirred for 2 hours at 0°C and then diluted with water (125 mL). The mixture was washed with ether (3 x 70 mL) and the combined organic layers dried over Na_2SO_4. The solvent was removed to give 16.0 g of the title compound (73%). The material was pure enough for the subsequent Grignard reaction and gave identical spectral data to that previously reported in the literature.[100] ^{1}H NMR ($CDCl_3$, 300 MHz): δ = 4.71 (d, 4H), 4.13 (dq, 8H), 1.34 (t, 12H).

2,3-Dipropyl-1,3-butadiene (12). The title compound was prepared following a modified literature method.[100] The Grignard reagent was prepared from 1-bromopropane (5.15 g, 41.8 mmol) and Mg (1.12 g, 41.8 mmol) turnings in dry THF (60 mL) in a conventional manner. The solution was cooled to 0°C followed by the dropwise addition of **11** (5.00 g, 13.9 mmol) in dry THF (30 mL). The reaction was warmed to room temperature and stirred overnight. Water (300 mL) was added to quench the reaction. The formed precipitate was filtered off and then washed with pentane (150 mL). The aqueous and organic layers were collected and separated. The aqueous layer was washed with pentane (4 x 80 mL). The organic layers combined and dried over Na_2SO_4 and the solvent removed under reduced pressure yielding 1.27 g of the title compound (62%). The material gave identical spectral data to that previously reported in the literature.[100] ^{1}H NMR ($CDCl_3$, 300 MHz): δ = 5.06 (s, 2H), 4.90 (s, 2H), 2.21 (t, 4H), 1.48 (sex, 4H), 0.91 (t, 6H).

p-Tolyl-[2-(trimethylsilyl)ethynyl]-sulfone (15). The title compound was prepared following a modified literature method.[84] A solution of $AlCl_3$ (9.4 g, 70.5 mmol) in dry DCM (40 mL) was cannula transferred to TsCl (13.43 g, 70.4 mmol) in DCM (30

mL) and stirred under N_2 atmosphere turning orange in color. A separate solution of **14** in DCM (40 mL) was cooled to 0°C in an ice bath. The mixture of $AlCl_3$/TsCl was transferred to the alkyne solution over a period of 10 minutes in small portions. The ice bath was removed and the reaction stirred overnight at room temperature. The mixture was poured into ice water (400 g) and the organic layer separated and collected. The aqueous layer was washed with DCM (3 x 50 mL). The combined organic layers were dried over $MgSO_4$ and the solvent removed. The crude material was extracted with hot hexanes and upon cooling yielded 10.01 g of the title compound (67%). The material gave identical spectral data to that previously reported in the literature.[85] ^{1}H NMR ($CDCl_3$, 300 MHz): δ = 7.90-7.89 (m, 2H), 7.38-7.35 (m, 2H), 2.46 (s, 3H), 0.21 (s, 9H).

Ethynyl p-tolyl sulfone (16). The title compound was prepared following a modified literature method.[86] A solution of **15** (8.01 g, 31.7 mmol) purged with argon in MeOH (65 mL) was cooled to 0°C. The cooled solution was treated dropwise with NaF (2.08 g, 49.5 mmol) in water (35 mL). The reaction was stirred for 90 minutes at 0°C and then diluted with water (100 mL). The organic layer was separated and collected. The aqueous layer was extracted with ether (3 x 100 mL). The combined organic layers were washed with water (2 x 100 mL), 10% aqueous $NaHCO_3$ (1 x 100 mL), and brine (1 x 100 mL). The organic layer was dried over $MgSO_4$ and the solvent removed. The crude material was recrystallized from hexanes to yield 5.70 g of the title compound (98%). The material gave identical spectral data to that previously reported in the literature.[86] ^{1}H NMR ($CDCl_3$, 75 MHz): δ = 7.91-7.88 (d, 2H), 7.40-7.37 (d, 2H), 3.45 (s, 1H), 2.47 (s, 3H).

1-Tosyl-1,4-cyclohexadiene (17a). The title compound was prepared following a modified literature method.[37] A thick walled 100 mL vessel with **16** (5.01 g, 27.8 mmol) was cooled to -78°C. Then an excess of **13** (20 mL) was added and the vessel sealed. The reaction was warmed to room temperature and stirred for 48 hours. After removal of excess 1,3-butadiene (**13**) a white oily solid was collected and recrystallized from diethyl ether to give 4.82 g of the title compound (74%). The material gave identical spectral data to that previously reported in the literature.[37] ^{1}H NMR ($CDCl_3$, 300 MHz): δ = 7.75-7.72 (d, 2H), 7.33-7.30 (d, 2H), 7.01 (m, 1H), 5.66-5.63 (m, 2H), 2.93-290 (m, 2H), 2.82-2.79 (m, 2H), 2.42 (s, 3H).

1-Tosyl-4,5-dipropyl-1,4-cyclohexadiene (17b). The title compound was prepared following a modified literature method.[101] In a thick walled flask with Teflon cap dry toluene (10 mL) and compound **16** (1.31 g, 7.3 mmol) with **12** (1.01 g, 7.3 mmol) under an argon atmosphere was heated at 130°C for 48 hours. The reaction was cooled to room temperature and the solvent removed under reduced pressure. The crude material was purified by column chromatography eluting with $CHCl_3$ to give a 1.58 g of a yellow oil (68%). ^{1}H NMR ($CDCl_3$, 300 MHz): δ = 7.76 (d, 2H), 7.33 (d, 2H), 6.96 (m, 1H), 2.86 (m, 2H), 2.74 (m, 2H), 2.42 (s, 3H), 1.96 (m, 4H), 1.32 (m, 2H), 1.30 (m, 2H), 0.87 (t, 3H), 0.86 (t, 3H); ^{13}C NMR ($CDCl_3$, 75 MHz): δ= 144.3, 137.9, 136.4, 135.3, 129.9, 128.3, 127.0, 126.4, 34.7, 34.3, 32.0, 28.2, 21.8, 21.4, 14.3; DART-MS $[M+H]^+$ 319.1737, calcd 319.1726.

2-Ethoxycarbonyl-4,7-dihydro-2H-isoindole (18a). The title compound was prepared following a modified literature method.[37] A solution of **17a** (2.5 g , 10.7 mmol) in dry THF (25 mL) was added dropwise at 0°C to one equivalent of ^{t}BuOK (1.44 g ,

12.8 mmol) and ethyl isocyanoacetate (1.31 g, 11.6 mmol). The reaction was stirred at room temperature for 4 hours. The solvent was removed and the crude material redissolved in DCM (140 mL). The organic layer was washed with water (2 x 80 mL), and brine (1 x 80 mL) and then dried over Na_2SO_4. The solvent removed and the crude material recrystallized from hexanes yielding 1.64 g of light yellow crystals (80%). The material gave identical spectral data to that previously reported in the literature.[37] ^{1}H NMR ($CDCl_3$, 300 MHz): δ = 8.97 (broad s, 1H), 6.72 (m, 1H), 5.94-5.82 (m, 2H), 4.31 (q, 2H), 3.46-3.43 (m, 2H), 3.24-3.21 (m, 2H), 1.35 (t, 3H).

2-Ethoxycarbonyl-4,7-dihydro-5,6-dipropyl-2H-isoindole (18b). The title compound was prepared according to the procedure for **18a**. A solution of ^{t}BuOK (930 mg, 8.3 mmol) in dry THF (30 mL) was cooled to 0°C followed by the addition of ethyl isocyanoacetate (0.9 mL, 8.2 mmol). The solution was stirred for 10 minutes then a solution of **17b** (2.4 g, 7.5 mmol) in dry THF (30 mL) was added dropwise. The reaction was warmed to room temperature and stirred for 4 hours. The solvent removed and the crude redissolved in DCM (120 mL). The organic layer was washed with water (2 x 80 mL) and brine (1 x 80 mL) then dried over Na_2SO_4. The solvent was removed producing an oil that was purified by column chromatography eluting with $CHCl_3$. The combined fractions were recrystallized from EtOH to give 1.09 g of the title compound (52%). ^{1}H NMR ($CDCl_3$, 300 MHz): δ = 8.89 (br s, 1H), 6.69 (d, 1H), 4.33 (q, 2H), 3.40 (m, 2H), 3.16 (m, 2H), 2.15 (q, 4H), 1.48 (m, 2H), 1.47 (m, 2H), 1.36 (t, 3H), 0.95 (t, 3H), 0.94 (t, 3H); ^{13}C NMR ($CDCl_3$, 75 MHz): δ= 161.7, 128.4, 127.7, 126.6, 120.5, 117.9, 117.2, 60.0, 35.7, 28.5, 26.9, 22.0, 14.8, 14.5; DART-MS 276.1968, calcd 276.1958.

2-Chloro-1,2,3,4-tetrahydro-3-(phenylsulfonyl)-naphthalene (20). The title compound was prepared following a modified literature method.[36] A solution of PhSCl (18.6 mmol) in dry DCM (40 mL) was added dropwise to **19** (2.0 g, 11.5 mmol) in DCM (30 mL) at 0°C. After the addition, the reaction was stirred at room temperature for two hours. The mixture was stored in a freezer over night and the precipitated removed by filtration. The filtrate was cooled to 0°C and diluted with DCM (50 mL). In one portion 77% *m*-CPBA (9.2 g, 41 mmol) was added and then stirred at room temperature for one hour. A chilled 10% aqueous Na_2SO_3 (80 mL) was added and the mixture stirred at room temperature for one hour. The organic layer was washed with 10% aqueous Na_2CO_3 (30 mL), 10% aqueous Na_2SO_3 (80 mL), and 10% aqueous Na_2CO_3 (80 mL). The organic layer collected and dried over K_2CO_3 and the solvent removed. The crude product recrystallized from EtOH to give 3.08 g of the title compound (87%). The material gave identical spectral data to that previously reported in the literature.[36] ^{1}H NMR ($CDCl_3$, 300 MHz): δ = 7.96-7.57 (m, 5H), 7.22-7.19 (m, 2H), 7.14-7.09 (m, 2H), 4.84 (m, 1H), 3.75-3.70 (m, 1H), 3.51-3.44 (dd, 1H), 3.51-3.27 (dd, 1H), 3.20-3.11 (dd, 1H), 3.07-3.06 (dd, 1H).

4,9-Dihydro-2H-benzo[f]isoindole-1-carboxylic acid ethyl ester (21). The title compound was prepared following a modified literature method.[36] Compound **20** (3.06 g, 10 mmol) in dry THF (10 mL) was added dropwise to a solution of ^{t}BuOK (3.1 g, 27.6 mmol) with ethyl isocyanoacetate (1.13 g, 10 mmol) in dry THF (40 mL) at 0°C. The reaction was warmed to room temperature and then refluxed for one hour under an argon atmosphere. The solvent was removed and the crude material dissolved in DCM (120 mL). The organic layer was washed with water (2 x 100 mL) and brine (1 x 100

mL) collected and dried over K_2CO_3. The crude material was recrystallized from EtOH and hexanes to yield 1.53 g (65%). The material gave identical spectral data to that previously reported in the literature.[36] ^{1}H NMR ($CDCl_3$, 300 MHz): δ = 9.04 (broad s, 1H), 7.33 (m, 1H), 7.24-7.17 (m, 2H), 6.81 (d, 1H), 4.37 (q, 2H), 4.17 (s, 2H), 3.89 (s, 2H), 1.40 (t, 3H).

4a,5,8,8a-tetrahydronaphthoquione-1,4-dione (23). The title compound was prepared following a modified literature method.[102] Compound **22** (6.0 g, 55.5 mmol) in AcOH (70 mL) was stirred at room temperature with **13** (12 g, 221.8 mmol) for 24 hours. The mixture was poured into ice water (200 mL) and rapidly stirred. The precipitate was collected and redissolved in warm ether and filtered to remove insoluble material. The solvent was removed to give 3.75 g of the title compound (42%). The material gave identical spectral data to that previously reported in the literature.[87] ^{1}H NMR ($CDCl_3$, 300 MHz): δ = 6.67 (s, 2H), 5.70 (m, 2H), 3.27-3.23 (m, 2H), 2.52-2.16 (m, 4H).

5,8-Dimethoxy-1,4-dihyronaphthalene (24). The title compound was prepared following a modified literature method.[102] In acetone (85 mL) **23** (5.4 g, 33.3 mmol) with an excess of K_2CO_3 (17.0 g) and dimethyl sulfate (20.0 g, 158.5 mmol) under N_2 atmosphere was refluxed for 40 hours. The mixture cooled to room temperature followed by the addition of water (25 mL). The mixture was concentrated and then poured into ice cold water (500 mL) with vigorous stirring. The formed precipitate was collected and washed thoroughly with water to remove any residual K_2CO_3. The crude product was recrystallized from MeOH to give 6.05 g of the title compound (96%). The material gave identical spectral data to that previously reported in the literature.[87] ^{1}H NMR ($CDCl_3$, 300 MHz): δ = 6.65 (s, 2H), 5.89 (s, 2H), 6.70 (s, 6H), 3.28 (s, 4H).

2-Chloro-1,2,3,4-tetrahydro-5,8-dimethoxy-3-(phenylsulfonyl)-naphthalene (25). The title compound was prepared following a modified literature method.[36] In dry DCM (50 mL) cooled to 0°C with **24** (3.5 g, 18.4 mmol) was treated dropwise with PhSCl (23.0 mmol) in DCM (40 mL). After the addition the reaction was stirred at room temperature for 2 hours. The mixture was stored in a freezer overnight and the formed precipitate removed by filtration. The solution was diluted with DCM (50 mL) and cooled to 0°C followed by the addition of 77% *m*-CPBA (7.95 g, 46.0 mmol) in one portion. The reaction was warmed to room temperature and stirred for one hour. A solution of chilled 10% aqueous Na_2SO_3 (100 mL) was added and the mixture stirred for one hour at room temperature. The organic layer was washed with 10% aqueous Na_2CO_3 (35 mL), 10% aqueous Na_2SO_3 (100 mL), and 10% aqueous Na_2CO_3 (100 mL). The organic layer was dried over K_2CO_3 and the solvent removed. The crude product was recrystallized from an EtOH and hexane mixture to give 4.30 g of the title compound (64%). The material gave identical spectral data to that previously reported in the literature.[36] ^{1}H NMR ($CDCl_3$, 300 MHz): δ = 7.94-7.90 (m, 2H), 7.67-7.54 (m, 3H), 6.66 (s, 2H), 4.85-4.80 (m, 1H), 3.77-3.67 (overlapping s+s+m, 3H+3H+1H), 3.40-3.33 (dd, 1H), 3.24-3.16 (m, 3H).

5,8-Dimethoxy-4,9-dihydro-2H-benzo[f]isoindole-1-carboxylic acid ethyl ester (26). The title compound was prepared following a modified literature method.[36] A solution of ^{t}BuOK (1.83 g, 16.3 mmol) in dry THF (60 mL) was cooled to 0°C followed by the addition of ethyl isocyanoacetate (2.21 g, 19.6 mmol). To this solution, **25** (3.0 g, 8.1 mmol) in THF (30 mL) was added dropwise. The reaction was warmed to room temperature and then refluxed for one hour. The solvent was removed and the material dissolved in DCM (120 mL).The organic layer was washed with water (2 x 100 mL) and

brine (1 x 100 mL) then dried over K_2CO_3. The solvent was removed yielding a red oil that precipitated yellow crystals upon the addition of EtOH. The precipitate was filtered and washed with hexanes to give 1.73 g of the title compound (70%). The material gave identical spectral data to that previously reported in the literature.[36] ^{1}H NMR ($CDCl_3$, 300 MHz): δ = 9.03 (br s, 1H), 6.82 (d, 1H), 6.71 (s, 2H), 4.39 (q, 2H), 4.08 (m, 2H), 4.06-3.82 (overlapping s+d, 6H+2H), 1.41 (t, 3H).

1,4,4a,9a-Tetrahydro-1,4-ethanoanthracene-9,10-dione (28). The title compound was prepared following a modified literature method.[103] A mixture of 1,3-cyclohexadiene (7.0 g, 87.3 mmol) and **27** (13.8 g, 87.3 mmol) in EtOH (90 mL) was refluxed for 3 hours. The reaction was cooled overnight in a freezer. The precipitated crystals were collected and then recrystallized from boiling EtOH to give 14.05 g of the title compound (67%). The material gave identical spectral data to that previously reported in the literature.[103] ^{1}H NMR ($CDCl_3$, 300 MHz): δ = 7.99-7.96 (m, 2H), 7.67-7.63 (m, 2H), 6.11 (dd, 2H), 3.32-3.30 (m, 2H), 3.18-3.17 (m, 2H), 1.77-1.73 (m, 2H), 1.39-1.34 (m, 2H).

1,2,3,4,4a,9,9a,10-Octahydro-1,4-ethanoanthracene-9,10-diol (29). The title compound was prepared following a modified literature method.[89] A solution of **28** (5.7 g, 23.9 mmol) in anhydrous MeOH (150 mL) was cooled to 0°C under N_2 atmosphere. In one portion $NaBH_4$ (2.5 g, 66.0 mmol) was added and the reaction stirred at 0°C for two hours. The solvent was removed and the crude material purified by column chromatography eluting with a hexane:THF (5:2) solvent mixture removing the first light yellow band. The solvent polarity was then increased to pure THF. The combined fractions afforded 5.15 g of the title compound (89%). The material gave identical

spectral data to that previously reported in the literature.[89] ^{1}H NMR ($CDCl_3$, 300 MHz): δ = 7.30 (s, 4H), 6.35 (broad s, 2H), 4.70-4.67 (m, 2H), 3.03-3.01 (m, 2H), 2.76 (broad s, 2H), 2.21 (broad s, 2H), 1.60-1.57 (m, 2H), 1.37-1.34 (m, 2H).

1,4-Dihydro-1,4-ethanoanthracene (30). The title compound was prepared following a modified literature method.[91] A mixture of TsCl (12.15 g, 63.7 mmol) and **29** (5.15 g, 21.3 mmol) in dry pyridine (40 mL) under N_2 atmosphere was stirred for 48 hours at room temperature. The reaction was poured over ice (300 g) and stirred. The precipitated material was collected and dried over $MgSO_4$. The crude product was purified by column chromatography eluting with hexanes yielding 3.25 g of the title compound (74%). The material gave identical spectral data to that previously reported in the literature.[90] ^{1}H NMR ($CDCl_3$, 300 MHz): δ = 7.80-7.77 (AA'BB', 2H), 7.59 (s, 2H), 7.43-7.39 (AA'BB', 2H), 6.60-6.57 (m, 2H), 4.06 (m, 2.12), 1.69-1.56 (m, 4H).

2-Chloro-1,2,3,4-tetrahydro-3-phenylsulfonyl-1,4-ethanoanthracene (31). The title compound was prepared following a modified literature method.[66] A solution of **30** (3.25 g, 15.8 mmol) in dry DCM (150 mL) was cooled to 0°C in an ice bath. The solution was then treated dropwise with PhSCl (18.9 mmol) in dry DCM (60 mL). The reaction was stirred at room temperature for one hour. The organic layer was washed with 10% aqueous $NaHCO_3$ (80 mL), water (80 mL), and brine (80 mL). The organic layer was collected and dried over Na_2SO_4.The solvent removed yielding a yellow oil that was diluted with hexanes and EtOH precipitating 4.3 g of white powder that was collected and dried. The crude material was dissolved in DCM (100 mL) and cooled to 0°C followed by the addition of 77% *m*-CPBA (6.8 g, 39.4 mmol) in one portion. The reaction was warmed to room temperature and stirred overnight. The precipitate was

filtered off and the solvent removed. The material was recrystallized from hexanes/EtOH to give 3.53 g of the title compound (59%). The material gave identical spectral data to that previously reported in the literature.[66] ^{1}H NMR ($CDCl_3$, 300 MHz): δ = 7.81-7.78 (m, 4H), 7.68 (s, 1H), 7.62-7.56 (m, 2H), 7.51-7.43 (m, 4H), 4.35-4.32 (m, 1H), 3.85-3.83 (m, 1H), 3.63-3.60 (m, 1H), 3.41-3.38 (m, 1H), 2.43-2.33 (m, 1H), 2.08-1.98 (m, 1H), 1.67-1.43 (m, 2H).

4,11-Dihydro-4,11-ethano-2H-napth[2,3f]isoindole-1-carboxylic acid ethyl ester (32). The title compound was prepared following a modified literature method.[66] A solution of dry THF (40 mL) and **31** (2.63 g, 6.9 mmol) was added dropwise at 0°C to ^{t}BuOK (1.85 g, 16.5 mmol) and ethyl isocyanoacetate (93 mg, 8.2 mmol). After the addition the reaction was warmed to room temperature and stirred overnight. The organic layer was washed with water (2 x 100 mL) and brine (1 x 100 mL) collected and dried over Na_2SO_4. The solvent was removed yielding an oil. The addition of hexane and EtOH precipitated the title compound as a white powder to give 805 mg (37%). The material gave identical spectral data to that previously reported in the literature.[66] ^{1}H NMR ($CDCl_3$, 300 MHz): δ = 8.45 (broad s, 1H), 7.74 (m, 2H), 7.68 (s, 1H), 7.61 (s, 1H), 7.38 (m, 2H), 6.07 (s, 1H), 4.90 (s, 1H), 4.39-4.34 (m, 3H), 1.81 (m, 4H), 1.44-1.40 (m, 3H).

1,4-Epoxy-1,4-dihydronaphthalene (33). The title compound was prepared following a modified literature method.[92] In dry THF (120 mL) anthranilic acid (9.5 g, 69.3 mmol) was cooled to 0°C followed by the addition of isoamyl nitrite (20 mL) dropwise. The mixture was then warmed to room temperature and stirred for one hour. The yellow precipitate was collected by filtration (Caution: explosion hazard do not allow

precipitate to dry or come in contact with metal) and transferred to a flask with dry THF (120 mL), furan (4.40 g, 64.6 mmol), and propylene oxide (6 mL). The mixture was slowly warmed to 70°C under a N_2 atmosphere until the precipitate disappeared with adequate venting. The solution was then heated to reflux for 20 minutes. The solvent was removed under reduced pressure and the crude product purified by column chromatography eluting with 10% ethyl acetate in hexanes. The material from the combined fractions was recrystallized from hexanes to give 4.60 g of the title compound (49%). The material gave identical spectral data to that previously reported in the literature.[93] ^{1}H NMR ($CDCl_3$, 300 MHz): δ = 7.23 (dd, 2H), 7.01 (s, 2H), 6.95 (dd, 2H), 5.70 (s, 2H).

9,10-Epoxy-1,4,4a,9,9a,10-hexahydroanthracene (34). The title compound was prepared following a modified literature method.[38] A 60 mL thick walled flask with Teflon screw cap with **33** (5.05 g, 35.0 mmol) and $NaHCO_3$ (2.5 g, 29.75 mmol) dissolved in pyridine (20 mL) freshly distilled over NaOH. To this solution 3-sulfolene (4.55 g, 38.5 mmol) was added in seven equal portions. The reaction was heated at 120°C for 10 hours after each addition of 3-sulfolene. The reaction was carefully vented prior to each new addition and heating cycle. The mixture was filtered through celite and the solvent removed. The crude material was dissolved in DCM and passed through a short (4”) column of silica-gel. The solvent was removed to give yellow oil that precipitated crystals upon addition of MeOH. The product was collected and dried to give 4.89 g of the title compound (70%). The material gave identical spectral data to that previously reported in the literature.[38] ^{1}H NMR ($CDCl_3$, 300 MHz): δ = 7.23 (AA’BB’, 2H),

7.13 (AA'BB', 2H), 5.95 (m, 2H), 5.00 (s, 2H), 2.52-2.46 (m, 2H), 2.09-2.01 (m, 2H), 1.95-1.89 (m, 2H).

1,4-Dihydroanthracene (35). The title compound was prepared following a modified literature method.[38] Compound **34** (4.89 g, 24.7 mmol) dissolved in a mixture of EtOH (100 mL) and HCl (10 mL) heated to reflux for 24 hours under an argon atmosphere. After cooling in an ice bath a crystalline precipitate formed and was collected. The material was recrystallized from MeOH and dried to give 3.64 g of the title compound (82%). The material gave identical spectral data to that previously reported in the literature.[38] ^{1}H NMR ($CDCl_3$, 300 MHz): δ = 7.77 (AA'BB', 2H), 7.64 (s, 2H), 7.42 (AA'BB', 2H), 6.06 (m, 2H), 3.60 (s, 4H).

2-Chloro-3-(phenylsulfonyl)-1,2,3,4-tetrahydroanthracene (36). The title compound was prepared following a modified literature method.[38] In dry DCM (80 mL) **35** (2.5 g, 13.9 mmol) was cooled to -78°C and treated dropwise with a solution of PhSCl (16.5 mmol) in dry DCM (80 mL). After the addition the reaction mixture was stirred for 4 hours at room temperature and then placed in a freezer for 2 hours. The precipitated was removed. The reaction mixture was then cooled to 0°C followed by the addition of 77% *m*-CPBA (7.18 g, 41.6 mmol). The reaction was warmed to room temperature and stirred under a N_2 atmosphere for 48 hours. The reaction was diluted with aqueous 10% Na_2SO_3 (50 mL) and stirred for 30 minutes. The organic layer was washed with aqueous 10% Na_2CO_3 (80 mL), aqueous10% Na_2SO_3 (80 mL), and aqueous 10% Na_2CO_3 (80 mL) then dried over K_2CO_3. The solvent was removed under reduced pressure and the crude material recrystallized from MeOH yielding 3.55 g of the title compound (72%). The material gave identical spectral data to that previously

reported in the literature.[38] ^{1}H NMR ($CDCl_3$, 300 MHz): δ = 7.99 (m, 2H), 7.77 (m, 2H), 7.70 (m, 1H), 7.64 (s, 1H), 7.61 (m, 2H), 7.46 (m, 2H), 4.97 (m, 1H), 3.79 (m, 1H), 3.58 (dd, 1H), 3.45 (dd, 1H), 3.34 (dd, 1H), 3.28 (dd, 1H).

2-(Phenylsulfonyl)-1,2-dihydroanthracene (37). The title compound was prepared following a modified literature method.[38] In dry DCM (30 mL) compound **36** (3.54 g, 9.91 mmol) was treated dropwise with one equivalent of DBU (1.51 g, 9.91 mmol). After the addition the reaction mixture was stirred at room temperature for one hour then diluted with water (30 mL). The layers were separated and the aqueous layer was washed with DCM (3 x 50 mL). The organic layers combined and dried over Na_2SO_4 and the solvent removed under reduced pressure. The crude material was recrystallized from MeOH yielding 2.80 g of the title compound (89%). The material gave identical spectral data to that previously reported in the literature.[38] ^{1}H NMR ($CDCl_3$, 300 MHz): δ = 7.75 (m, 2H), 7.66 (m, 2H), 7.43-7.37 (m, 3H), 7.34 (m, 1H), 7.29-7.20 (m, overlap with solvent, 3H), 6.80 (d, 1H), 6.13 (dd, 1H), 4.13 (m, 1H), 3.61 (dd, 1H), 3.40 (dd, 1H).

Ethyl-4,11-dihydro-2H-naphtho[2,3-*f*]isoindole-1-carboxylate (38). The title compound was prepared following a modified literature method.[38] In dry THF (30 mL) ^{t}BuOK (1.4 g, 12.5 mmol) was stirred at 0°C followed by the addition of ethyl isocyanoacetate (988 mg, 8.73 mmol) and stirred at room temperature. Compound **37** (2.80 g, 8.73 mmol) in dry THF (30 mL) was added dropwise at 0°C. The mixture was warmed to room temperature and stirred overnight. The solvent was removed and the crude material redissolved in DCM (120 mL). The organic layer was washed with water (2 x 100 mL) and brine (1 x 100 mL) and dried over K_2CO_3. The solvent removed under

reduced pressure and the crude material purified by column chromatography eluting with DCM/Hexanes (80:20). The combined fractions recrystallized from MeOH yielding 1.163 g of the title compound (46%). The material gave identical spectral data to that previously reported in the literature.[38] ^{1}H NMR ($CDCl_3$, 300 MHz) δ = 8.96 (br s, 1H), 7.80 (s overlapped, 1H), 7.76 (m, 2H), 7.74 (s overlapped, 1H), 7.44 (m, 2H), 6.86 (d, 1H), 4.43 (q overlapped, 2H), 4.39 (s, 2H), 4.06 (s, 2H), 1.44 (t, 3H).

4,7-dihydro-2H-isoindole (BP). A suspension of **18a** (600 mg, 3.1 mmol) in ethylene glycol (20 mL) with KOH (880 mg, 15.7 mmol) was thoroughly purged with argon. The mixture was heated to 170°C for 1 hour. The reaction was immediately cooled in an ice bath and diluted with DCM (100 mL). The organic layer was washed with water (2 x50 mL) and brine (1 x 50 mL) collected and dried over Na_2SO_4. The solvent was removed producing a dark amber colored oil that was vacuum dried to a consistent weight to give 287 mg of the title compound (77%). TLC analysis verified that no starting material was present. The title compound was immediately used in a porphyrin synthesis without further purification due its instability. ESI-TOF [M+H]+ and [2M+H]+ 120.0813, 239.1545, calcd 120.0808, 239.1543.

4,9-Dihydro-2H-benzo[f]isoindole (NP). The title compound was prepared from **21** following the procedure used for **BP** (86 %). APCI-MS $[M+H]^+$ 170.0961, calcd 170.0964.

5,8-Dimethoxy-4,9-dihydro-2H-benzo[f]isoindole (NP2). The title compound was prepared from **26** following the procedure used for **BP** (61%). ESI-TOF $[M+H]^+$ and $[M+Na]^+$ 230.1176, 252.0990, calcd 230.1176, 252.0990.

4,11-Dihydro-4,11-ethano-2H-napth[2,3f]isoindole (AP). The title compound was prepared from **32** following the procedure used for **BP** (87%). ESI-TOF m/z 246.1275, calcd 246.1277.

4,11-Dihydro-2H-naphtho[2,3-f]isoindole (AP2). The title compound was prepared from **38** following the procedure used for **BP** (82%). CI-MS $[M]^+$ and $[M+H]^+$ 219.1054, 220.1132 calcd 219.1048, 220.1126.

Tetraphenyltetrabenzoporphyrin (39a). The title compound was prepared following a modified literature method.[37] A solution of **BP** (287 mg, 2.4 mmol) and **1** (255 mg, 2.4 mmol) in dry DCM (250 mL) was stirred under an argon atmosphere protected from light. After the addition $BF_3{\cdot}O(Et)_2$ (60 mg, 0.4 mmol) the reaction was stirred for 3 hours at room temperature. In one portion DDQ (603 mg, 2.7 mmol) was added and the reaction stirred for one hour. The solvent was removed and the material redissolved in toluene (80 mL) with DDQ (655 mg, 2.9 mmol) heated to reflux under argon for one hour. The solvent was removed and the crude material dissolved in DCM (120 mL). The organic layer was washed with aqueous 10% Na_2SO_3 (2 x 100 mL), water (2 x 100 mL) and brine (1 x 100 mL) collected and dried over Na_2SO_4. The crude material was loaded on silica and purified by column chromatography eluting with 2% MeOH in DCM. The first bright green band was collected and the solvent removed. The material was dissolved in a minimal amount of boiling $CHCl_3$ vigorously stirred and diluted with MeOH (10x volume) precipitating small green crystalline flakes. The precipitate was collected and repeatedly washed with MeOH yielding 140 mg of the title compound (29%). The NMR spectra were recorded on a Varian Inova 500 MHz, operating at 500 MHz for ^1H, 125 MHz for ^{13}C, and 50 MHz for ^{15}N. The probe was an

indirect detection triple resonance probe, with z-axis gradients. The proton spectrum at 25°C displayed a broad signal for the protons of the orthophenylene moiety, due to the exchange of the NH protons.[104] This broad signal was resolved at -50°C into two AA'BB' patterns, while the NH protons displayed a sharp signal at -1.34 ppm, as the exchange became slower. Because of the limited solubility of H_2TPTBP in the NMR solvent, ^{13}C chemical shifts were measured by indirect detection, in a gHMBC spectrum. The material gave identical spectral data to that previously reported in the literature.[104] ^{1}H NMR ($CDCl_3$, 500 MHz): δ = 8.40 (m, 8H), 7.96 (m, 4H), 7.88 (m, 8H), 7.43 (AA'BB', 4H), 7.34 (AA'BB', 4H), 7.18 (AA'BB', 4H), 6.98 (AA'BB', 4H), -1.34 (s, 2H); ^{13}C NMR ($CDCl_3$, 125 MHz) δ = 115.9, 124.2, 124.9, 126.1, 126.7, 129.5, 131.6, 133.7, 134.7, 140.1, 141.9; ESI-TOF $[M+H]^+$ 815.3169, calcd 815.3169.

Tetra(3,5-di-*tert*-butylphenyl)tetrabenzoporphyrin (39b). The title compound (H_2Ar_4TBP) was prepared from a solution of **BP** (296 mg, 2.5 mmol) and **3** (542 mg, 2.5 mmol) in dry DCM (250 mL) according to the procedure for **39a**. The crude product was purified by column chromatography eluting with DCM collecting the second large green band. The solvent was removed and the material dissolved in boiling methanol after cooling 158 mg of the title compound was collected by filtration (20%). ^{1}H NMR (pyridine-d_5, 500 MHz): δ = 8.48 (s, 8H), 8.25 (s, 4H), 7.66 (d, 8H), 7.47 (m, 8H), 1.59 (s, 72H); ^{13}C NMR (pyridine-d_5, 125 MHz) δ = 152.6, 138.4, 130.2, 126.4, 125.5, 122.7, 118.0, 35.7, 32.0; MALDI-MS $[M]^+$ and $[M+H]^+$ 1262.8042, 1263.8179, calcd 1262.8099, 1263.8177.

Tetra(4-(9,9-dihexyl-fluorenyl)-phenyl)tetrabenzoporphyrin (39c). The title compound (H_2ArF_4TBP) was prepared from a solution of **BP** (143 mg, 1.2 mmol) and **9**

(520 mg, 1.2 mmol) in dry DCM (150 mL) according to the procedure for **39a**. The crude product was purified by column chromatography eluting with 20% EtOAc in hexane collecting the first large green band. The solvent was removed and the material precipitated from DCM and MeOH to give 110 mg of the title compound (17%).^{1}H NMR (pyridine-d_5, 500 MHz): δ = 8.67 (d, 8H), 8.50 (d, 8H), 8.24 (d, 4H), 8.19(d, 4H), 8.05 (d, 4H), 7.85 (d, 8H), 7.70 (d, 4H), 7.55 (m, 8H), 7.42 (m, 8H), 2.44 (dd, 8H), 2.35 (dd, 8H), 1.28 (m, 16H), 1.23 (m, 32H), 1.13 (m, 16H), 0.88 (t, 24H); ^{13}C NMR (pyridine-d_5, 125 MHz) δ = 153.0, 152.3, 143.2, 142.2, 141.9, 141.8, 140.5, 138.0, 136.2, 128.4,128.2, 128.0, 127.5, 127.0, 125.4, 124.1, 122.8, 121.2, 120.9, 116.8, 56.5, 41.1, 32.1, 30.4, 24.9, 23.1, 14.4; MALDI-MS $[M]^+$ and $[M+H]^+$ 2143.3074, 2144.3104, calcd 2143.3107, 2144.3185.

Tetraphenyltetranaphthoporphyrin (40a). The title compound was prepared following a modified literature method.[36] In dry DCM (250 mL), **NP** (430 mg, 2.54 mmol) and **1** (270 mg, 2.54 mmol) was stirred under argon atmosphere and protected from light. After the addition of $BF_3{\cdot}O(Et)_2$ (72 mg, 0.5 mmol) the reaction was stirred at room temperature for 90 minutes. In one portion DDQ (2.88 g, 12.7 mmol) was added and the reaction brought to reflux for one hour. The organic layer was washed with 10% aqueous Na_2SO_3 (2 x 100 mL), and water (2 x 100 mL) and dried over K_2CO_3. The solvent removed and the crude material loaded on neutral silica eluting with DCM collecting the first major green band. The material was redissolved in boiling $CHCl_3$ and diluted with excess MeOH precipitating fine green crystals to give 116 mg of the title compound (20%). The material gave identical spectral data to that previously reported

in the literature.[36] ^{1}H NMR ($CDCl_3$-TFA, 300 MHz): δ = 8.63-8.60 (m, 8H), 8.08-7.97 (m, 20H), 7.75-7.72 (m, 8H), 7.53-7.50 (m, 8H), 2.49 (s, 4H).

1,4,10,13,19,22,28,31-Octamethoxy-7,16,25,34-tetrakis(3,5-di-tertbutylphenyl)-tetranaphthoporphyrin (40b). The title compound ($H_2Ar_4TNP(OMe)_8$) (**40b**) was prepared according to the procedure for **40a** from a solution of **NP2** (242 mg, 1.0 mmol) and **3** (230 mg, 1.0 mmol) in dry DCM (180 mL). The solvent was removed and the crude material purified by chromatography eluting with DCM followed by multiple precipitations from DCM and MeOH to give 72 mg of the title compound (16%). ^{1}H NMR (pyridine-d_5, 500 MHz): δ = 8.66 (s, 8H), 8.49 (s, 8H), 8.37 (s, 4H), 6.86 (d, 8H), 4.03 (s, 24H), 1.60 (s, 72H); ^{13}C NMR (pyridine-d_5, 125 MHz) δ = 152.9, 151.1, 142.8, 136.1, 128.5, 125.3, 122.6, 120.2, 119.5, 116.8, 103.5, 55.7, 35.4, 31.8; MALDI-TOF MS $[M]^+$ 1703.9685, calcd 1703.9603.

8,19,30,41-tetrakis(3,5-di-butylphenyl)-6,10,17,22,27,32,39,43-octahydro-6,43:10,17:21,28:32,39-tetraethano-45H,47H-tetraanthraporphyrin (41). The title compound was prepared following a modified literature method.[66] A mixture of **3** (200 mg, 0.9 mmol) with **AP** (225 mg, 0.9 mmol) in dry DCM (170 mL) was stirred protected from light under an argon atmosphere. After the addition of $BF_3{\cdot}O(Et)_2$ (58 mg, 0.4 mmol) the reaction was stirred at room temperature for 18 hours. In one portion DDQ (1.08 g, 4.75 mmol) was added and the mixture stirred for 90 minutes. The organic layer was washed with 10% aqueous Na_2SO_3 (2 x 100 mL), water (1 x 100 mL), and brine (1 x 100 mL) collected and dried over Na_2SO_4. The solvent removed and the crude material passed through a silica column eluting with DCM. The combined fractions dissolved in warm THF (25 mL) and diluted with MeOH (250 mL). The solution became

turbid and was placed in the refrigerator overnight. The formed precipitate was filtered and washed repeatedly with MeOH. The precipitate was collected and dried to give 209 mg of the title compound (51%). The material gave identical spectral data to that previously reported in the literature.[66] ^{1}H NMR ($CDCl_3$, 300 MHz): δ = 8.41-7.26 (mixture of isomers, overlap with solvent, 36H), 3.95 (m, 8H), 1.83-1.63 (m, bridge + t-Bu, 88H).

Tetra(3,5-di-*tert*-butylphenyl)tetraanthroporphyrin (42). The title compound was prepared following a modified literature method.[38] The solvents used in this procedure were thoroughly purged with argon or subjected to freeze pump thaw cycles due to the oxygen sensitivity of **42**. A mixture of **AP2** (150 mg, 0.67 mmol) and **3** (149 mg, 0.68 mmol) in dry DCM (100 mL) was stirred under an argon atmosphere protected from light. The reaction was stirred for one hour after the addition of $BF_3{\cdot}OEt_2$ (20 µL). A solution of DDQ (232 mg, 1.0 mmol) in toluene (4 mL) was subjected to freeze pump thaw cycles in a schlenk flask prior to addition. After the addition the reaction was stirred for one hour at room temperature and then quenched by the addition of aqueous 10% Na_2SO_3 (100 mL). The organic layer was separated and washed with aqueous 10% Na_2SO_3 (100 mL), aqueous 10% Na_2CO_3 (100 mL), and brine (100 mL). The organic layer was dried over Na_2SO_4 and the solvent removed under reduced pressure. The material was purified by column chromatography eluting with DCM. The combined fractions were concentrated and the material precipitated by the addition of excess MeOH. The precipitate was collected to give 95 mg of the title compound (33%). ^{1}H NMR (pyridine-d_5, 500 MHz): δ = 8.67 (s, 8H), 8.65 (s, 8H), 8.58 (s, 4H), 8.37 (s, 8H), 8.15 (s, 8H), 7.52 (t, 8H), 1.67 (s, 72H); ^{13}C NMR (pyridine-d_5, 125 MHz) δ = 32.2, 35.9,

116.3, 123.2, 125.7, 126.1, 128.2, 129.1, 129.6, 130.8, 132.8, 136.7; MALDI-TOF MS $[M]^+$ 1663.9403, calcd 1663.9384.

Bis(3-ethoxycarbonyl-4,7-dihydro-2H-isoindolyl)methane (43a). The title compound was prepared following a modified literature method.[59] A solution of **18a** (1.606 g, 8.4 mmol) and dimethoxy methane (319 mg, 4.2 mmol) in AcOH (130 mL) and TsOH (165 mg, 0.9 mmol) under N_2 atmosphere was stirred for 24 hours. The reaction was poured into ice water (200 mL) and vigorously stirred. The precipitated material was collected and washed with water (1x 100 mL) and cold MeOH (2 x 50 mL). The title compound was dried under vacuum to give 1.38 g (85%). The material gave identical spectral data to that previously reported in the literature.[59] ^{1}H NMR ($CDCl_3$-d_6-DMSO, 300 MHz): δ = 11.19 (br s, 2H), 5.77 (m, 4H), 4.17 (q, 4H), 3.71 (s, 2H), 3.24 (m, 4H overlap with solvent), 3.02 (m, 4H), 1.27 (t, 6H).

Bis(3-ethoxycarbonyl-4,7-dihydro-5,6-dipropyl-2H-isoindolyl)methane (43b). The title compound was prepared from a solution of **18b** (920 mg, 3.3 mmol), dimethoxy methane (127 mg, 1.7 mmol), TsOH (75 mg, 0.4 mmol) in 75 mL of AcOH following the procedure for **43a**. The crude material was reprecipitated from boiling $CHCl_3$ and excess MeOH to give 470 mg of the title compound (50%). ^{1}H NMR ($CDCl_3$, 300 MHz): δ = 9.43 (s, 2H), 4.26 (q, 3H), 3.88 (s, 2H), 3.37 (m, 4H), 3.51 (m, 4H), 2.16 (m, 8H), 1.46 (m, 8H), 1.30 (t, 6H), 0.95 (t, 3H), 0.94 (t, 3H); ^{13}C NMR ($CDCl_3$, 75 MHz): δ= 162.2, 128.7, 128.4, 127.3, 117.5, 116.0, 60.0, 35.7, 28.9, 26.6, 23.3, 22.0, 14.7, 14.6; ESI- MS $[M+H]^+$ 563.3851, calcd 563.3843.

Bis(4,7-dihydro-2H-isoindolyl)methane (44a). The title compound was prepared according to the procedure used for **BP**. A suspension of **43a** (650 mg, 1.65

mmol) in ethylene glycol (40 mL) with KOH (925 mg, 16.5 mmol) was thoroughly purged with argon and heated to 170°C for 1 hour. The isolated material was dried under vacuum to a consistent weight to give 351 mg of the title compound (84%). Due to instability **44a** was used immediately and not subjected to further purification. DART-MS $[M+H]^+$ 251.1563, calcd 251.1543.

Bis(4,7-dihydro-5,6-dipropyl-2H-isoindolyl)methane (44b). The title compound was prepared according to the procedure used for **44a** from **43b** (450 mg, 0.8 mmol) to give 255 mg of the title compound (76%)**.** ESI-MS $[M+H]^+$ 419.3429, calcd 419.3421.

5,15-Diphenyltetrabenzoporphyrin (45a). The title compound was prepared following a modified literature method.[59] In dry DCM (200 mL) **44a** (352 mg, 1.4 mmol) and **1** (149 mg, 1.4 mmol) were stirred protected from light under an argon atmosphere. After the addition of TFA (30 mg, 0.3 mmol) the reaction was stirred for 18 hours at room temperature. DDQ (478 mg, 2.1 mmol) was added in one portion and the reaction stirred for one hour. The solvent was removed under reduced pressure. The material was redissolved in toluene (120 mL) with DDQ (634 mg, 2.8 mmol) and refluxed for 30 minutes. The solvent was removed and the crude material dissolved in DCM (120 mL). The organic layer was washed with aqueous 10% Na_2SO_3 (2 x 100 mL), water (2 x 100 mL), and brine (1 x 100 mL). The organic layer was collected and dried over Na_2SO_4. The material loaded on silica and purified by column chromatography eluting with DCM. The combined fractions were dissolved in a minimal amount of boiling $CHCl_3$ and precipitated by the slow addition of MeOH (excess) under vigorous stirring. The precipitate was collected and repeatedly washed with MeOH to give 178 mg of the title

compound (38%). The material gave identical spectral data to that previously reported in the literature.[59] ^{1}H NMR ($CDCl_3$-TFA, 300 MHz): δ = 10.98 (s, 2H), 9.38 (d, 4H), 8.44 (m, 4H), 8.17 (ddd, 4H), 8.12 (m, 2H), 8.04 (m, 4H), 7.83 (ddd, 4H), 7.58 (d, 4H), 3.51 (br s, 4H).

5,15-Di(3,5-di-*tert*-butylphenyl)tetrabenzoporphyrin (45b). The title compound was prepared following a modified literature method.[59] Following the procedure for **45a** the title compound was prepared from a solution of **44a** (309 mg, 1.2 mmol) and **3** (269 mg, 1.2 mmol) in dry DCM (180 mL). The crude material was purified by column chromatography eluting with DCM. Then precipitated by dissolving in a minimum amount of boiling $CHCl_3$ diluting with MeOH to give 158 mg of the title compound after filtration and repeated washing with MeOH (29%). The material gave identical spectral data to that previously reported in the literature.[59] ^{1}H NMR (CD_2Cl_2, 300 MHz): δ = 11.15 (s, 2H), 9.73 (d, 4H), 8.17 (m, 4H), 8.12 (m + d overlapped, 6H), 7.77 (m, 4H), 7.53 (m, 4H), 1.56 (s, 36H), -1.25 (br s, 2H).

5,15-Di((3,5-di-*tert*-butylphenyl)-phenyl)tetrabenzoporphyrin (45c). The title compound was prepared from a solution of **44a** (369 mg, 1.5 mmol) and **6** (546 mg, 1.5 mmol) in dry DCM (180 mL) following the procedure used for **45a**. The material was purified by column chromatography on silica-gel eluting with DCM. The fractions were concentrated and the title compound precipitated from the addition of excess MeOH to give 220 mg (25%). ^{1}H NMR (pyridine-d_5, 500 MHz): δ = 1.44 (s, 36H), 7.67 (d, 8H), 7.94 (t, 4H), 8.14 (d, 8H), 8.21 (t, 4H), 8.29 (d, 4H), 8.90 (s, 2H), 8.92 (s, 4H), 10.00 (d, 4H), 11.56 (s, 2H); ^{13}C NMR (pyridine-d_5, 125 MHz) δ =31.8, 35.0, 94.3, 117.7, 122.4,

125.9, 126.8, 128.0, 128.3, 130.8, 138.0, 138.5, 140.3, 143.5, 150.5,151.9; DART-MS $[M+H]^+$ 1191.6296, calcd 1191.6299.

5,15-Di(3,5-di-*tert*-butylphenyl)octapropyltetrabenzoporphyrin (45d). The title compound was from a solution of **44b** (255 mg, 0.6 mmol) and **3** (133 mg, 0.6 mmol) in dry DCM (110 mL). The material was purified by column chromatography on silica-gel eluting with 2% MeOH in DCM to give 68 mg of the title compound following the procedure for **45a** (18%). ^{1}H NMR (pyridine-d_5, 500 MHz): δ = 11.66 (s, 2H), 9.90 (s, 4H), 8.45 (s, 4H), 8.42 (s, 2H), 7.75 (s, 4H), 3.26 (t, 8H), 3.08 (t, 8H), 2.07 (sex, 8H), 1.93 (sex, 8H), 1.72 (s, 36H), 1.25 (t, 12H), 1.24 (t, 12H); ^{13}C NMR (pyridine-d_5, 125 MHz) δ = 152.8, 141.0, 140.7, 140.2, 138.6, 136.6, 128.0, 126.2, 123.2, 122.1, 117.9, 93.6, 36.6, 36.4, 35.8, 32.2, 25.5, 25.2, 14.8, 14.7; DART-MS $[M+H]^+$ 1223.8763, calcd 1223.8803.

. **Platinum Tetraphenyltetrabenzoporphyrin (Pt-39a).** A solution of **39a** (49 mg, 60.1 μmol) and platinum acetate (83 mg, 60.1 μmol) in benzonitrile (25 mL) was thoroughly purged with argon. The reaction was then submerged in a pre-heated oil bath at 200 °C and refluxed until the Q-band of **39a** disappeared from the UV-Vis spectrum. The solvent was removed under reduced pressure and the crude material dissolved in DCM and filtered through a plug of Celite. The material was then loaded on silica and purified via column chromatography eluting with 30% DCM in Hexanes yielding 45 mg of the title compound (74%). ^{1}H NMR (pyridine-d_5, 500 MHz): δ = 8.35 (d, 8H), 7.96 (t, 4H), 7.92 (t, 8H), 7.42 (m, 8H), 7.37 (m, 8H); ^{13}C NMR (pyridine- d_5, 125 MHz) δ = 142.1, 138.2, 136.7, 134.2, 129.9, 129.9, 126.3, 124.8; ESI-TOF m/z 1006.2549, calcd 1006.2562.

Platinum Tetra(3,5-di-*tert*-butylphenyl)tetrabenzoporphyrin (Pt-39b). The title compound was prepared from **39b** (80 mg, 63.3 μmol) and platinum acetate (87 mg, 63.3 μmol) in benzonitrile (30 mL) using the procedure for **Pt-39a**. The crude material was purified via column chromatography eluting with 30% DCM in hexanes yielding 32 mg of the title compound (35%). ^{1}H NMR (pyridine- d_5, 500 MHz): δ = 8.31 (s, 8H), 8.17 (s, 8H), 7.51 (m, 8H), 7.44 (m, 8H), 1.46 (s, 72H); ^{13}C NMR (pyridine- d_5, 125 MHz) δ = 153.3, 138.9, 136.6, 129.0, 126.4, 125.6, 122.9, 120.5, 35.6, 32.0; DART-MS $[M+H]^+$ 1457.7687, calcd 1457.7694.

Platinum Tetra(4-(9,9-dihexyl-fluorenyl)-phenyl)tetrabenzoporphyrin (Pt-39c). The title compound was prepared from **39c** (76 mg, 35.4 μmol) and platinum acetate (49 mg, 35.4 μmol) in benzonitrile (25 mL) using the procedure for **Pt-39a**. The crude material was purified by chromatography eluting with 20% hexanes in DCM. The fractions combined and concentrated in DCM then diluted with excess MeOH to give 78 mg of the title compound (94%). ^{1}H NMR (pyridine- d_5, 500 MHz): δ = 8.50 (m, 12H), 8.21 (d, 4H), 8.18 (d, 4H), 8.04 (d, 4H), 7.69 (d, 8H), 7.66 (d, 4H), 7.53 (t, 8H), 7.30 (m, 8H), 2.37 (t, 4H), 2.27 (t, 4H), 1.14 (m, 16H), 1.11 (q, 16H), 0.99 (m, 16H), 0.95 (m, 16H), 0.77 (t, 24H); ^{13}C NMR (pyridine- d_5, 125 MHz) δ = 152.9, 152.0, 142.8, 142.2, 141.7, 141.2, 140.0, 138.5, 137.2, 135.1, 128.7, 128.4, 127.9, 127.4, 126.6, 125.1, 124.0, 121.4, 121.0, 119.3, 41.0, 32.1, 30.4, 24.8, 23.2, 14.5; MALDI-TOF MS $[M+H]^+$ 2338.2735, calcd 2338.2709.

Platinum Tetraphenyltetranaphthoporphyrin (Pt-40a). The title compound was prepared from **40a** (112 mg, 110.3 μmol) and platinum acetate (150 mg, 109.3 μmol) in benzonitrile (25 mL) using a procedure similar tor **Pt-39a** heating at 180°C**.** The

crude material was passed a column of neutral silica eluting with DCM:THF (9:1). The first dark green band was collected and the solvent removed. The material was precipitated from DCM and acetonitrile. The precipitate was collected and washed repeatedly with cold MeOH yielding 70 mg of the title compound (53%). The ^{1}H and gHMBC spectrum of compound Pt-TPTNP were taken on a Varian Inova 500 NMR spectrometer, equipped with a 5 mm indirect detection probe and with z-axis gradients, and operating at 500 MHz for ^{1}H and 125 MHz for ^{13}C. The chemical shifts were referenced to the residual solvent signals, 7.22 ppm in ^{1}H and 123.9 in ^{13}C. Because of the limited solubility of Pt-TPTNP in the NMR solvent, ^{13}C chemical shifts were measured by indirect detection, in a gHMBC spectrum. ^{1}H NMR (pyridine- d_5, 500 MHz) δ 8.47-8.44 (m, 8H), 8.22-8.14 (m, 4H), 8.10-8.03 (m, 8H), 7.93 (s, 8H), 7.90-7.84 (m, 8H), 7.61 (8H, overlap with solvent); ^{13}C NMR (pyridine- d_5, 125 MHz) δ 142.4, 135.9, 134.2, 131.6, 130.5, 130.0, 129.7, 126.7, 124.1, 117.9; ESI-TOF m/z 1206.3188, calcd 1206.3157.

Platinum 1,4,10,13,19,22,28,31-Octamethoxy-7,16,25,34-tetrakis(3,5-di-*tert*-butylphenyl)tetranaphthoporphyrin (Pt-40b). The title compound was prepared from **40b** (115 mg, 67.5 μmol) and platinum acetate (92 mg, 67 μmol) in benzonitrile (30 mL) using the procedure for **Pt-39a.** The crude material was passed through a column of neutral silica eluting with DCM. The first dark green band was collected and the solvent removed. The material was precipitated from warm $CHCl_3$ and MeOH. The precipitate was collected and washed repeatedly with cold MeOH yielding 110 mg of the title compound (85%). ^{1}H NMR (pyridine- d_5, 500 MHz): δ = 8.56 (s, 8H), 8.30 (s, 8H), 8.29 (s, 4H), 6.82 (d, 8H), 3.93 (s, 24H), 1.46 (s, 72H); ^{13}C NMR (pyridine- d_5, 125 MHz) δ =

153.6, 151.1, 136.4, 127.5, 125.0, 123.5, 119.7, 119.5, 103.3, 55.8, 35.7, 32.0; MALDI-TOF MS $[M]^+$ 1896.9161, calcd 1896.9090.

Platinum Tetra(3,5-di-*tert*-butylphenyl)tetraanthroporphyrin (Pt-42) Due to the sensitivity with oxygen in the presence of room light for the title compound and **42** all manipulations were preformed under inert atmospheres and flask protected from light with foil. A schlenk flask charged with benzonitrile (6 mL), **42** (59 mg, 35.5 µmol) and platinum acetate (48 mg, 35.5 µmol) was degassed by freeze pump thaw cycles. The mixture was heated at 180°C under a positive pressure of argon until the disappearance of the Q-band of **42** (approx. 3 hours). The solvent was removed by vacuum distillation and the crude was purified by passing through a short plug of neutral silica under an argon atmosphere with DCM. The solvent was removed under reduced pressure to give 25 mg of the title compound (38%). ^{1}H NMR (pyridine- d_5, 500 MHz): δ = 8.71 (s, 8H), 8.53 (s, 4H), 8.53 (overlap s, 8H), 8.30 (s, 8H), 8.11 (d, 8H), 7.52 (t, 8H), 1.58 (s, 72H); ^{13}C NMR (pyridine- d_5, 125 MHz) δ = 154.5, 136.6, 132.8, 130.4, 129.1, 128.7, 128.2, 126.3, 125.2, 123.4, 118.5, 35.8, 32.1; MALDI-TOF MS $[M]^+$ 1856.8951, calcd 1856.8872.

Platinum 5,15-Diphenyltetrabenzoporphyrin (Pt-45a). The title compound was prepared from **45a** (50 mg, 75.4 µmol) and platinum acetate (104 mg, 75.7 µmol) in benzonitrile (25 mL) using the procedure for **Pt-39a**. The material was loaded on silica, eluting with DCM removing the green band (**45a**). The solvent was changed to an increasing gradient with a THF:DCM mixture (30:70). The dark blue band was collected yielding 16 mg of the title compound (25%). Analogously to the reported palladium complex NMR analysis was not possible due to low solubility of **Pt-45a** in common NMR

solvents.[61] The material was characterized by UV-VIS and mass spectrometry. UV-Vis, Toluene, λ_{max}: 409 nm, 547 nm, 595 nm, 604 nm; MALDI-TOF MS $[M]^+$ 852.4518, 854.1971, 855.2001, 856.2019, 857.2050, 858.2057, 859.2082, 860.2094, 861.4855, calcd 852.1919, 854.1935, 855.1960, 856.1974, 857.1999, 858.2004, 859.2026, 860.2054.

Platinum 5,15-Di(3,5-di-*tert*-butylphenyl)tetrabenzoporphyrin (Pt-45b). The title compound was prepared from **45b** (65 mg, 73.3 μmol) and platinum acetate (100 mg, 73.3 μmol) in benzonitrile (30 mL) using the procedure for **Pt-39a**.The solvent was removed and the crude material loaded on silica eluting with 15% DCM in Hexane collecting the blue band. The material was further purified from multiple precipitations from boiling $CHCl_3$ and MeOH. The precipitate was collected and repeatedly washed with MeOH yielding 25 mg of the title compound (32%). ^{1}H NMR (pyridine- d_5, 500 MHz): δ = 11.55 (s, 2H), 9.80 (d, 4H), 8.35 (s, 4H), 8.31 (s, 4H), 8.08 (t, 4H), 7.78 (t, 4H), 7.54 (d, 4H); ^{13}C NMR (pyridine- d_5, 125 MHz) δ = 153.1, 141.5, 139.0, 138.2, 136.6, 136.2, 128.1, 127.7, 126.4, 122.8, 121.5, 121.0, 97.5, 35.9, 32.0; ESI-TOF [M]+ 1080.4543, calcd 1080.4481.

Platinum 5,15-Di((3,5-di-*tert*-butylphenyl)-phenyl)tetrabenzoporphyrin (Pt-45c). The title compound was prepared from **45c** (110 mg, 92.3 μmol) and platinum acetate (127 mg, 92.3 μmol) in benzonitrile (25 mL) using the procedure for **Pt-39a**. Separation with column chromatography failed due to solubility and small differences in R_f values. The title compound was purified by multiple precipitations from DCM and MeOH to give 70 mg (55%). ^{1}H NMR (pyridine- d_5, 500 MHz): δ = 11.60 (s, 2H), 9.86 (d, 4H), 8.93 (s, 2H), 8.84 (s, 4H), 8.12 (d, 8H), 8.08 (t, 4H), 7.99 (d, 4H), 7.81 (t, 4H),

7.63 (d, 8H), 1.34 (s, 36H); ^{13}C NMR (pyridine- d_5, 125 MHz) δ = 151.8, 143.5, 139.1, 138.3, 138.2, 136.8, 130.5, 128.2, 128.0, 127.8, 126.9, 126.9, 126.3, 121.8, 120.0, 35.0, 31.7; DART-MS $[M+H]^+$ 1383.5772, calcd 1383.5770.

Platinum 5,15-Di(3,5-di-*tert*-butylphenyl)octapropyltetrabenzoporphyrin (Pt-45d). The title compound was prepared from **45c** (33 mg, 23.2 μmol) and platinum acetate (32 mg, 23.2 μmol) in benzonitrile (20 mL) using the procedure for **Pt-39a**. After vacuum distillation to remove benzonitrile the crude material was loaded on silica and eluted with a hexane:DCM mixture (85:15) collecting the first blue band. The fractions were concentrated and the material precipitated by the addition of excess MeOH. The precipitate was collected to give 22 mg of the title compound (58%). ^{1}H NMR (pyridine- d_5, 500 MHz): δ = 11.86 (s, 2H), 9.83 (s, 4H), 8.36 (s, 2H), 8.33 (s, 4H), 7.42 (s, 4H), 3.11 (t, 8H), 2.95 (t, 8H), 1.90 (sex, 8H), 1.82 (sex, 8H), 1.63 (s, 36H), 1.18 (t, 12H), 1.12 (t, 12H); ^{13}C NMR (pyridine- d_5, 125 MHz) δ =153.0, 140.7, 140.4, 137.6, 136.8, 127.7, 126.8, 123.5, 121.7, 120.3, 97.0, 36.4, 35.9, 32.2, 25.6, 15.0; ESI-TOF m/z 1416.8265, calcd 1416.8301.

CHAPTER 3
PHOTOPHYSICS AND DEVICE RESULTS

Introduction

Photoluminescence is the process of photons being emitted by either a fluorophore to give fluorescence or alternatively a phosphor to give phosphorescence described earlier in Chapter 1. Electroluminescence is the process of generating an excited state by the application of an electric field and the emission of photons upon relaxation of the excited species. The first report of electroluminescence was by Destriau using microcrystals of ZnS suspended in an insulating medium sandwiched between two electrodes.[105, 106] This sparked the development and commercialization of numerous inorganic materials with a wide variety of emission wavelengths.

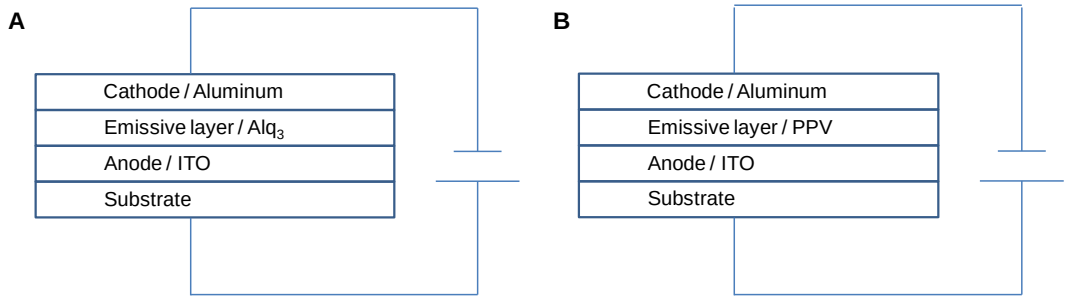

Figure 3-1. Single layer device structure for the first reported OLED and PLED. A) Vapor deposited small molecule OLED with Alq_3 as the emissive material. B) Solution processed polymer based PLED with PPV as the emissive material.

Electroluminescence from organic materials was first described in 1963.[107, 108] The use of anthracene crystals as the emitting species resulted in low efficiency and required high-field strengths and resulted in an overall lack of interest in the use of organic based materials for electroluminescence. A breakthrough occurred almost twenty five years later when Tang and Van Slyke reported green emission upon application of an electric field to single-layer devices fabricated by thermal vapor

deposition of aluminum *tris*-(-8-hydroxyquinolinate) (AlQ_3) onto indium-tin-oxide (ITO) followed by the thermal vapor deposition of an aluminum electrode shown in Figure 3-1A.[55]

Another important milestone was reached in 1990 when the Friend *et al* prepared the first polymer light-emitting diode (PLED).[109] The device was fabricated from a sandwiched thin film of poly(p-phenylenevinylene) (PPV) between two electrodes Al and ITO outlined in Figure 3-1B. The application of a voltage to the device produced yellow green light. Thus this work along with the work from Tang and Van Slyke can be regarded as the seminal works for the development of the organic LED field. The present day research area of OLEDs and PLEDs has grown significantly with devices in both areas at the point of commercialization.[110-113]

Electroluminescence Mechanisms

The simplest description of electroluminescence would be the conversion of electrons and holes into photons. The actual process can be broken down into four steps: (1) charge injection into the device, (2) charge transport to the emissive layer, (3) charge-recombination resulting in the formation of an excited state on the radiative material and (4) radiative relaxation of the generated excited state. One mechanism for generating electroluminescence known as intrinsic electroluminescence has been demonstrated by Bernanose using cellophane films or in perylene and anthracene crystals.[114-116] This requires the acceleration of electrons known as hot carriers to impact the radiative material generating the excited state. However because high ac voltages are often required which leads to electrical breakdown, it is difficult to generate intrinsic electroluminescence in organic materials.

A more successful method of introducing charge carriers into organic materials involves sandwiching the electroactive materials between electrodes. Application of an electric field at the electrodes effectively injects electrons and holes into the material. The use of a low work function metal at the cathode allows for electrons to be easily injected into the lowest unoccupied molecular orbital (LUMO) and in chemical terms reduces the electroactive material. This is analogous to injecting electrons into the conduction band (E_c) of inorganic semiconductors. The cathode is typically made from calcium, magnesium, or aluminum. Once the electrons are injected into the device near the cathode, simultaneously the anode injects holes into the highest occupied molecular orbital (HOMO) of the active material in an analogous fashion to the valence band (E_v) inorganic semiconductors. The formation of holes or more simply the removal of electrons is the oxidation of the electroactive material. The anode is most often indium tin oxide primarily for its high work function and good transmission properties (transparency) in the visible region. Now that both holes and electrons have been injected into the active material they begin to drift towards the oppositely charged electrode. This eventually leads to recombination of both holes and electrons on the emissive material generating an excited state that may radiatively or non-radiatively decay.

The choice of whether to use fluorescent or phosphorescent emitters becomes clear upon examination of the recombination process of electrons with holes. This can lead to an electron configuration on the emissive material to be either a singlet state (S= ½) or a triplet state (S=1). Recombination of electrons and holes affords a statistical distribution of singlet excitons (25%) and triplet excitons (75%). This means that use of

fluorescent emitters (i.e. emission from the S_1) are limited to a maximum efficiency of 25%. However the use of phosphorescent materials allows for use of both singlet and triplet states. Where the singlet states can intersystem cross to the triplet state and then radiatively decay (phosphorescence) device efficiency can reach the theoretical limit of 100% internal quantum efficiency. Materials with very high phosphorescence quantum yields are desirable and can potentially be used to fabricate highly efficient PLEDs and OLEDs.

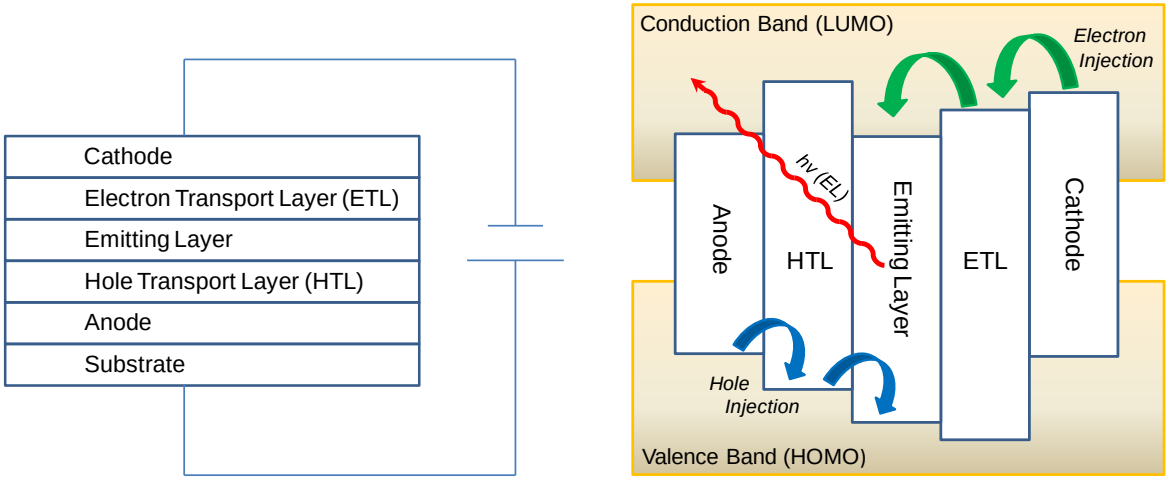

Figure 3-2. Device structure of a multilayer light emitting diode with a diagram of electroluminescence mechanism.

Organic Light Emitting Diodes

The term OLED refers to devices fabricated from the thermal vapor deposition (sublimation) of small molecules the substrate. The term PLED refers to devices fabricated from spin coating solution processable polymers on to the substrate.

The electron configuration of the excited material after the recombination of electrons with holes is not the only contributing factor to device efficiency. The rates at which the holes and electrons migrate through the materials to eventually recombine on the desired emitting species are important. Typically in most organic materials the hole

mobility is far higher than the electron mobility. This problem is circumvented by more complicated device structures with layers of materials that either increase or decrease the carrier mobilities. An example of this device structure is shown in Figure 3-2.

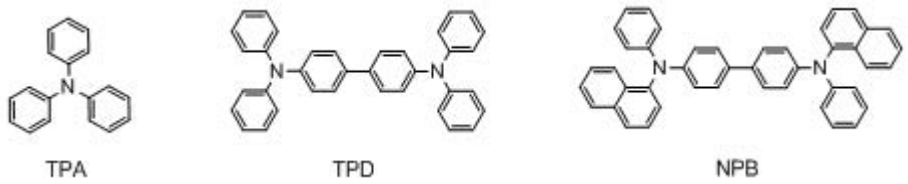

Figure 3-3. Examples of small molecule hole transport materials. TPA is triphenylamine, TPD is (N,N'-diphenyl-N,N'bis(3-methylphenyl)-1,1'biphenyl-4,4'-amine and NPB is N,N'-bis(naphthalene-1-yl)-N,N'-bis(phenyl)benzidine.

Electron transport layers (ETL) and hole transport layers (HTL) serve dual purposes in that they can alter the overall electron and hole mobilities respectively, while at the same time restricting the transport or injection of the opposite carrier. This allows the holes and electrons to be trapped in the emissive layer (EML) of the device. The hole transport layers are generally materials with large energy gaps ($\Delta E_{HOMO-LUMO}$) usually consisting of amines with low ionization potentials. These properties allow for the holes to be more easily injected while also providing a large barrier to electron injection from the EML. Examples of small molecules that can be vapor deposited for HTLs are shown in Figure 3-3.

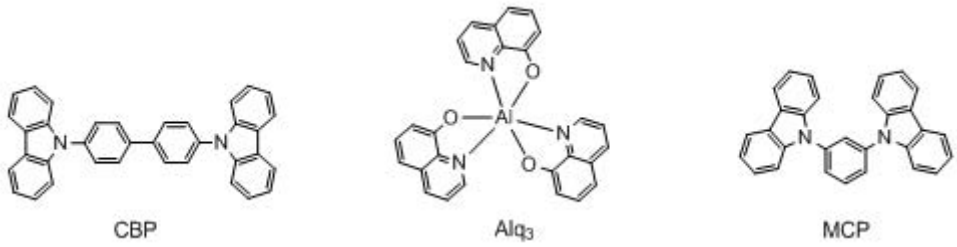

Figure 3-4. Examples of small molecule host materials. CBP is 4,4'-bis(N-carbazolyl)-1,1'-biphenyl, Alq_3 is tris-(8-hydroxyquinoline)aluminum and MCP is 1,3-bis(carbazol-9-yl)benzene.

The emissive layer of the device can either be a single material (neat) or an emissive material doped into a polymer or small molecule host at some concentration. The first OLEDs and PLEDs were fabricated as single layer devices (Figure 3-1). However it has been shown to be advantageous to use a host material to prevent various quenching mechanisms induced by having a neat layer of the emitting species. Common host materials used in the fabrication of OLEDs are outlined in Figure 3-4. The host materials are paired with the emitting species based on spectral overlap of the host emission spectrum (usually fluorescence) with the absorption of the emitter. This allows for efficient Förster energy transfer efficiently quenching the host emission. The materials may also be prepared such that the HOMO and LUMO of the emitting species lie within the HOMO and LUMO levels of the host, thus leading to charge trapping on the emitting species.

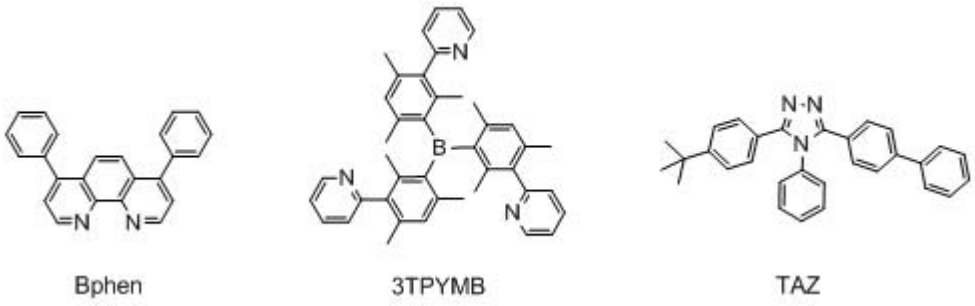

Figure 3-5. Examples of small molecule electron transport materials. Bphen is 4,7-diphenyl-1,10-phenanthroline, 3TPYMB is tris(2,4,6-trimethyl-3-(pyridine-3-yl)phenyl)borane, and TAZ is 3-(4-biphenylyl)-4-phenyl-5-*tert*-butylphenyl-1,2,4-triazole.

In between the cathode and the EML a layer of electron transport materials are deposited to facilitate balanced charge transport within the device with more efficient electron injection. In general these materials exhibit high electron mobilities and are chosen to have deep HOMO energy levels to block hole transport to the cathode.

Common materials used for OLED electron transport layers (ETL) are shown in Figure 3-5. The ability to block holes from reaching the cathode helps in trapping the carriers in the EML for hole and electron recombination on the emissive species.

Polymer Light Emitting Diodes

The devices composed of polymers for either the EML or as a host material are known as polymer light emitting diodes (PLEDs). Figure 3-6 outlines common polymers used for these devices. Most of the advantages in using polymeric materials for LEDs stem from the ability to solution process the materials over the thermal vapor deposition method used for OLEDs. However, in most cases device efficiencies for PLEDs are lower than a small molecule based OLED using the same emitter. The main reasons for the differences in device efficiencies are the difficulty in confining the holes and electrons to the EML. Since the use of common solvents in processing prevents deposition of multiple layers, multilayer device architectures in which the holes and electrons are confined to the active layer are generally not used. Without the addition of HTL and ETL layers, the carriers in PLEDs can migrate across the device and reach the opposite electrode without recombination, thus resulting in lower efficiency.

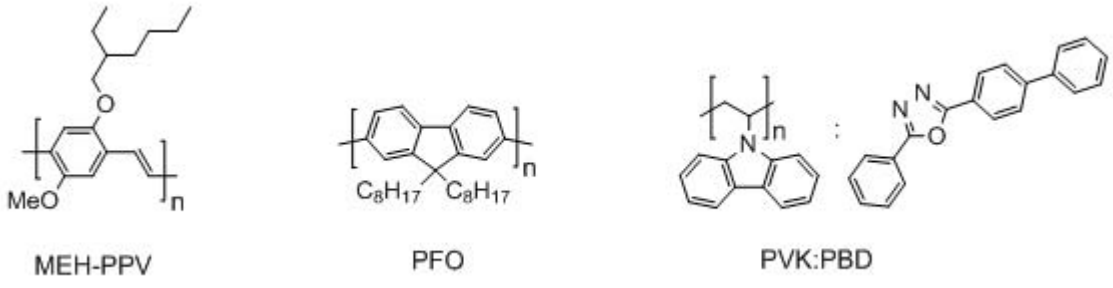

MEH-PPV PFO PVK:PBD

Figure 3-6. Examples of polymer host materials for polymer light emitting diodes. MEH-PPV is poly[2-methoxy-5-(2-ethylhexyloxy)-1,4-phenylenevinylene], PFO is poly(9,9-di-n-octylfluorenyl-2,7-diyl and PVK:PBD is poly(9-vinylcarbazole) blended with 2-(4-biphenylyl)-5-phenyl-1,3,4-oxadiazole.

Results and Discussion

Presented herein are the photophysical properties for three series of π-extended platinum porphyrins previously outlined in Chapter 2 (Figure 2-2). Also reported are the performance of these materials in PLEDs and OLEDs using each series of π-extended platinum porphyrins as the near-IR phosphors. Specifically this work advances the field of near-IR LEDs by the realization of electroluminescence in new wavelength regions of the near-IR using these novel phosphors. For the first time the solution photophysics of π-extended platinum porphyrins are reported setting PL efficiency records in their respective wavelengths regions. Record device efficiencies are obtained from use of these phosphors for near-IR LED applications.

Series 1- Photophysical Properties

The structures of the free-base and platinum complexes for π-extended porphyrins for Series 1are shown in Figure 3-7. The goal of these target compounds is to red shift the emission wavelengths further into the near-IR through increasing the conjugation to the porphyrin macrocycle. Platinum complexes for TNP and TAP systems have not been reported and this work represents the first known report of the photophysical properties for these targets. Gouterman showed early on that the major effect of extending conjugation to the porphyrin macrocycle (via fused benzo-rings) was a large red shift in the Q-band with the transition becoming significantly more allowed (intense), however only a small red shift is observed for the Soret band.[18-20] The absorption and photoluminescence in air saturated toluene for series 1 free-base porphyrins is shown in Figure 3-8, while the absorption and emission wavelength maxima, molar absorption coefficients, emission quantum yields and S_1 lifetimes are listed in Table 3-1.

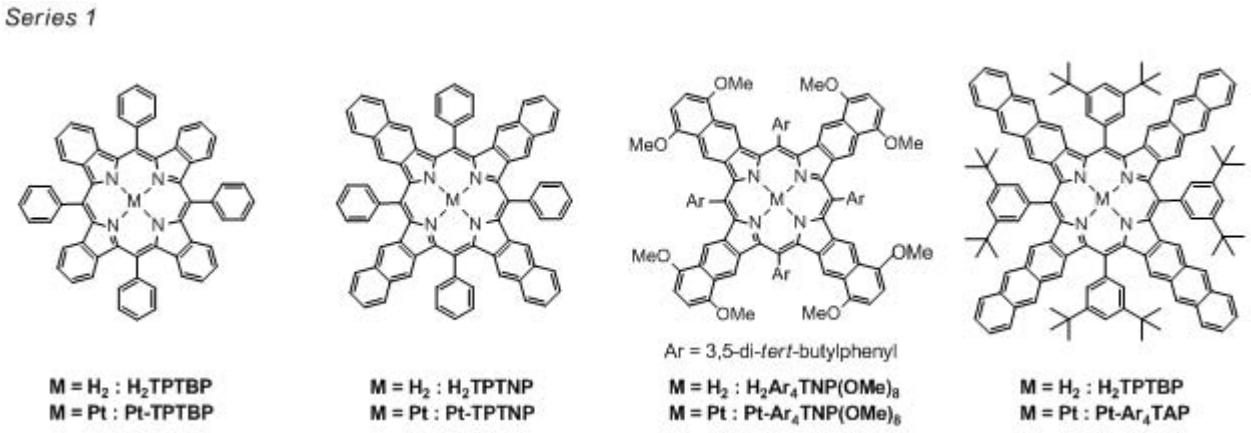

Figure 3-7. Structures for series 1 π-extended free-base and platinum porphyrins.

The addition of fused-benzo rings to the porphyrin macrocycle from H_2TPTBP to H_2Ar_4TAP results in approximately a 200 nm red shift of the Q-band. This results in the transition being shifted from the red region of the visible (H_2TPTBP) to being completely in the near-IR region (H_2Ar_4TAP). The Q-band becomes more allowed across the series and is noted by the increase in molar absorptivity constant ($\varepsilon = 3.32 \times 10^4 – 1.95 \times 10^5$ M^{-1} cm^{-1}) by an order of magnitude from H_2TPTBP to H_2Ar_4TAP. However the Soret band across the series is only red shifted 50 nm from H_2TPTBP to H_2Ar_4TAP. The transition is strongly allowed and remains in the visible region of the spectrum (ε ~2-3 x 10^5 M^{-1} cm^{-1}).

The photoluminescence for series 1 free-base porphyrins were obtained by excitation of the Soret band (Figure 3-8). The quantum yields (QY) were referenced to ZnTPP in toluene (QY 0.04)[117] while the S_1 decays were obtained by single photon counting and were all mono-exponential in nature shown in Figure A-1. A small Stokes shift is observed with the S_1 emission maxima relative to the lowest energy absorption. The emission maxima are red shifted approximately 140 nm (H_2TPTBP to H_2Ar_4TAP) across the series. The quantum yield for H_2TPTBP in toluene is in agreement with the

reported literature value.[61] The increase in the QYs for H_2TPTNP and $H_2Ar_4TNP(OMe)_8$ reflect the increase in k_r values consistent with an increase in the allowedness of the S_1-S_o transition, and in line with other values reported for H_2Ar_4TNP systems.[58] Ono *et al* have reported the PL spectra for two fluorescent ZnTAPs, however photophysical characterization of a free-base TAP has not been reported.[66] The PL for H_2Ar_4TAP is dominated by emission at 841 nm with a vibronic should at 932 nm. The low intensity broad emission in the visible region is likely from the anthracene fragments in the TAP macrocycle. The QY for H_2Ar_4TAP (6.8%) is higher than the reported QYs for ZnTAPs (3.7-4.3%) which are expected to be lower due to the increase rate in ISC.

Table 3-1. Photophysical properties of Series 1 free-base π-extended porphyrins in air saturated toluene. Fluorescence quantum yields were measured relative to ZnTPP (0.04) with excitation at 420 nm in toluene. The S_1 decays were obtained by single photon counting method.

Free-base Porphyrins	Absorption λ_{max} (Soret, Q-band) nm (ε_{max} = M^{-1} cm^{-1})	Fluorescence λ_{max} nm	φ_{fl}	τ_{fl} (ns)
H_2TPTBP	465, 633 ε_{465} = 3.03 x 10^5 ε_{633}= 3.32 x 10^4	704, 785	4.1% ±0.1	3.1
H_2TPTNP	500, 728 ε_{500} = 2.25 x 10^5 ε_{728}= 1.06 x 10^5	756, 840	19% ±0.2	3.9
$H_2Ar_4TNP(OMe)_8$	502, 730 ε_{502} = 2.64 x 10^5 ε_{730}= 1.18 x 10^5	755, 837	23% ±0.1	4.6
H_2Ar_4TAP	510, 824 ε_{510} = 2.11 x 10^5 ε_{824}= 1.95 x 10^5	841, 932	6.8% ±0.5	1.0

The decrease in the S_1 lifetime and quantum yield for H_2Ar_4TAP compared to H_2TPTBP follows the energy gap law.[118, 119] This states that as the difference in energy between the ground state and excited state gets smaller the rate of non-radiative decay

will increase, thus decreasing the radiative rate and QY. The deactivation rate constants for the S_1 state for series 1 free-base π-extend porphyrins were calculated and summarized in Table 3-2. The radiative rate constant (k_r) across the series increases from H_2TPTBP to H_2Ar_4TAP about 5.2 times. The non-radiative rate constant (k_{nr}) also increases across the series about 3 times. This results in the observed decrease in S_1 lifetimes across the series.

Table 3-2. Deactivation rate constants for S_1 state of series 1 free-base π-extended porphyrins in air saturated toluene. Radiative decay rate constant (k_r), calculated as $k_r = \varphi_{fl}k$, and the non-radiative decay rate constant ($k_{nr} = k_{ic} + k_{isc}$), calculated as $k_r = k - k_{nr}$.

Free-base Porphyrins	$k = 1/\tau_{fl}$ (s^{-1})	k_r (s^{-1})	k_{nr} (s^{-1})	τ_{fl} (ns)
H_2TPTBP	3.2×10^8	1.3×10^7	3.1×10^8	3.1
H_2TPTNP	2.6×10^8	4.9×10^7	2.1×10^8	3.9
$H_2Ar_4TNP(OMe)_8$	2.2×10^8	5.1×10^7	1.7×10^8	4.6
H_2Ar_4TAP	1.0×10^9	6.8×10^7	9.3×10^8	1.0

The absorption and photoluminescence in deoxygenated toluene for series 1 π-extended platinum porphyrins is shown in Figure 3-9. The absorption and emission wavelength maxima for the series are summarized in Table 3-3 along with the molar absorption coefficients, phosphorescence QYs and T_1 lifetimes.

The insertion of platinum changes the porphyrin symmetry to D_{4h}. The absorption spectra are blue shifted relative to the respective free-base absorptions. This is due to the donated d-electrons from platinum into the π*-orbitals of the porphyrin resulting in metal-to-ring charge transfer giving *irregular hypso*-type spectra. The relative intensities between the Soret and Q-bands have also changed. The insertion of the metal makes the Q-band transition more allowed (ε ~4-5 x 10^4 - 1-2 x 10^5 M^{-1} cm^{-1}). In the case of

platinum TNP and TAP systems the Q-band surpasses the Soret in intensity giving very strong absorptions in the deep-red to near-IR region of the spectrum.

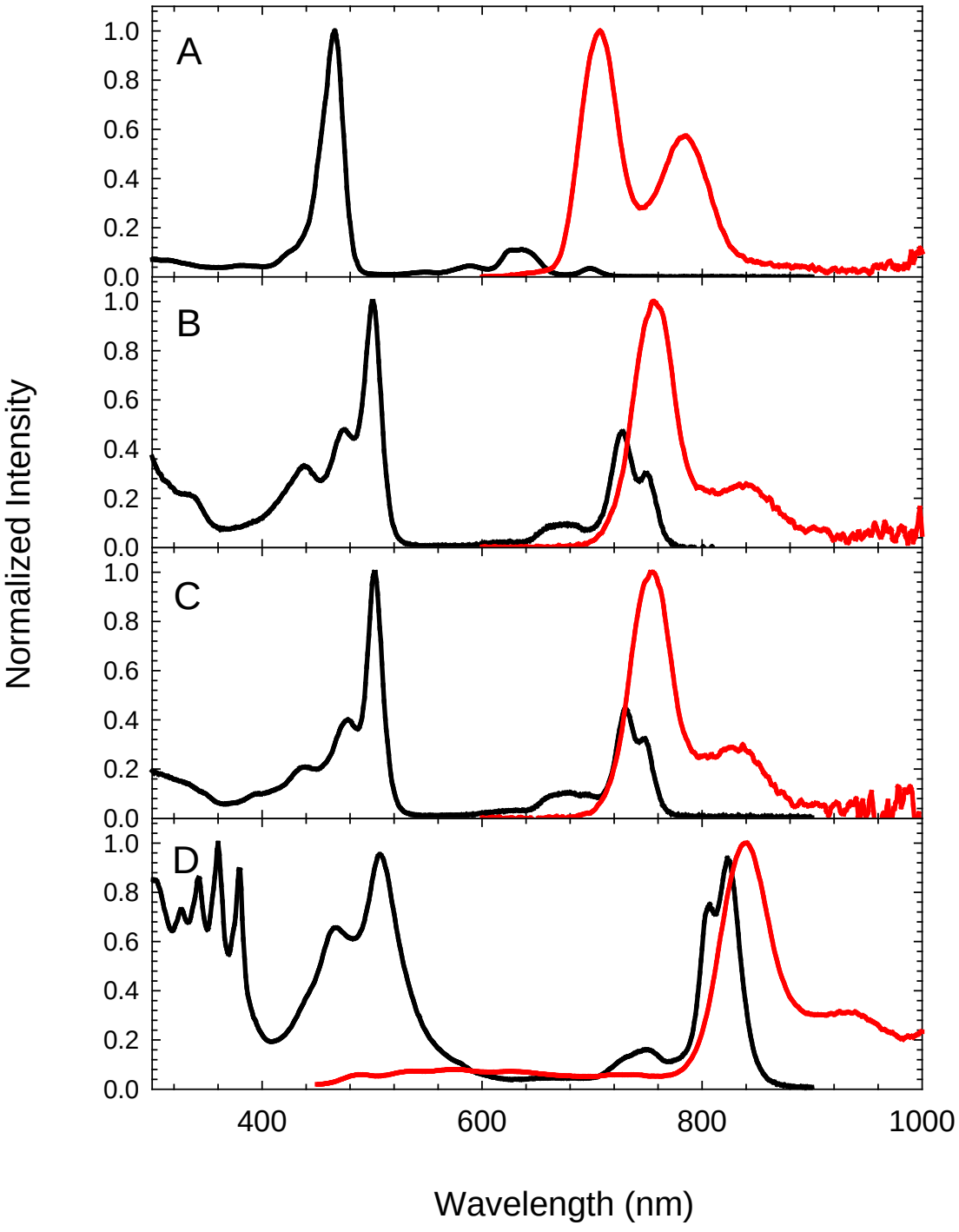

Figure 3-8. Normalized absorption (black) and photoluminescence (red) of Series 1 free-base π-extended porphyrins in toluene: A) H_2TPTBP, B) H_2TPTNP, C) $H_2Ar_4TNP(OMe)_8$, D) H_2Ar_4TAP.

Table 3-3. Photophysical data for series 1 π-extended platinum porphyrins in deoxygenated toluene. Quantum yields were measured relative to ZnTPP (0.04) by excitation at 420 with the exception of Pt-Ar_4TAP which was measured relative to H_2TPTBP (0.041) with excitation at 420 nm. The T_1 lifetimes were obtained by transient absorption spectroscopy.

Platinum Porphyrins	Absorption λ_{max} (Soret, Q-band) nm (ε_{max} = M^{-1} cm^{-1})	Phosphorescence λ_{max} nm	Φ_{phos}	τ_{T-T} (μs)	E_{ST} (eV)
Pt-TPTBP	430, 612 ε_{430} = 1.91 x 10^5 ε_{612}= 1.35 x 10^5	773	46% ±5	29.9	0.33
Pt-TPTNP	436, 689 ε_{436} = 9.17 x 10^4 ε_{689}= 1.50 x 10^5	891	20% ±0.1	12.7	0.34
Pt-Ar_4TNP$(OMe)_8$	455, 690 ε_{455} = 8.30 x 10^4 ε_{690}= 1.32 x 10^5	883	16% ±0.5	15.3	0.32
Pt-Ar_4TAP	455, 762 ε_{455} = 2.99 x 10^4 ε_{762}= 4.64x 10^4	1022	11% ±2	3.2	0.35

Table 3-4. Deactivation rate constants for T_1 state of series 1 π-extended platinum porphyrins in deoxygenated toluene. Radiative decay rate constant (k_r), calculated as $k_r = \varphi_{phos}k$, and the non-radiative decay rate constant ($k_{nr} = k_{ic} + k_{isc}$), calculated as $k_r = k - k_{nr}$.

Platinum Porphyrins	$k = 1/\tau_{T-T}$ (s^{-1})	k_r (s^{-1})	k_{nr} (s^{-1})	τ_{T-T} (μs)
Pt-TPTBP	3.3 x 10^4	1.5 x 10^4	1.8 x 10^4	29.9
Pt-TPTNP	7.9 x 10^4	1.6 x 10^4	6.3 x 10^4	12.7
Pt-Ar_4TNP$(OMe)_8$	6.5 x 10^4	1.0 x 10^4	5.5 x 10^4	15.3
Pt-Ar_4TAP	3.1 x 10^5	3.5 x 10^4	2.8 x 10^5	3.2

The photoluminescence spectra from series 1 π-extended platinum porphyrins are dominated by a single phosphorescence band with a weak vibronic shoulder. The platinum center dramatically increases the rate of ISC from S_1 to the T_1 state via the

heavy atom effect. The porphyrins are now strongly phosphorescent and no longer fluorescent. Moving across the series from Pt-TPTBP to Pt-Ar_4TAP the expected trend based on the energy gap law of a decrease in both the lifetime and quantum yield are observed. The Singlet-Triplet energy splitting (E_{ST}) was calculated from approximating the singlet energy level at the onset of the lowest energy Q-band and the emission maximum and remains relatively constant across the series. The non-radiative rate constant (Table 3-4) increases about 3 times from Pt-TPTBP to the Pt-TNPs and for Pt-Ar_4TAP is an order of magnitude higher compared to Pt-TPTBP. The QYs were measured in deoxygenated toluene using ZnTPP as an actinometer, except for Pt-Ar_4TAP which was measured relative to H_2TPTBP. The T_1 lifetimes were determined from transient absorption spectroscopy.

The photoluminescence spectrum for Pt-TPTBP is identical to that reported in the literature. The reported quantum yield and lifetime (53 μs, 0.70) for Pt-TPTBP by Thompson *et al* are different from our measurements (29.9 μs, 0.43) but in line with those from Kilmant *et al*.[53, 57] However, absent from the literature was a report for a platinum TNP and its photophysical properties. The PL spectra for Pt-TPTNP is red shifted (~100 nm) relative to Pt-TPTBP. The quantum yield (0.20) and lifetime (12.7 μs) are lower compared to that of Pt-TPTBP. Based on a literature report for a palladium octamethoxy substituted TNP it was expected that the PL for Pt-Ar_4TNP$(OMe)_8$ would be red shifted relative to Pt-TPTNP; however this is not observed. The red shift reported in the literature is believed to originate from a push-pull effect created by ester substituents (electron withdrawling) in the 3,5-positions in the *meso*-aryl substituents.[120]

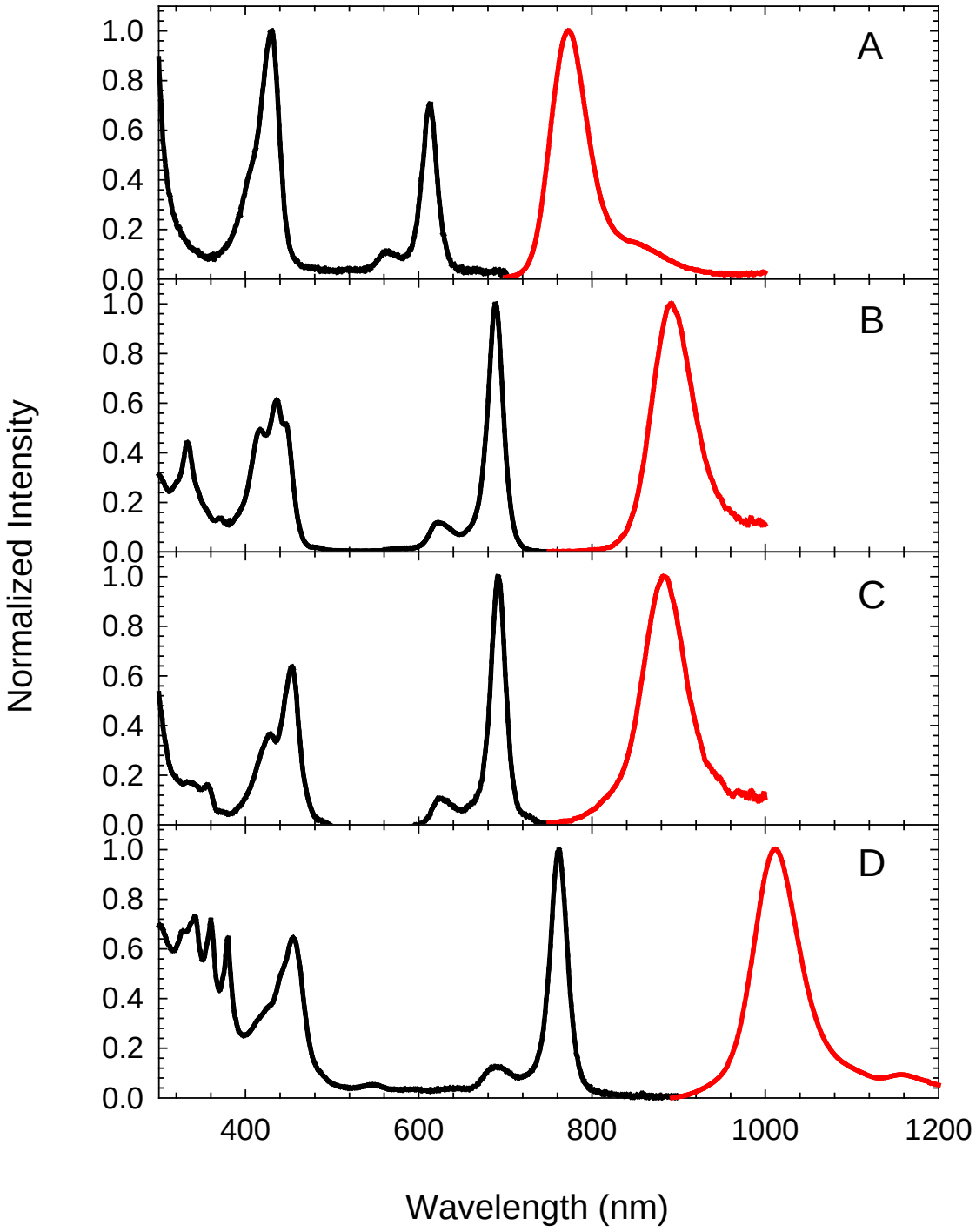

Figure 3-9. Normalized absorption (black) and photoluminescence (red) for series 1 π-extended platinum porphyrins in toluene: A) Pt-TPTBP, B) Pt-TPTNP, C) Pt-Ar_4TNP$(OMe)_8$, D) Pt-Ar_4TAP.

A Pd-TAP derivative has been reported without PL spectra (phosphorescence) in the literature with a QY of less than 0.5% with emission reported at 1.12 eV (1107 nm).

To our knowledge this represents the first full report and photophysical characterization of a phosphorescent TAP and more specifically a platinum TAP. The PL spectrum for Pt-Ar_4TAP is centered at 1022 nm with a life time of 3.2 μs measured by transient absorption spectroscopy. The phosphorescence QY was measured relative to H_2TPTBP as the Soret bands are separated by ~20 nm and S_1 emission (704,788 nm) is in a region of good sensitivity for the near-IR detector. The QY measured for Pt-Ar_4TAP was 11%. Multiple measurements could not be made from the same solution as severe bleaching occurred and so error bars of ~20% are assumed. Nonetheless the room temperature phosphorescence yields of series 1 π-extended platinum porphyrins represent the highest that have ever been reported for materials that emit at approximately ~800, 900, and 1000 nm regions of the near-IR.

Series 1- PLED Device Results

PLEDs were fabricated by the Reynolds group (Ken Graham) at the University of Florida. Spin-coating the active layer on top of a PEDOT:PSS layer, followed by evaporation of the metal electrode materials to give the following device structure: glass/ITO/PEDOT:PSS(40 nm)/2% Pt-porphyrin:PVK:PBD(7:3) (110 nm)/LiF(1 nm)/Ca(10 nm)/Al. However, PLEDs fabricated with this device structure displayed very poor performance for Pt-Ar_4TAP. A hybrid device structure adopted by thermal vapor deposition of an ETL (Bphen) to give a new device structure of glass/ITO/PEDOT:PSS(40 nm)/PVK:PBD(7:3):2% Pt-Ar_4TAP(110 nm)/Bphen(40 nm)/LiF(1 nm)/Al was used in efforts to increase device efficiency.

Electroluminescence (EL) across the series for series 1 PLEDs is centered at 771, 898, 892, and 1005 nm for Pt-TPTBP, Pt-TPTNP, Pt-Ar_4TNP$(OMe)_8$, and Pt-Ar_4TAP respectively with no host emission observed (Figure 3-10A). Light emission from the

PLEDS turns on at an applied voltage of ~8-17 V observed in the *R*-V plot (Figure 3-10C). Similar current densities are observed in the *J*-V plot (Figure 3-10B) but expected as only the near-IR phosphor is changing in the device structures. Overall the PLEDs operate at relatively high voltages due to the thickness of the emissive layer and the high electron and hole injection barriers.

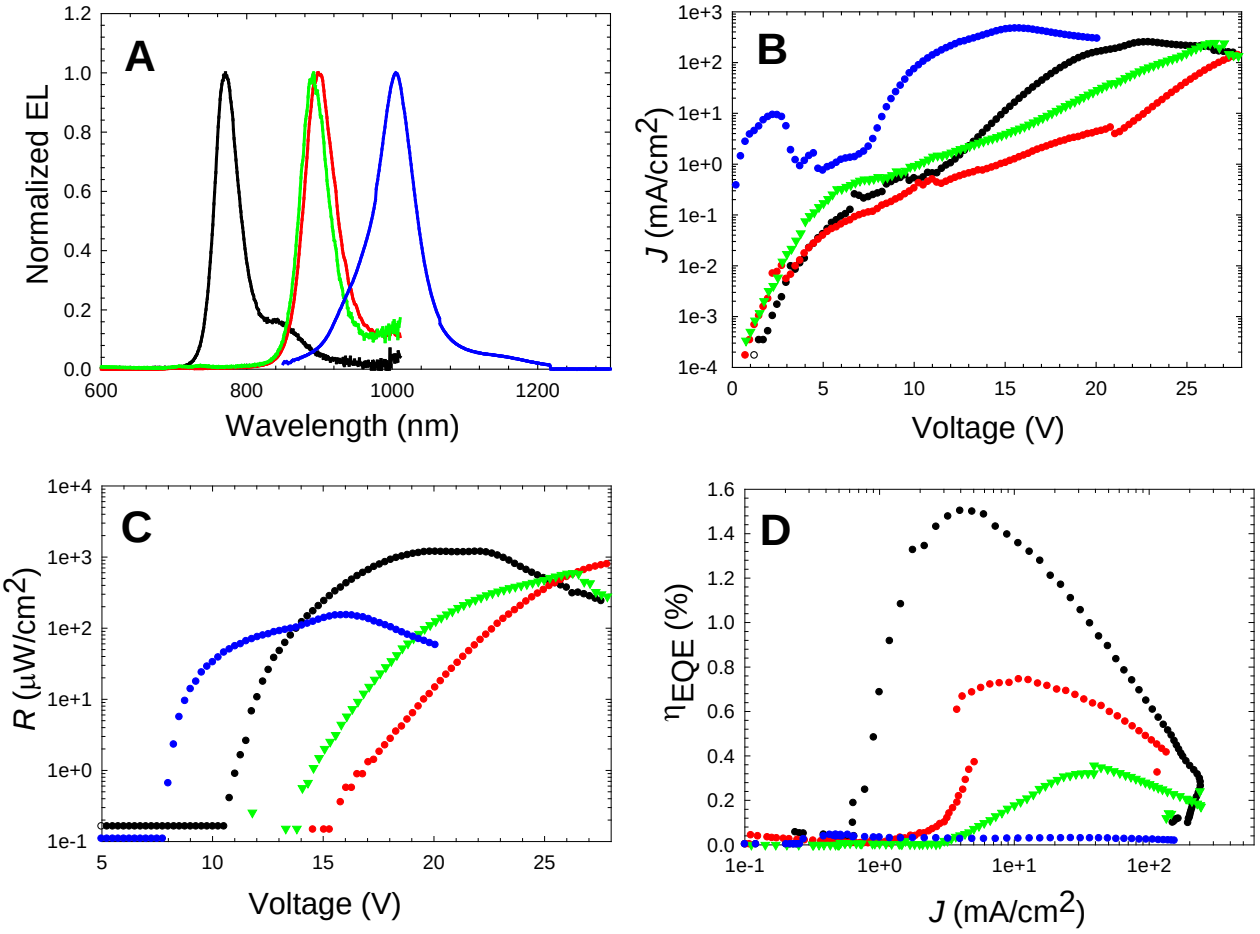

Figure 3-10. PLED device results for series 1 π-extended platinum porphyrins. Pt-TPTBP (black), Pt-TPTNP (red), Pt-Ar_4TNP$(OMe)_8$ (green), and Pt-Ar_4TAP (blue) with the following device structure: glass/ITO/PEDOT:PSS(40 nm)/2% Pt-porphyrin:PVK:PBD(7:3) (110 nm)/LiF(1 nm)/Ca(10 nm)/Al. A) EL spectra for PLEDs, B) *J*-V plot, C) *R*-V plot, D) External quantum efficiency.

Although the hybrid PLED device structure for Pt-Ar_4TAP has a significantly lower turn on voltage due to the ETL (Figure 3-11B). The PLEDs across the series exhibit

maximum radiant emittance of approximately 100-1000 μW/cm^2. The maximum external quantum efficiencies (EQE) for the series range from 0.04-1.5%. The PLED fabricated from Pt-TPTBP gave the highest EQE while Pt-Ar$_4$TAP gave the lowest EQE of 0.04% shown in Figure 3-10D. The Pt-TPTNP and Pt-Ar$_4$TNP(OMe)$_8$ based PLEDs gave maximum EQE values of 0.74 and 0.36%.

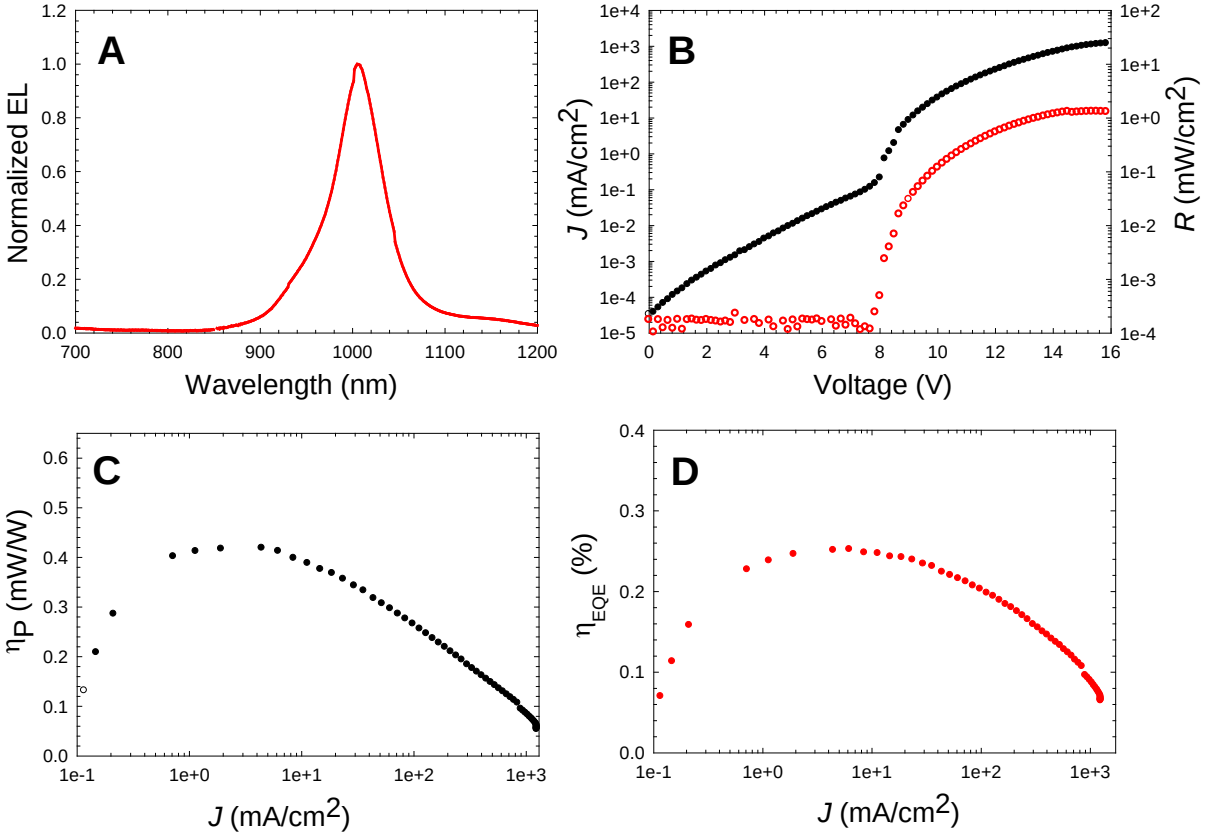

Figure 3-11. Hybrid PLED device for Pt-Ar$_4$TAP with device structure: glass/ITO/PEDOT:PSS(40 nm)/PVK:PBD(7:3):2% Pt-Ar$_4$TAP(110 nm)/Bphen(40 nm)/LiF(1 nm)/Al. A) EL spectrum, B) *J*-V plot (closed circles) and *R*-V (open circles), C) Power efficiency, D) External quantum efficiency.

The device performance of Pt-Ar$_4$TAP in the hybrid PLED device structure is shown in Figure 3-11. EL from the device is identical to that from the Pt-Ar$_4$TAP based PLED (Figure 3-11A). The device featured maximum radiant emittance of ~1 mW/cm^2 at approximately 12 volts shown in Figure 3-11B. The maximum EQE value (Figure 3-11D)

for the hybrid device was ~0.25 which is around 5 times higher than the Pt-Ar_4TAP based PLED.

Series 1- OLED Device Results

Due to the high molecular weight of Pt-Ar_4TNP$(OMe)_8$ and Pt-Ar_4TAP thermal vapor deposition for OLEDs was not possible. Thus, OLEDs were only constructured using Pt-TPTBP and Pt-TPTNP. Thompson *et al* have previously reported an OLED using Pt-TPTBP as the near-IR phosphor with an overall EQE of 8.5%.[53, 67] Multilayer OLEDs were fabricated by the Xue group at the University of Florida (Yixing Yang) with Pt-TPTBP having the following device structure: ITO/NPB(40 nm)/Alq_3:4% Pt-TPTBP(25 nm)/Bphen(80 nm)/LiF(1 nm)/Al. Another multilayer device was fabricated with Pt-TPTNP representing the first reported use of this material in an OLED with the following device structure: ITO/NPB(40 nm)/CBP:8% Pt-TPTNP(20 nm)/Bphen(100 nm)/LiF(1 nm)/Al.

Electroluminescence from the Pt-TPTBP and Pt-TPTNP OLEDs is centered at 773 nm and 890 nm, respectively, similar to the EL for the respective PLEDs (Figure 3-12A). The *R*-V plot (Figure 3-12B) shows that light emission for both devices is observed at a rather low turn on voltage of ~2 V. The maximum radiant emittance for the Pt-TPTBP based OLED is 1 mW/cm^2 obtained at ~12V (Figure 3-11B). Similarly the maximum radiant emittance of the Pt-TPTNP based OLED is 1 mW/cm^2 obtained at ~10 V (Figure 3-11B). The EQE data shown in Figure 3-12D for the OLED fabricated with Pt-TPTBP gave a maximum EQE of 8.0%, in good agreement with the literature value of 8.5%. The Pt-TPTNP based OLED displays a maximum EQE of 3.8%. The lower EQE of a Pt-TPTNP based OLED relative to a Pt-TPTBP based OLED follows the trend for the phosphorescence QYs and lifetimes of the materials (3.8%, 0.201, and 12.7 μs) and

(8.0%, 0.459, and 29.9 μs) respectively. Although the EQE value for Pt-TPTNP based OLEDs is lower it represents a new record for devices emitting beyond 800 nm.

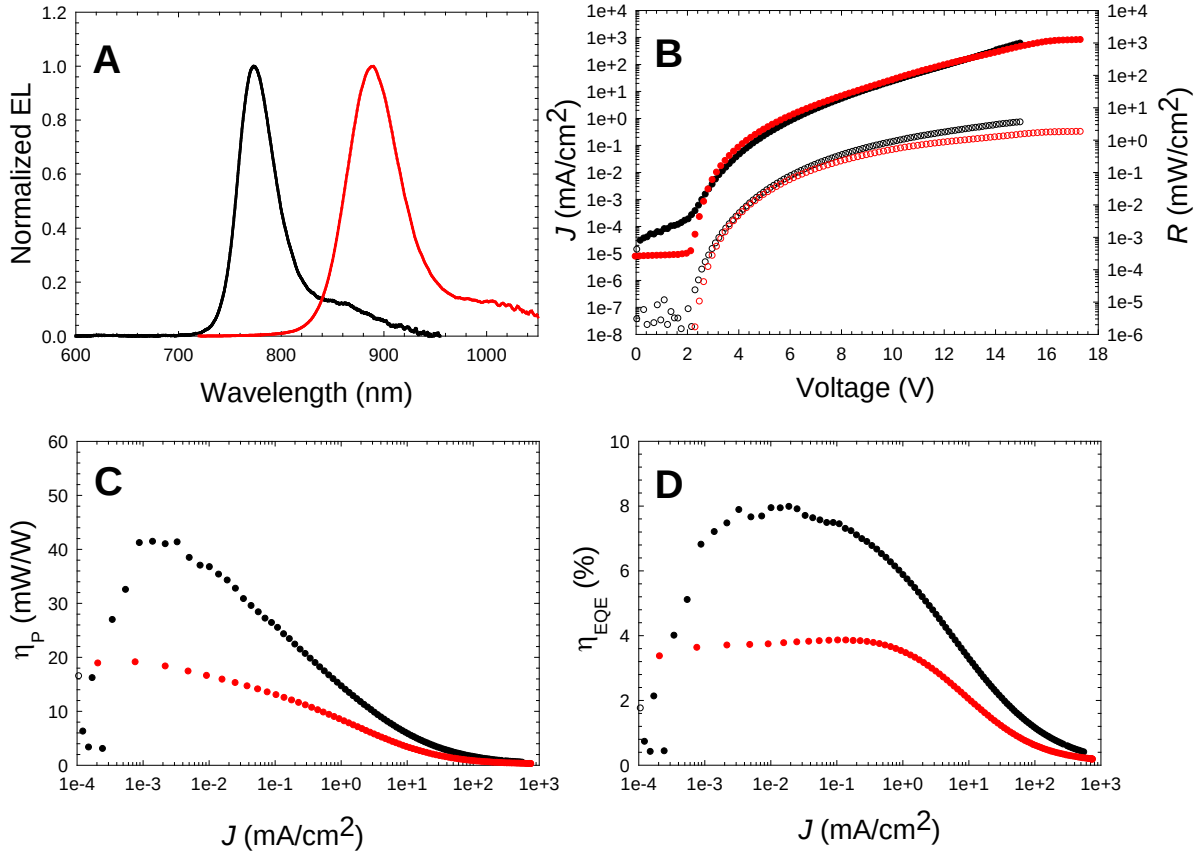

Figure 3-12. OLED device results for series 1 π-extended platinum porphyrins. Pt-TPTBP (black), Pt-TPNP (red), with device structures: glass/ITO/NPB(40 nm)/Alq_3:4% Pt-TPTBP(25 nm)/Bphen(80 nm)/LiF(1 nm)/Al and glass/ITO/NPB(40 nm)/CBP:8% Pt-TPTNP(20 nm)/Bphen(100 nm)/LiF(1 nm)/Al. A) EL spectra for OLEDs, B) *J*-V plot (closed circles) and *R*-V (open circles), C) Power efficiency, D) External quantum efficiency.

Series 2- Photophysical Properties

The recent report of Pd-5,15-diaryl-TBPs by Vinogradov *et al* is the primary basis for developing the free-base and Pt-TBPs for series 2 outlined in Figure 3-13.[61] They report the solution phosphorescence QY for Pd-DPTBP to be twice that of Pd-TPTBP and half that of a soluble *meso*-unsubstituted Pd-TBP. This trend is observed due to an increase in macrocycle planarity which decreases the non-radiative decay rate thus

increasing the lifetime and QY. Ikai *et al* have also reported that 3,5-di-*tert*-butylphenyl *meso*-aryl substituents provide facial sterics leading to enhanced device efficiency in platinum porphyrin based LEDs.[78] The following series was developed to expand the known literature work on Pt-TBPs. It is expected, that the Pt-5,15-diaryl-TBPs will exhibit a QY twice that of Pt-TPTBP and Pt-Ar_4TBP based on an increase in the planarity of the macrocycle. Also examined are the effect of bulky *meso*-aryl substituents (3,5-^{t}BuPh) on device efficiency across the series. This represents the first known report for the synthesis and photophysical characterization of platinum 5,15-diaryl-TBPs.

Series 2

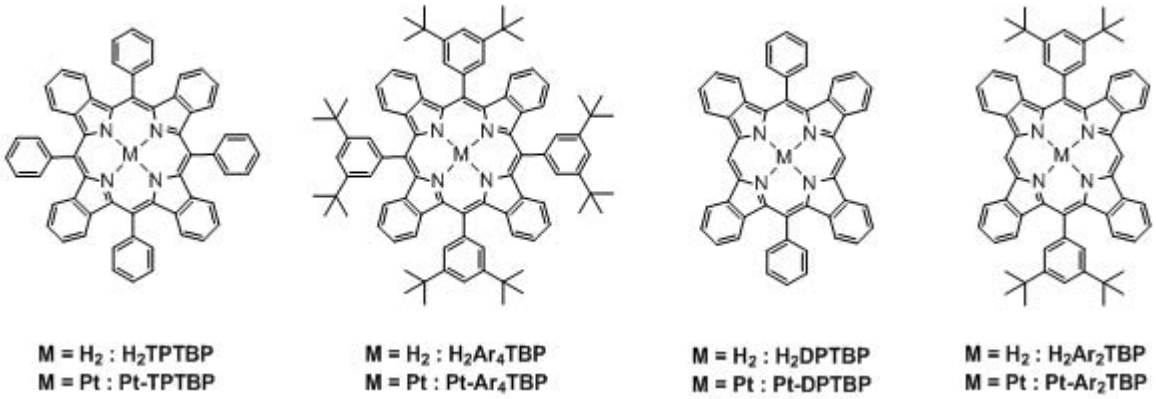

Figure 3-13. Structures of free-base and platinum complexes for series 2 TBPs.

The absorption and photoluminescence in air saturated toluene for series 2 free-base TBPs is shown in Figure 3-14. The absorption spectra for H_2TPTBP and H_2DPTBP are identical to those previously reported in the literature. The absorption spectra for H_2Ar_4TBP and H_2Ar_2TBP are identical to the respective phenyl derivatives with only a small red shift observed (1-2 nm) in each case. In both diaryl- and tetraryl-TBPs the Soret band is strongly allowed in the visible region with high molar absorptivity values (2-3 x 10^5 M^{-1} cm^{-1}). The absorption spectra for H_2DPTBP and H_2Ar_2TBP show well

resolved vibronic structure in both the Soret and Q-band. The large splitting (841 cm^{-1}) in the Soret band of 5,15-diaryl TBPs is attributed to the strong mixing of the Soret and Q-band states.[19, 121, 122] These spectra resemble red shifted *meso*-unsubstituted TBPs and strongly suggest there is little difference in macrocycle planarity between 5,15-diaryl TBPs and *meso*-unsubstituted TBPs. This increase in planarity results in both the absorption and PL being sharper and blue shifted relative to the tetraaryl derivatives. The photophysical data for series 2 free-base TBPs is summarized below in Table 3-5.

Table 3-5. Photophysical properties of Series 2 free-base TBPs in air saturated toluene. Fluorescence quantum yields were measured relative to ZnTPP (0.04) with excitation at 420 nm in toluene. The S_1 decays were obtained by single photon counting method.

Free-base Porphyrins	Absorption λ_{max} (Soret, Q-band) nm (ε_{max} = M^{-1} cm^{-1})	Fluorescence λ_{max} nm	φ_{fl}	τ_{fl} (ns)
H_2TPTBP	465, 633 ε_{465} = 3.03 x 10^5 ε_{633}= 3.32 x 10^4	704, 785	4.1% ±0.1	3.1
H_2Ar_4TBP	462, 630 ε_{462} = 3.21 x 10^5 ε_{630}= 4.14 x 10^4	701, 779	4.3% ±0.1	3.5
H_2DPTBP	440, 612 ε_{440} = 3.62 x 10^5 ε_{612}= 6.81 x 10^4	671, 738	37% ±4.0	10.6
H_2Ar_2TBP	440, 612 ε_{440} = 3.83 x 10^5 ε_{612}= 6.70 x 10^4	671, 738	38% ±4.0	10.3

The absorption and photoluminescence in deoxygenated toluene for series 2 platinum TBPs is shown in Figure 3-15. The photophysical data for series 2 platinum TBPs is summarized and reported in Table 3-7. The absorption spectra for series 2 platinum TBPs are blue shifted relative to the free-base TBPs and indicative of porphyrins with local D_{4h} symmetry (metal center).

Table 3-6. Deactivation rate constants for S_1 state of series 2 free-base TBPs in air saturated toluene. Radiative decay rate constant (k_r), calculated as $k_r = \varphi_{fl}k$, and the non-radiative decay rate constant ($k_{nr} = k_{ic} + k_{isc}$), calculated as $k_r = k - k_{nr}$.

Free-base Porphyrins	$k = 1/\tau_{fl}$ (s^{-1})	k_r (s^{-1})	k_{nr} (s^{-1})	τ_{fl} (ns)
H_2TPTBP	3.2×10^8	1.3×10^7	3.1×10^8	3.1
H_2Ar_4TBP	2.9×10^8	1.2×10^7	2.7×10^8	3.5
H_2DPTBP	9.4×10^7	3.5×10^7	5.9×10^7	10.6
H_2Ar_2TBP	9.7×10^7	3.7×10^7	6.0×10^7	10.3

Table 3-7. Photophysical data for series 2 platinum TBPs in deoxygenated toluene. Quantum yields were measured relative to ZnTPP (0.04) by excitation at 420 nm in toluene. The T_1 lifetimes were obtained by transient absorption spectroscopy.

Platinum Porphyrins	Absorption λ_{max} (Soret, Q-band) nm ($\varepsilon_{max} = M^{-1}\ cm^{-1}$)	Phosphorescence λ_{max} nm	Φ_{phos}	$\tau_{T\text{-}T}$ (μs)
Pt-TPTBP	430, 612 $\varepsilon_{430} = 1.91 \times 10^5$ $\varepsilon_{612} = 1.35 \times 10^5$	773	46% ±5	29.9
Pt-Ar_4TBP	432, 610 $\varepsilon_{432} = 1.81 \times 10^5$ $\varepsilon_{610} = 1.05 \times 10^5$	772	44% ±0.3	32.0
Pt-DPTBP	409, 604 $\varepsilon_{409} = 2.68 \times 10^4$ $\varepsilon_{604} = 2.13 \times 10^4$	770	40% ±2	28.0
Pt-Ar_2TBP	410, 604 $\varepsilon_{410} = 1.73 \times 10^5$ $\varepsilon_{604} = 1.32 \times 10^5$	770	65% ±8	53.0

As expected the absorption spectra for Pt-TPTBP and Pt-Ar_4TBP are virtually identical. The vibronic structure observed in the Q-bands for platinum 5,15-diaryl TBPs most likely results from the unsymmetrical nature of the macrocycle. As stated earlier the insertion of the metal makes the Q-band transition more allowed with the molar absorptivity

constants in the platinum 5,15-diaryl TBPs being ~20% higher than Pt-TPTBP or Pt-Ar_4TBP. The Soret band is the most intense transition (1-2 x 10^5 M^{-1} cm^{-1}) across the series in the absorption spectra located in the visible region. The very low solubility of Pt-DPTBP is likely the reason for the low ε value.

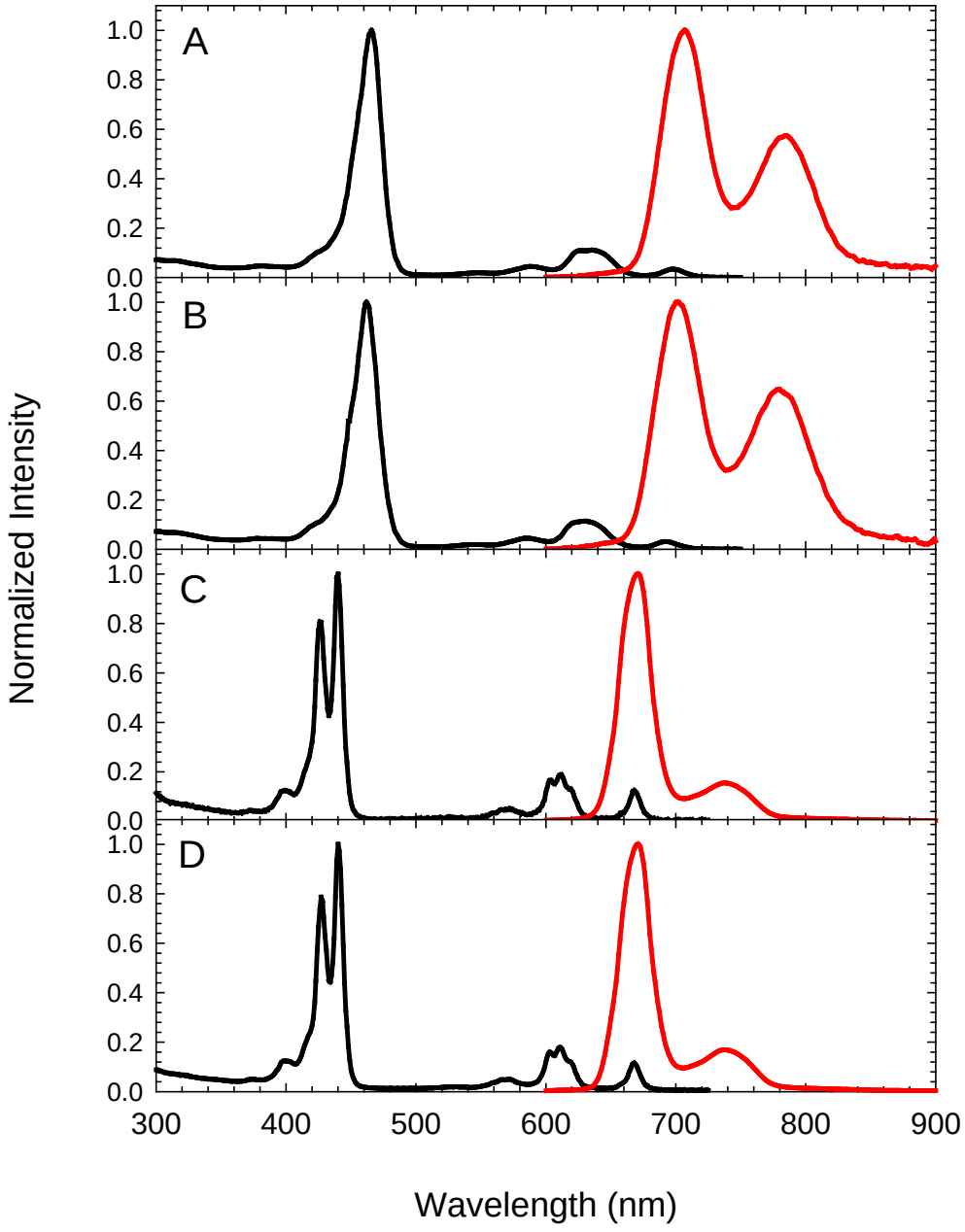

Figure 3-14. Normalized absorption (black) and photoluminescence (red) of series 2 free-base TBPs in toluene: A) H_2TPTBP, B) H_2Ar_4TBP, C) H_2DPTBP, D) H_2Ar_2TBP.

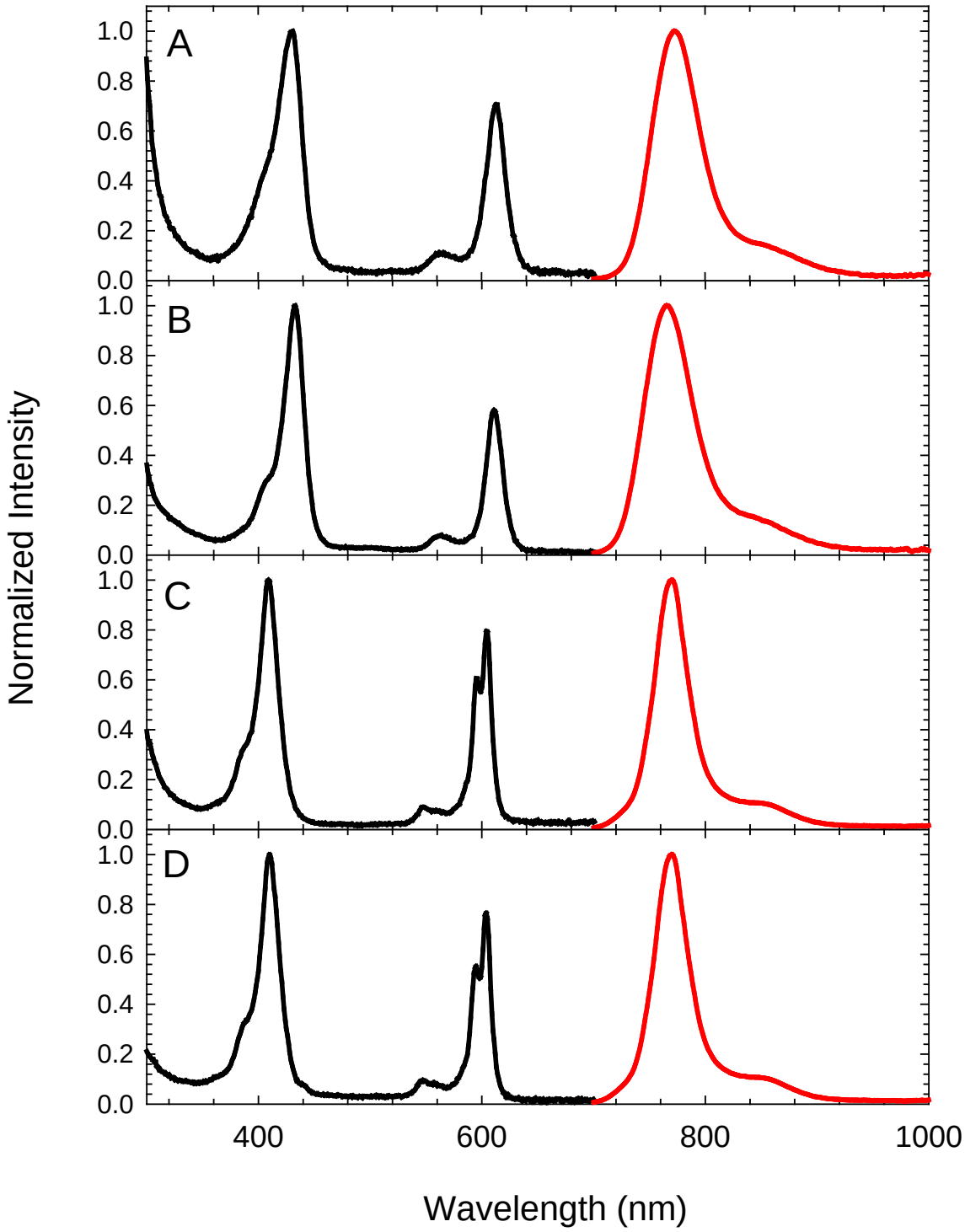

Figure 3-15. Normalized absorption (black) and photoluminescence (red) for series 2 platinum TBPs in toluene: A) Pt-TPTBP, B) Pt-Ar_4TBP, C) Pt-DPTBP, D) Pt-Ar_2TBP.

The photoluminescence spectra for series 2 platinum TBPs are shown in Figure 3-15. The PL spectra are dominated by a single phosphorescence band with a weak vibronic shoulder. The maximum emission wavelengths for Pt-TPTBP and Pt-Ar_4TBP are centered at 773 and 772 nm respectively. The PL spectra for Pt-DPTBP and Pt-Ar_2TBP are slightly blue shifted (770 nm) and have a narrower full width at half maximum (FWHM) due to the increased planarity of the TBP macrocycle. The T_1 lifetimes for the entire series were measured by transient absorption spectroscopy. The values for Pt-TPTBP and Pt-Ar_4TBP as expected gave very similar T_1 lifetimes of 29.9 and 32.0 μs respectively. The QYs should be very similar as they are directly proportional to the lifetimes. The QYs were measured relative to ZnTPP (0.04) in toluene for Pt-TPTBP and Pt-Ar_4TBP to give values of 0.46 and 0.44 respectively. This is in good agreement with the lifetime data and reported values.[57]

However the lifetime and QY measured for Pt-DPTBP was not expected based on the recent trend observed in the Pd-TBPs reported by Vinogradov *et al* discussed herein elsewhere. The T_1 lifetime (28.0 μs) and phosphorescence QY (0.40) for Pt-DPTBP are nearly identical to Pt-TPBP and Pt-Ar_4TBP. The QY was expected to increase (~double) due to the increased macrocycle planarity and reduction of the non-radiative decay rate (Table 3-8). However, other literature reports exist suggesting that the rotation of the *meso*-phenyl substituent serves as a non-radiative decay path way negating the effects of increased planarity.[43, 78] Once this rotation is blocked (i.e. bulky group) the observed T_1 lifetime increases as in the case of Pt-Ar_2TBP (53.0 μs). The QY for Pt-Ar_2TBP (0.65) has been measured as high as 0.90 but difficulty exists in reproducing this measurement. A decrease in the non-radiative decay rate (k_{nr}) from

the increased planarity is observed (Table 3-8). Pt-Ar_2TBP has the highest PL efficiency ever reported for a phosphor in this wavelength region.

Table 3-8. Deactivation rate constants for T_1 state of series 2 platinum TBPs in deoxygenated toluene. Radiative decay rate constant (k_r), calculated as $k_r = \varphi_{phos}k$, and the non-radiative decay rate constant ($k_{nr} = k_{ic} + k_{isc}$), calculated as $k_r = k - k_{nr}$.

Platinum Porphyrins	$k = 1/\tau_{T-T}$ (s^{-1})	k_r (s^{-1})	k_{nr} (s^{-1})	τ_{T-T} (μs)
Pt-TPTBP	3.3×10^4	1.5×10^4	1.8×10^4	29.9
Pt-Ar_4TBP	3.1×10^4	1.4×10^4	1.8×10^4	32.0
Pt-DPTBP	3.6×10^4	1.4×10^4	2.1×10^4	28.0
Pt-Ar_2TBP	1.9×10^4	1.2×10^4	6.5×10^3	53.0

Series 2- PLED Device Results

PLEDs were fabricated by spin-coating the active layer on top of a PEDOT:PSS layer, followed by evaporation of the metal electrode materials to give the following device structure: glass/ITO/PEDOT:PSS(40 nm)/2% Pt-porphyrin:PVK:PBD(7:3) (110 nm)/LiF(1 nm)/Ca(10 nm)/Al. Due to the limited solubility of Pt-DPTBP it was excluded from device fabrication.

Electroluminescence from the PLEDs is centered at ~770 nm with no host emission observed (Figure 3-16A). Light emission from the PLEDS turns on at an applied voltage of ~12 V observed in Figure 3-16C. Overall the PLEDs operate at relatively high voltages due to the thickness of the emissive layer (110 nm) and the high electron and hole injection barriers. The PLEDs exhibit maximum radiant emittance of approximately 1000 μW/cm^2 (Figure 3-16C). The maximum external quantum efficiencies for the series range from 1.0-1.5%. The PLED fabricated from Pt-TPTBP gave the highest EQE (1.50%) while Pt-Ar_4TBP gave a slightly lower EQE of 1.05%.

Although Pt-Ar_2TBP has a much higher solution phosphorescence quantum yield the PLED EQE is slightly lower (1.43%) than that of Pt-TPTBP.

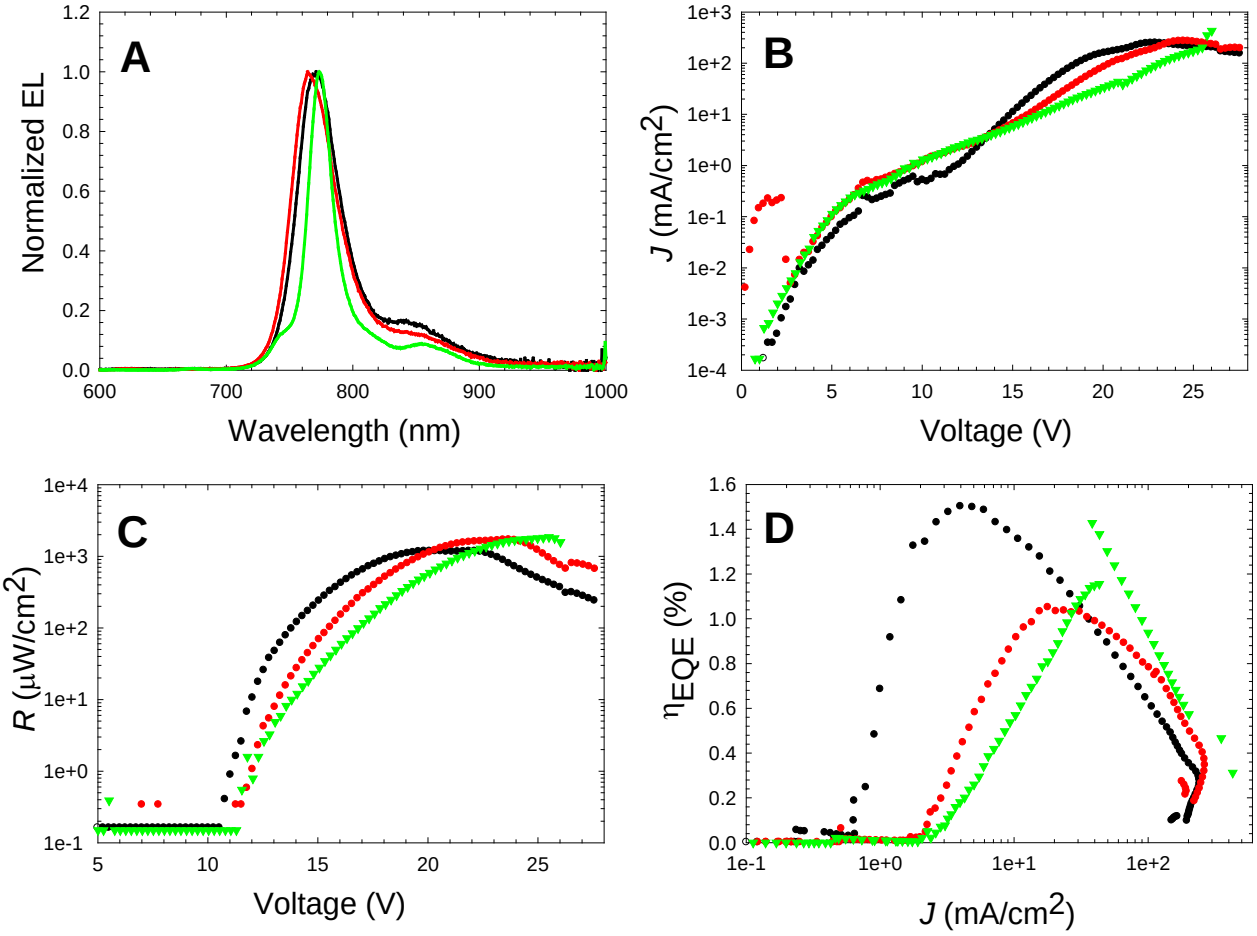

Figure 3-16. PLED device results for series 2 platinum TBPs. Pt-TPTBP (black), Pt-Ar_4TBP (red), and Pt-Ar_2TBP (green) with the following device structure: glass/ITO/PEDOT:PSS(40 nm)/2% Pt-porphyrin:PVK:PBD(7:3) (110 nm)/LiF(1 nm)/Ca(10 nm)/Al. A) EL spectra, B) *J*-V plot, C) *R*-V plot, D) External quantum efficiency.

Series 2- OLED Device Results

Multilayer OLEDs were fabricated from thermal vapor deposition to give the following device structure: glass/ITO/NPB(40 nm)/Alq_3:4% Pt-TBP(25 nm)/Bphen(80 nm)/LiF(1 nm)/Al for series 2 platinum TBPs. Electroluminescence from the OLEDs is centered at ~770 nm and is shown in Figure 3-17A. Light emission is observed at a

rather low turn on voltage of ~2 V with the maximum radiant emittance of 1 mW/cm^2 obtained at ~12V (Figure 3-17B). The current densities across the series are similar and expected due to little difference in the device structure with the only changes coming from substituent patterns in the platinum TBPs (Figure 3-17B).

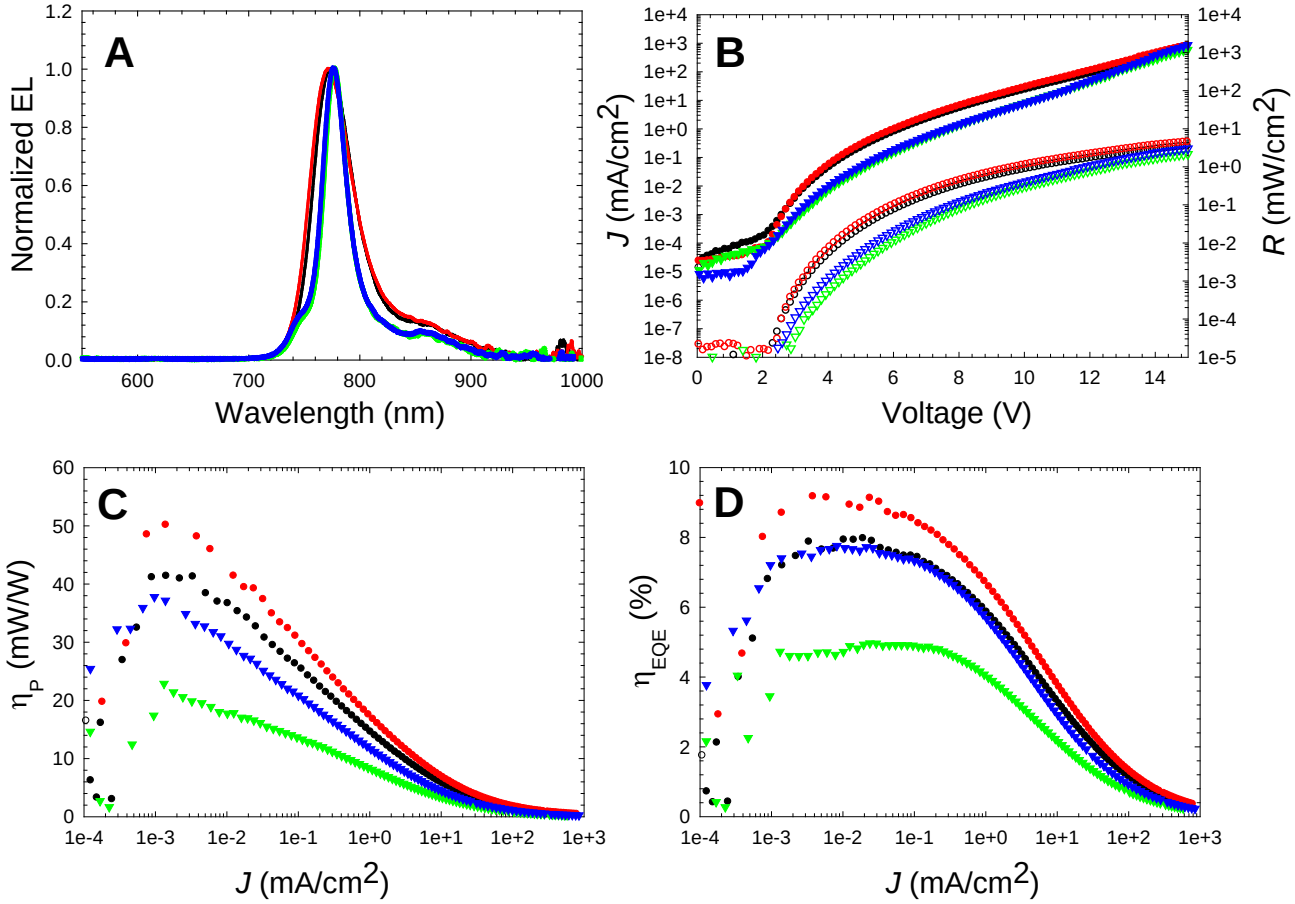

Figure 3-17. OLED device results for series 2 platinum TBPs. Pt-TPTBP (black), Pt-Ar_4TBP (red), Pt-DPTBP (green), and Pt-Ar_2TBP (blue) with device structure: glass/ITO/NPB(40 nm)/Alq_3:4% Pt-TBP(25 nm)/Bphen(80 nm)/LiF(1 nm)/Al. A) EL spectra for OLEDs, B) *J*-V plot (closed circles) and *R*-V (open circles), C) Power efficiency, D) External quantum efficiency.

The EQE data shown in Figure 3-17C for the series follows a different trend than the PLED EQE data. In contrast to the PLED data, Pt-Ar_4TBP gave a higher maximum EQE (9.2%) than Pt-TPTBP (8.0%). Although Pt-DPTBP was not soluble enough for PLED fabrication it was readily incorporated into a multilayer OLED giving a maximum

EQE of 5.0%. The significantly lower efficiency is likely due to bimolecular interactions or aggregates of Pt-DPTBP within the host matrix. Interestingly the T_1 lifetimes and phosphorescence QYs for Pt-TPTBP, Pt-Ar_4TBP and Pt-DPTBP are nearly identical. However, these materials give maximum OLED EQEs ranging from 5.0-9.2%. The differences in efficiency are likely due to some physical property of the porphyrin or porphyrin:host morphology.

Thompson *et al* have shown that platinum porphyrins with high phosphorescence QYs like Pt-OEP (0.45) give higher maximum EQEs (1.3%) in OLEDs compared to Pt-DPP (0.16, 0.25%).[43] However, despite the significant increase in the solution QY for Pt-Ar_2TBP the maximum EQE (7.8%) is comparable to that of Pt-TPTBP (8.0%).

Series 3- Photophysical Properties

The EQE data for series 2 OLEDs strongly suggest some form of aggregation of the phosphor or phosphor: host incompatibility from a morphology standpoint. Recent literature reports of both porphyrin systems and other dyes have displayed improvement in device efficiencies through the addition of bulky substituents.[69, 71, 73, 77, 78] This creates a dye encapsulation effect that prevents self-quenching mechanisms. The platinum TBPs in series 3 were designed in order to examine the effects of bulky substituents on the photophysical properties and device efficiencies shown and are shown Figure 3-18.

The absorption and photoluminescence in air saturated toluene for series 3 free-base TBPs is shown in Figure 3-19. The absorption and emission wavelength maxima for series 3 free-base TBPs are summarized in Table 3-9 along with the molar absorption coefficients, QYs and S_1 lifetimes. The Soret and Q-band for H_2ArF_4TBP are each red shifted about 10 nm and they resemble the absorption spectrum for H_2TPTBP.

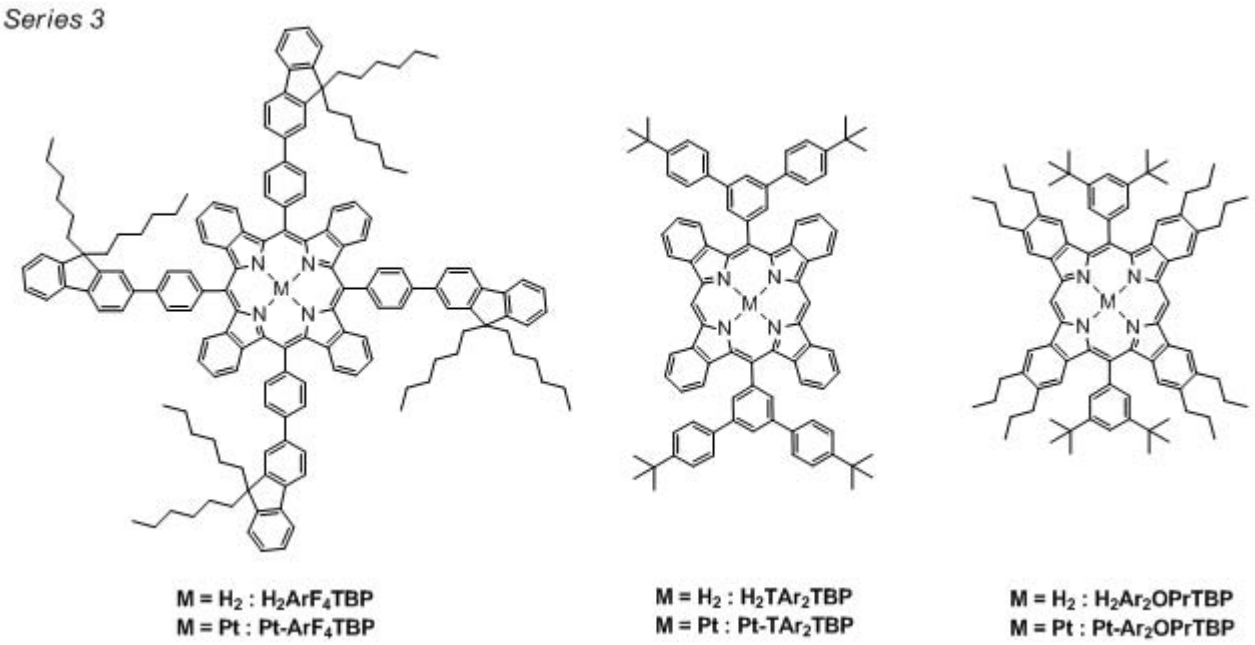

Figure 3-18. Structures of free-base and platinum complexes for series 3 TBPs.

This trend is similar to the reported H_2TPP and H_2TPP-Fluorenyl derivatives.[77] Aside from the red shift in the Soret and Q-band the addition of the fluorenyl-substituents contributes to an additional absorption at ~300 nm. The Soret bands for H_2TAr_2TBP and $H_2Ar_2OPrTBP$ both display a small red shift of 2 and 5 nm respectively relative to H_2DPTBP. The Q-bands however are not red shifted and identical to H_2DPTBP. The molar absorptivity values measured for series 3 free-base TBPs are in line with the values obtained for series 2.

The PL spectra in air saturated toluene are shown in Figure 3-19. The emission maxima for H_2ArF_4TBP is red shifted 7 nm relative to H_2TPTBP. The lower energy band is also significantly higher in intensity than in H_2TPTBP (Appendix A-6). This suggests the fluorenyl-substituents are increasing the saddling of the TBP macrocycle leading to the observed shorter lifetime. Consequently a smaller quantum yield relative to

H_2TPTBP would be expected however the increase is probably attributed to a reduction in solution interactions similar to the reported TPP derivatives.[77]

Table 3-9. Photophysical properties of Series 3 free-base TBPs in air saturated toluene. The fluorescence quantum yield for H_2ArF_4TBP was measured relative to ZnTPP (0.04) with excitation at 420 nm in toluene. The fluorescence quantum yield for H_2TAr_2TBP and $H_2Ar_2OPrTBP$ was measured relative to H_2Ar_2TBP (0.38) with excitation at 420 nm in toluene. The S_1 decays were obtained by single photon counting method.

Free-base Porphyrins	Absorption λ_{max} (Soret, Q-band) nm (ε_{max} = M^{-1} cm^{-1})	Fluorescence λ_{max} nm	Φ_{fl}	τ_{fl} (ns)
H_2ArF_4TBP	474, 642 ε_{474} = 3.03 x 10^5 ε_{642}= 3.63 x 10^4	711, 788	6.0% ±0.4	2.8
H_2TAr_2TBP	442, 612 ε_{442} = 3.43 x 10^5 ε_{612}= 5.68 x 10^4	670, 735	39% ±1	10.4
$H_2Ar_2OPrTBP$	445, 625 ε_{445} = 3.22 x 10^5 ε_{625}= 7.23 x 10^4	674, 743	43% ±3	10.6

Table 3-10. Deactivation rate constants for S_1 state of series 3 free-base TBPs in air saturated toluene. Radiative decay rate constant (k_r), calculated as $k_r = \varphi_{fl}k$, and the non-radiative decay rate constant ($k_{nr} = k_{ic} + k_{isc}$), calculated as $k_r = k - k_{nr}$.

Free-base Porphyrins	$k = 1/\tau_{fl}$ (s^{-1})	k_r (s^{-1})	k_{nr} (s^{-1})	τ_{fl} (ns)
H_2ArF_4TBP	3.6 x 10^8	2.1 x 10^7	3.4 x 10^8	2.8
H_2TAr_2TBP	9.6 x 10^7	3.8 x 10^7	5.8 x 10^7	10.4
$H_2Ar_2OPrTBP$	9.4 x 10^7	4.1 x 10^7	5.4 x 10^7	10.6

The fluorescence QY and S_1 lifetime for H_2TAr_2TBP and $H_2Ar_2OPrTBP$ are identical to that of H_2Ar_2TBP. Replacing the *tert*-butyl substituents on the *meso*-aryl substituents of H_2Ar_2TBP with 4-*tert*-butylphenyl to give H_2TAr_2TBP has shown to reduce solution interactions thus increasing the QY in TPP derivatives but was not

expected to significantly increase the QY, but may prevent aggregation in solid state films.[77] The choice of the propyl-substituents in $H_2Ar_2OPrTBP$ was determined from X-ray crystallography data reported for free-base 5,15-diaryl porphyrins in efforts to interrupt the dominant offset π-stacking in the crystal structures.[123] The emission maxima for H_2TAr_2TBP (670 nm) is identical to H_2DPTBP. The PL spectrum of $H_2Ar_2OPrTBP$ is red shifted ~4 nm and it is unclear if this is from an inductive effect from the propyl groups or an out of plane distortion of the macrocycle.

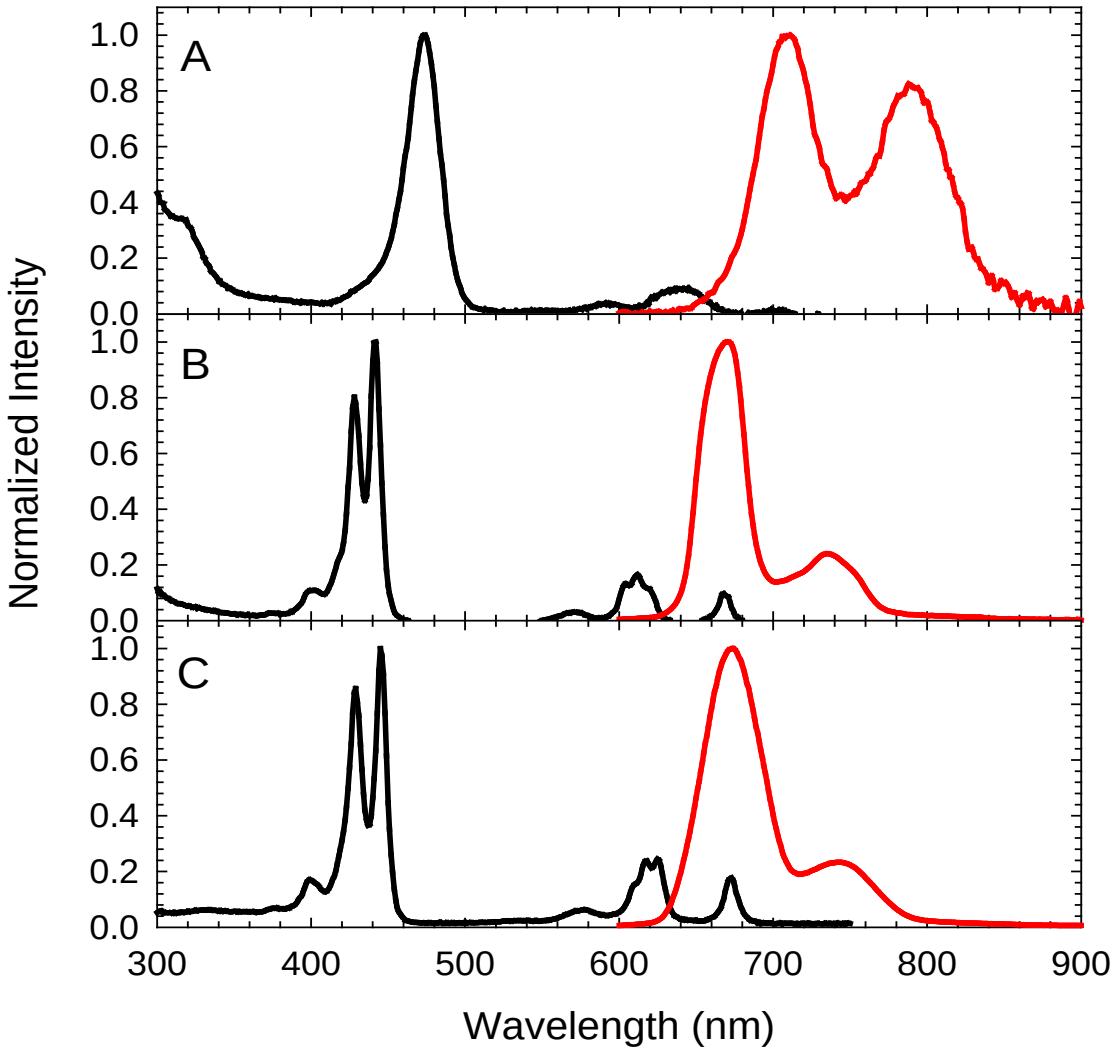

Figure 3-19. Normalized absorption (black) and photoluminescence (red) for series 3 free-base TBPs in air saturated toluene: A) H_2ArF_4TBP, B) H_2TAr_2TBP, C) $H_2Ar_2OPrTBP$.

The absorption and photoluminescence in deoxygenated toluene for series 3 platinum TBPs is shown in Figure 3-20. The photophysical data for series 3 platinum TBPs is summarized and reported in Table 3-11. The radiative and non-radiative rates were calculated and shown in Table 3-12. The Soret and Q-band for Pt-ArF4TBP are red shifted 8 and 5 nm, respectively, with similar molar absorptivity constants compared to Pt-TPTBP. The absorption spectrum for Pt-TAr_2TBP is nearly identical to Pt-DPTBP and Pt-Ar_2TBP. The Soret band for Pt-Ar_2OPrTBP has a small red shift of 1 nm relative to Pt-Ar_2TBP. A larger red shift is observed in the Q-band of ~20 nm. The molar absorptivity constants for Pt-TAr_2TBP and Pt-Ar_2OPrTBP are in line with the Pt-diaryl TBPs from series 2.

Table 3-11. Photophysical data for series 3 platinum TBPs in deoxygenated toluene. Quantum yields were measured relative to ZnTPP (0.04) by excitation at 420 nm in toluene. The triplet lifetimes were obtained by transient absorption spectroscopy.

Platinum Porphyrins	Absorption λ_{max} (Soret, Q-band) nm (ε_{max} = M^{-1} cm^{-1})	Phosphorescence λ_{max} nm	Φ_{phos}	τ_{T-T} (μs)
Pt-ArF_4TBP	438, 617 ε_{438} = 2.22 x 10^5 ε_{617}= 1.13 x 10^5	772	34% ±1	20.1
Pt-TAr_2TBP	411, 605 ε_{411} = 2.15 x 10^5 ε_{605}= 1.67 x 10^5	769	58% ±3	51.7
Pt-Ar_2OPrTBP	411, 625 ε_{411} = 2.06 x 10^5 ε_{614}= 1.47 x 10^5	786	60% ±1	51.8

The absorption and photoluminescence in deoxygenated toluene for series 3 platinum TBPs is shown in Figure 3-20. The emission maximum for Pt-ArF_4TBP is centered at 772 nm. The T_1 lifetime of 20.1 μs for Pt-ArF_4TBP is significantly shorter than that of Pt-TPTBP and Pt-Ar_4TBP. This leads to the expected decrease in the

phosphorescence QY (0.341) relative to Pt-TPBP and Pt-Ar_4TBP. The non-radiative decay rate constant for Pt-ArF_4TBP is doubled compared to Pt-TPTBP. Although no significant red shift is observed in either the absorption or PL for Pt-ArF_4TBP the increase in k_{nr} still suggests non-planar distortions are likely the reason.

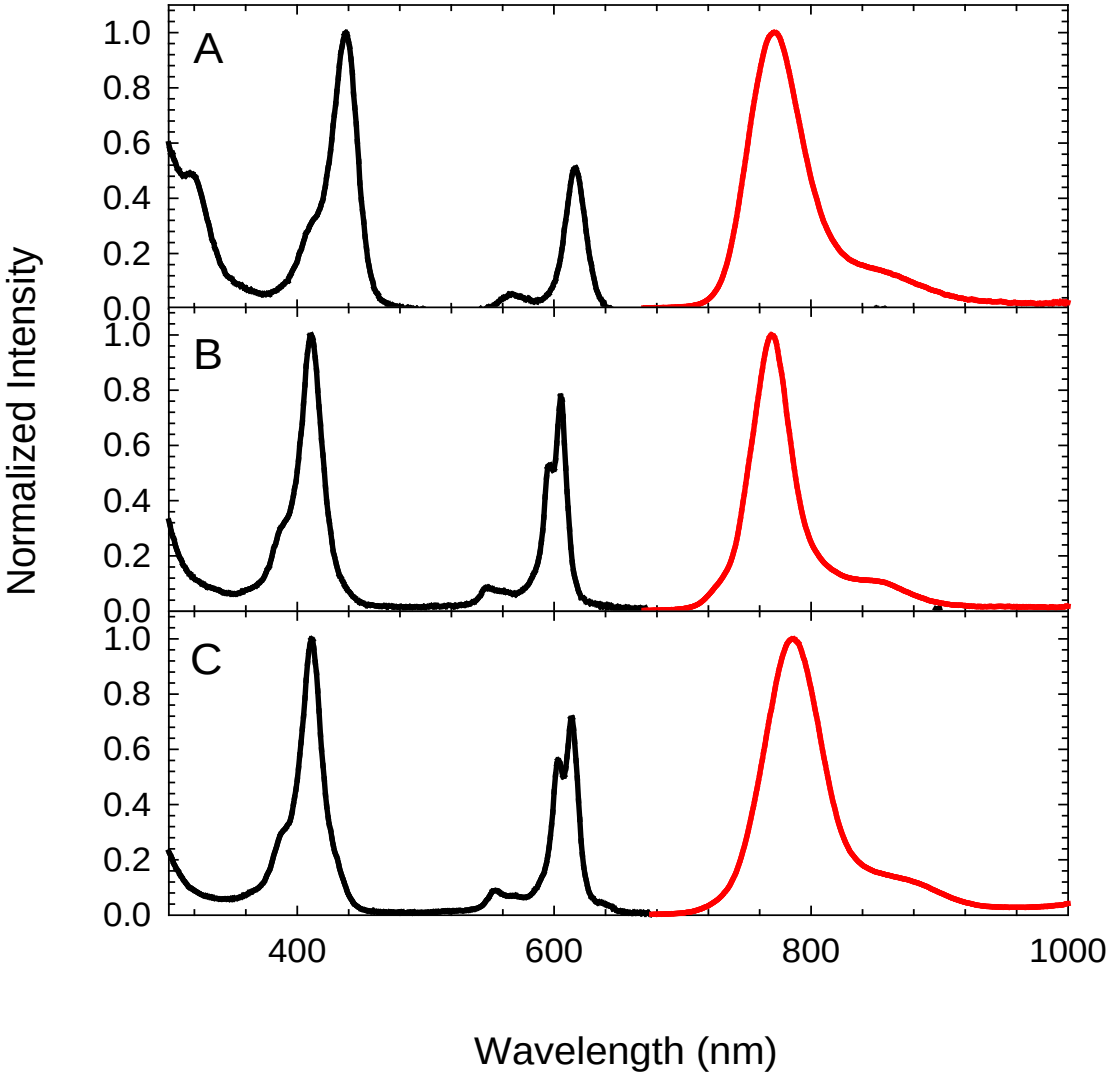

Figure 3-20. Normalized absorption (black) and photoluminescence (red) for series 3 platinum TBPs in toluene: A) Pt-ArF_4TBP, B) Pt-TAr_2TBP, C) Pt-Ar_2OPrTBP.

The emission maximum for Pt-TAr_2TBP of 769 nm is blue shifted 1 nm relative to Pt-Ar_2TBP. Similar to H_2Ar_2OPrTBP, the emission maximum for Pt-Ar_2OPrTBP of 786 nm is red shifted 16 nm relative to Pt-Ar_2TBP. The T_1 lifetimes for Pt-TAr_2TBP and Pt-

Ar_2OPrTBP of 51.7 and 51.8 μs are very close to those of Pt-Ar_2TBP (53.0 μs) measured by transient absorption spectroscopy. Consequently, the QYs should be very similar as they are directly proportional to the lifetimes but are difficult to accurately measure. The reported trend by Vinogradov *et al* of the QY doubling from Pd-TPTBP to Pd-DPTBP is supported by other literature data. Since the emission from platinum and palladium porphyrins is largely porphyrin based (π-π*) this trend should also hold true for Pt-Ar_2TBP, Pt-TAr_2TBP, and Pt-Ar_2OPrTBP.[124, 125]

Table 3-12. Deactivation rate constants for T_1 state of series 3 platinum TBPs in deoxygenated toluene. Radiative decay rate constant (k_r), calculated as $k_r = \varphi_{phos}k$, and the non-radiative decay rate constant ($k_{nr} = k_{ic} + k_{isc}$), calculated as $k_r = k - k_{nr}$.

Platinum Porphyrins	$k = 1/\tau_{T\text{-}T}$ (s^{-1})	k_r (s^{-1})	k_{nr} (s^{-1})	$\tau_{T\text{-}T}$ (μs)
Pt-ArF_4TBP	5.0×10^4	1.0×10^4	4.0×10^4	20.1
Pt-TAr_2TBP	1.9×10^4	1.1×10^4	8.1×10^3	51.7
Pt-Ar_2OPrTBP	1.9×10^4	1.2×10^4	7.8×10^3	51.8

Series 3- PLED Device Results

PLEDs were fabricated in an identical manner to those in series 2, by spin-coating the active layer on top of a PEDOT:PSS layer, followed by evaporation of the metal electrode materials to give the following device structure: glass/ITO/PEDOT:PSS(40 nm)/2% Pt-porphyrin:PVK:PBD(7:3) (110 nm)/LiF(1 nm)/Ca(10 nm)/Al.

Electroluminescence from PLEDs fabricated from Pt-ArF_4TBP and Pt-TAr_2TBP is centered at ~775 nm shown in Figure 3-21A. The PLED fabricated from Pt-Ar_2OPrTBP exhibits an electroluminescence maximum at 790 nm, red shifted similar to the PL emission. No host emission is observed in each device with light emission from the phosphors turning on at applied voltages (~12 V) identical to series 2 (Figure 3-21C).

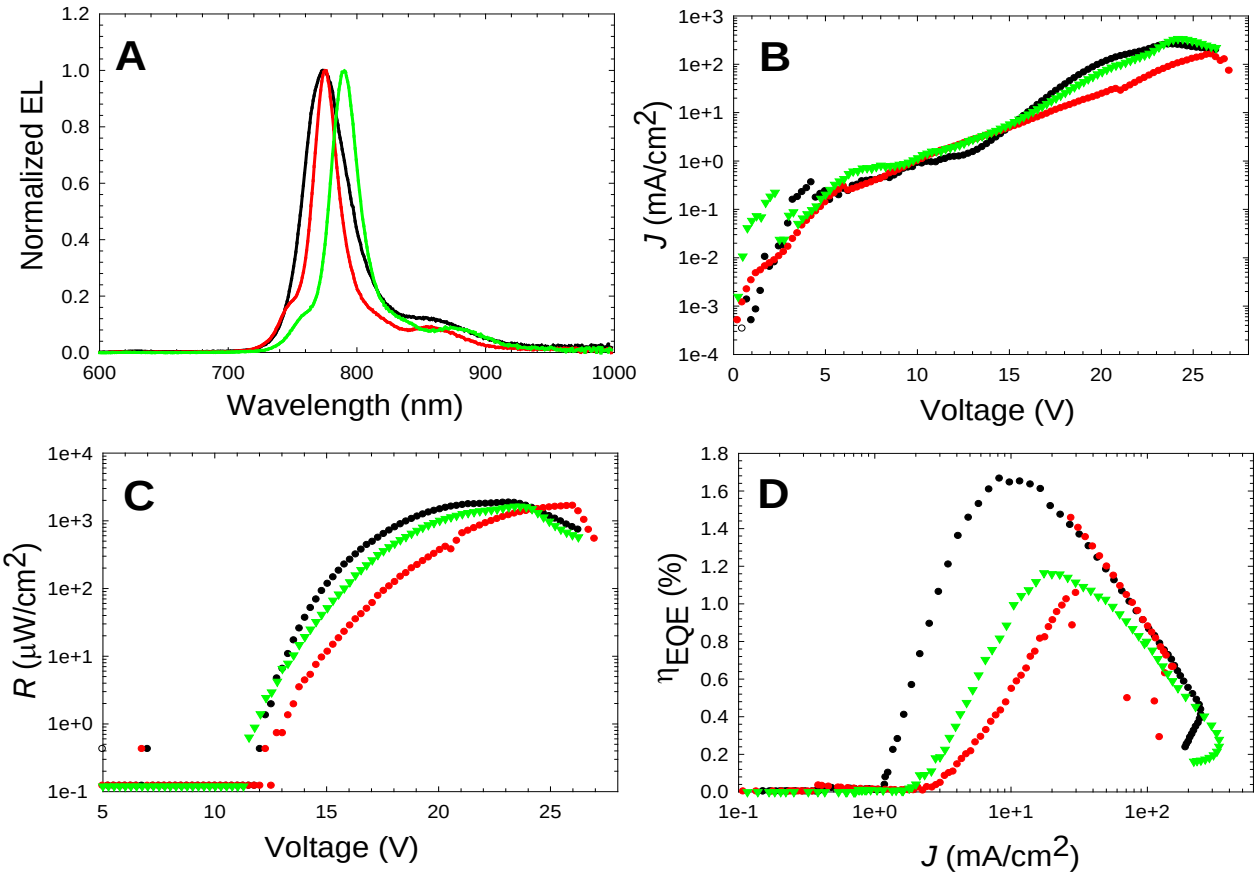

Figure 3-21. PLED device results for series 3 platinum TBPs with the following device structure: glass/ITO/PEDOT:PSS(40 nm)/2% Pt-porphyrin:PVK:PBD(7:3) (110 nm)/LiF(1 nm)/Ca(10 nm)/Al. Pt-ArF_4TBP (black), Pt-TAr$_2$TBP (red), and Pt-Ar$_2$OPrTBP (green). A) EL spectra for PLEDs, B) *J*-V plot, C) *R*-V plot, D) External quantum efficiency.

The PLEDs exhibit maximum radiant emittance of approximately 1.6-1.8 mW/cm^2 (Figure 3-21C). The maximum EQEs for the series range from 1.2-1.7%. The PLED fabricated from Pt-ArF_4TBP gave the highest EQE (1.7%) slightly higher than Pt-TPTBP (1.5%). Pt-TAr$_2$TBP and Pt-Ar$_2$OPrTBP both have significantly higher phosphorescence QYs compared to Pt-TPTBP and Pt-ArF_4TBP but no significant gain is observed in device efficiency. The maximum EQE for Pt-TAr$_2$TBP and Pt-Ar$_2$OPrTBP are 1.5 and 1.2% respectively. Comparison of series 2 and 3 PLEDS from platinum TBPs with similar solution QYs and lifetimes give the following trends with respect to the maximum

EQE data: Pt-ArF_4TBP > Pt-TPTBP > Pt-Ar$_4$TBP and Pt-TAr$_2$TBP > Pt-Ar$_2$TBP > Pt-Ar$_2$OPrTBP. The two major conclusions can be drawn from the observed trend. The frist is that despite the increased solution QYs of the platinum diaryl-TBPs large increases are not observed in device efficiency. This is likely due to bimolecular interactions that lead to self quenching pathways. The second, is that the addition of bulky substituents in the *meso*-aryl positions lead to small to moderate increases in device efficiency demonstrating that the substituents have little affect on the porphyrin:host polymer morphology.

Series 3- OLED Device Results

Multilayer OLEDs were fabricated by thermal vapor deposition of Pt-TAr$_2$TBP and Pt-Ar$_2$OPrTBP to give the following device structure: glass/ITO/NPB(40 nm)/Alq$_3$:4% Pt-TBP(25 nm)/Bphen(80 nm)/LiF(1 nm)/Al. Thermal vapor deposition was not attempted due to the high molecular weight of Pt-ArF_4TBP. Electroluminescence from the OLEDs for Pt-TAr$_2$TBP and Pt-Ar$_2$OPrTBP is centered at 775 and 790 nm respectively and is shown in Figure 3-22A. Turn on voltages of ~2 V and maximum radiant emittance of 1 mW/cm^2 obtained at ~12V are in line with the data from series 2 OLEDs (Figure 3-22B). The current densities from the *J*-V plot for both devices are similar and expected due to the identical device structure (Figure 3-22B).

The EQE data shown in Figure 3-22D for both devices follows a different trend than the PLED EQE data. Pt-TAr$_2$TBP exhibits a lower maximum EQE (3.2%) than Pt-Ar$_2$OPrTBP (6.9%). While Pt-TAr$_2$TBP and Pt-Ar$_2$OPrTBP have identical solution photophysics as Pt-Ar$_2$TBP the overall OLED EQEs range from 3.2-7.8%. The variations in performance are not well understood and likely originate from some physical property of the porphyrin:Alq$_3$ films. The observed trend demonstrates that the

additional substituents have a negative impact on the device efficiency. In the case of Pt-TAr$_2$TBP the maximum EQE is two times lower than that of the Pt-Ar$_2$TBP based OLED. This suggests that the additional substituents in Pt-TAr$_2$TBP and Pt-Ar$_2$OPrTBP do not enhance mixing with the host (Alq$_3$) or prevent bimolecular quenching pathways.

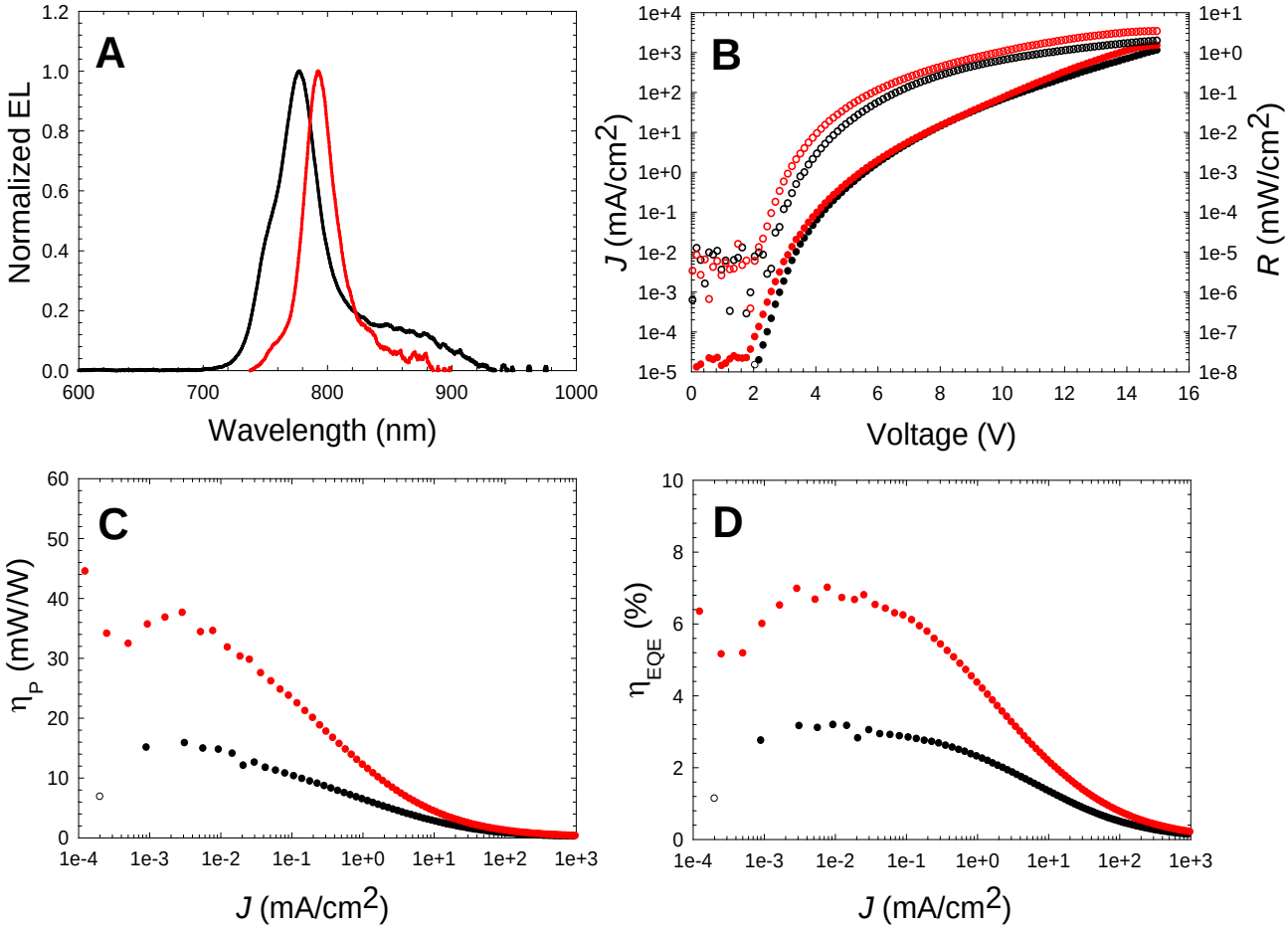

Figure 3-22. OLED device results for series 3 platinum TBPs. Pt-TAr$_2$TBP (black), Pt-Ar$_2$OPrTBP (red) with device structure: glass/ITO/NPB(40 nm)/Alq$_3$:4% Pt-TBP(25 nm)/Bphen(80 nm)/LiF(1 nm)/Al. A) EL spectra for PLEDs, B) *J*-V plot (closed circles) and *R*-V plot (open circles), C) Power efficiency, D) External quantum efficiency.

Conclusion

Electroluminescent OLEDs and PLEDs have been prepared by thermal vapor deposition with small molecule hosts and solution blending with polymers respectively

for each series of π-extended platinum porphyrins. The device wavelengths of the near-IR electroluminescence range from 770 to 1005 nm based on the π-extended platinum porphyrin system used. OLEDs have been prepared with record efficiencies of 9.2% and 3.8% at 770 and 898 nm respectively. In general, as the wavelength increases a decrease in overall device efficiency is observed for both PLEDs and OLEDs in accord with the energy gap law. Unexpectedly, devices fabricated using phosphors with significantly larger PL efficiency did not directly translate into higher device efficiency. Large ranges in device efficiency for phosphors with similar photophysical properties suggest a physical property of the platinum porphyrin in the solid state or a porphyrin:host morphology plays a major role in device efficiency.

Experimental

Optical Characterization. Absorption spectra for all free-base and platinum π-extended porphyrins were measured using a PerkinElmer Lambda 25 UV-vis spectrometer. The PL spectra were obtained by excitation at the Soret band absorption maximum for each compound. The spectra were recorded with an ISA Spex Triax 180 spectrograph coupled to a Spectrum-1 liquid nitrogen silicon charge coupled device detector. This spectrometer has a relatively flat spectral response to 900 nm, although there is some loss in efficiency due to the grating, which is blazed in the visible region. The PL for Pt-Ar_4TAP was measured separately on a PTI fluorimeter equipped with InGaAs near-IR detector and a Spex Fluorolog II equipped with InGaAs near-IR detector. The solution fluorescence and phosphorescence quantum yields were calculated relative to ZnTPP in toluene (0.04) unless otherwise noted according to a previously described method.[117 126] The sample and actinometer solutions had matched optical density at a shared excitation wavelength. The emission spectra were corrected

for the spectrometer response prior to being used to compute the quantum yield. Time-resolved transient absorption spectra for π-extended platinum porphyrins in toluene were collected by using previously described laser systems for the visible and near-IR regions.[127]

Device Fabrication and Characterization. PLEDs were fabricated by Ken Graham from the Reynolds group at the University of Florida using the following method. PLEDs were fabricated on pre-patterned indium tin oxide (ITO) coated glass substrates with a sheet resistance of ~20 Ω/ . The ITO substrates were cleaned sequentially with a sodium dodecyl sulfate solution, acetone, and isopropyl alcohol followed by exposure to an oxygen plasma. A layer of PEDOT:PSS (Baytron P VP Al4083) was spin-coated on the ITO immediately following oxygen plasma exposure and then annealed at 120ºC under vacuum for 2 h. The active layer solutions consisting of varying weight percentages of π-extended platinum porphyrins in PVK:PBD were prepared and spin-coated from chlorobenzene in an MBraun glovebox with <0.1 ppm oxygen and water. The cathode consisting of LiF (1 nm), Ca (10 nm), and Al (80 nm) was deposited in a thermal evaporator under a vacuum of 10^{-6} Torr. Radiant emittance (*R*)-voltage (V) measurements were carried out using a calibrated UDT Instruments silicon detector. Current density (*J*)-voltage (V) measurements were carried out using a Keithley 2400 sourcemeter. The electroluminescence (EL) spectra were collected using the ISA SPEX Triax 180 spectrograph or a Spex Fluorolog II equipped with InGaAs near-IR detector with the devices driven using the Keithley sourcemeter. Each 2.5 x 2.5 cm substrate features eight independently addressable pixels with area 0.07 cm^2, and the results presented herein represent measurements averaged over three pixels.

The OLEDs were fabricated by Yixing Yang in Dr. Xue's group Department of Materials Science at the University of Florida. The OLEDs were fabricated on glass substrates commercially coated with an ITO anode with a sheet resistance of ~20 Ω/ . The substrates were cleaned in ultrasonic baths of deionized water, acetone, and isopropyl alcohol consecutively for 15 min each and then exposed to an ultraviolet ozone environment for 15 min immediately before loading into a high vacuum chamber (base pressure ~10^{-7} Torr). All the layers including the cathode, were deposited using vacuum thermal evaporation following procedures published previously.[128] The thicknesses of the HTL and EML were 40 and 20 nm, respectively, whereas the ETL layer thickness was 100 nm, optimized to achieve the highest device efficiencies. A 1 nm layer of LiF followed by a 100 nm Al layer was then deposited as the cathode. Radiant emittance (*R*)-current density (*J*)-voltage (V) characteristics were measured under ambient conditions using an Alilent 4155C semiconductor parameter analyzer and a calibrated Newport silicon detector. The EL spectra were collected as described above, with the device driven at a constant current. The radiant emittance for both OLEDs and PLEDs was calibrated assuming Lambertian emission, and the EQE and electrical-to-optical power efficiency values were derived on the basis of the recommended methods.[129] Each 2.5 x 2.5 cm substrate features four independently addressable pixels with area 4mm^2, and the results presented herein represent measurements averaged over at least eight pixels.

CHAPTER 4
CONCLUSIONS

The previous chapters detail the investigation of π-extended platinum porphyrins as near-IR phosphors for use in near-IR LED applications. Reported are the synthesis, characterization and photophysical properties with the PLED and OLED device data for three novel series of π-extended platinum porphyrins. The photophysical properties of porphyrins make them excellent candidates for use in LED applications due to their narrow emission. The use of phosphors over fluorophores has been shown to give theoretical device efficiencies of a 100%. Therefore high efficiency devices can only be achieved with materials that posses phosphorescence quantum yields approaching unity. The insertion of a transition metal such as palladium or platinum forming a metalloporphyrin induces intersystem crossing to give phosphors with high phosphorescence quantum yields that are ideal candidates for LED applications.

The photophysical properties of porphyrins with fused-benzo rings have long been of interest with the platinum complexes of this class of porphyrins almost completely absent from the literature. Herein is the first full report of the photophysical properties for π-extended platinum porphyrins. The high PL efficiencies of the platinum complexes for TBP, TNP and TAP systems make them ideal choices for near-IR phosphors. OLEDs and PLEDs have been fabricated in order to demonstrate the application of these materials in near-IR LEDs.

Conclusions and Future work. The synthetic work and photophysical characterization for each series with the reported PLED and OLED device data has significantly advanced the field of near-IR LEDs based upon the use of π-extended platinum porphyrins a near-IR phosphors. The advancements from series 1 include

devices with EL reaching further into the near-IR (900 and 1000 nm) while also achieving new device efficiency records for each new wavelength region. The preparation and characterization of series 2 platinum TBPs produced the brightest platinum TBP ever reported. This record quantum yield expands farther than platinum TBPs and is the highest known for this wavelength region of any reported material. The structures designed for series 3 platinum TBPs attempted to prevent quenching mechanisms in the device from porphyrin-porphyrin interactions through chemical modification of the porphyrin macrocycle. This series represents some of the most complex TBPs reported to date while also furthering the understanding of substituent effects on the photophysical properties on the TBP macrocycle.

While this body of work has answered many questions concerning the use of π-extended platinum porphyrins for near-IR LED applications it has also raised many more. The large increase in the solution quantum yield observed in series 2 did not directly translate into significantly higher device EQEs. This result along with the device data from series 3 platinum TBPs suggest that the translation of solution photophysical properties to the solid state for these novel phosphors is not well understood. Future work should be directed towards gaining an understanding of how these materials behave in the solid state. A clear understanding of the solid state photophysical properties is necessary to completely achieve optimized device efficiencies. It would also be advantageous to thoroughly examine the photophysical properties as a function of concentration in a select variety of host materials. The device data for series 2 and 3 shows significant variations for materials with identical solution photophysical properties. This strongly suggest a physical property or unique morphology exist

between the phosphor and host material ultimately contributing to an increase or decrease in device efficiency. The investigation and answers to these questions may provide the data necessary to utilize the record quantum yield of near-IR phosphors like Pt-Ar_2TBP achieving much higher device efficiencies.

APPENDIX A
FIGURES

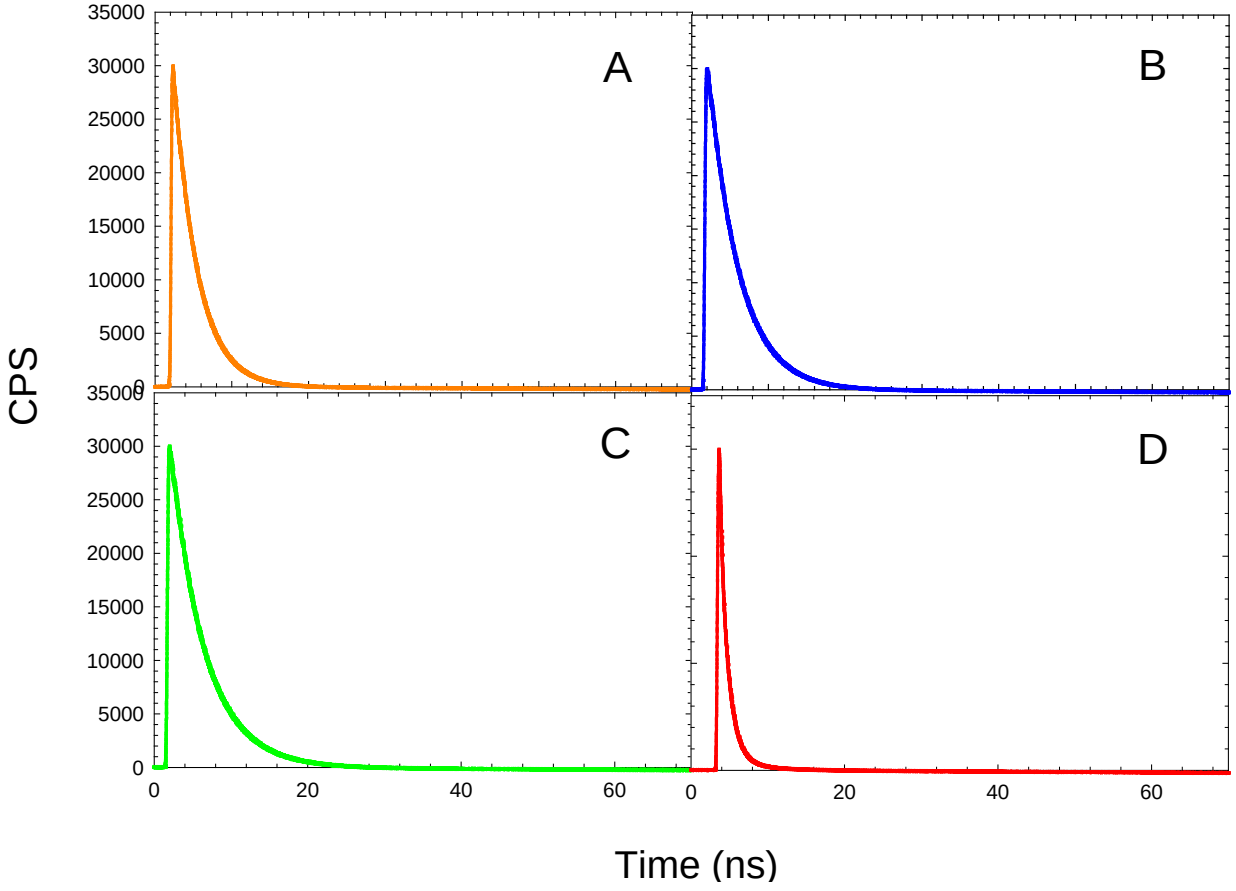

Figure A-1. Fluorescence lifetimes for Series 1 free-base π-extended porphyrins in air saturated toluene: A) H_2TPTBP, B) H_2TPTNP, C) H_2Ar_4TNP$(OMe)_8$, D) H_2Ar_4TAP.

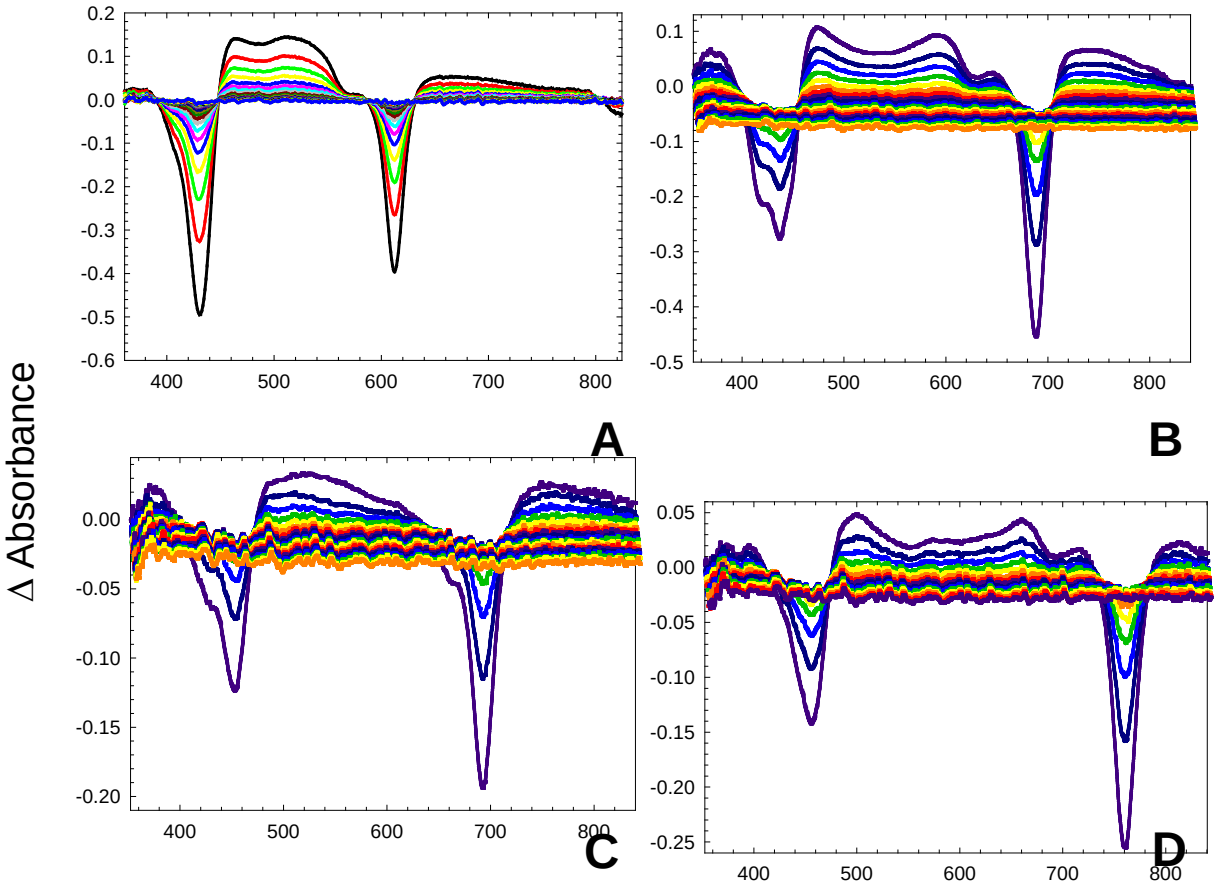

Figure A-2. T_1-T_n absorption data for series 1 π-extended platinum porphyrins in deoxygenated toluene: A) Pt-TPTBP, B) Pt-TPTNP, C) Pt-Ar_4TNP$(OMe)_8$, D) Pt-Ar_4TAP.

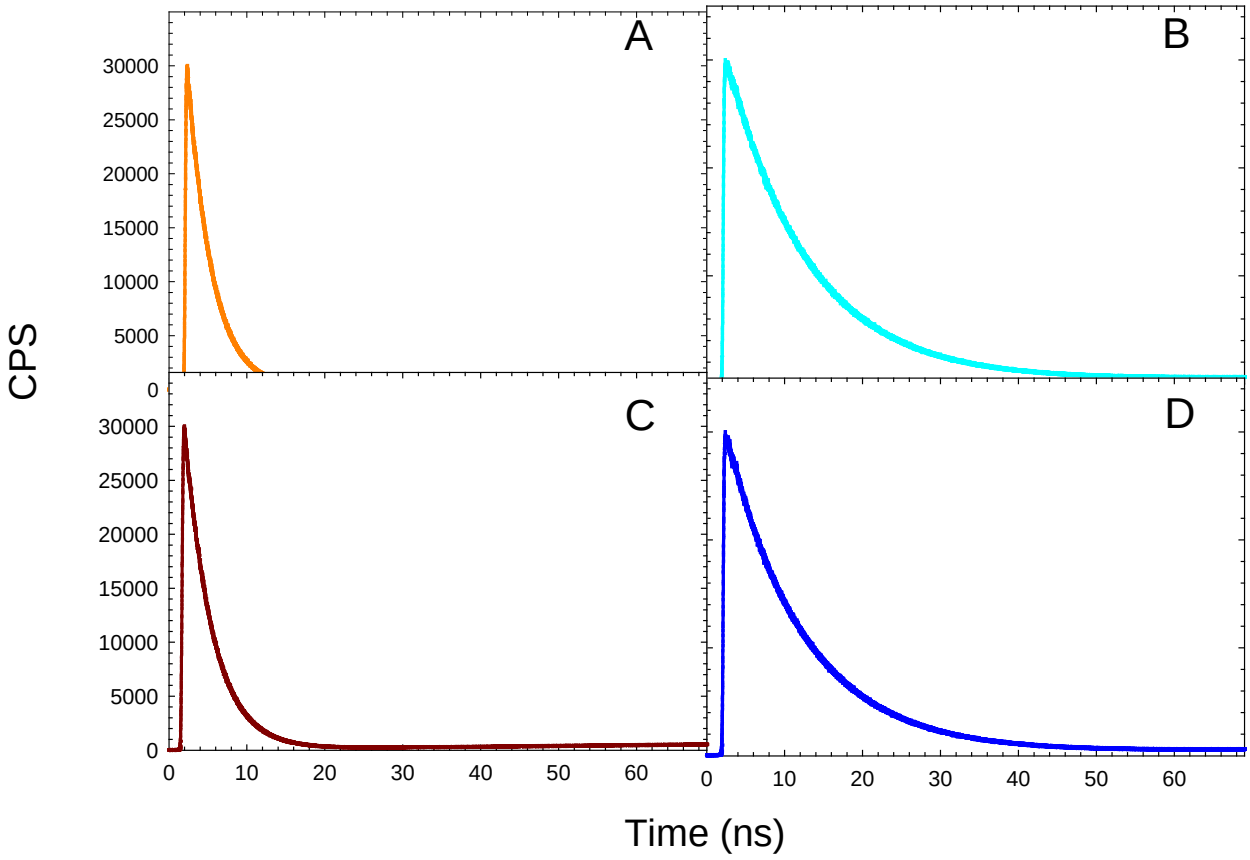

Figure A-3. Fluorescence lifetimes for Series 2 free-base π-extended TBPs in air saturated toluene: A) H_2TPTBP, B) H_2DPTBP, C) H_2Ar_4TBP, D) H_2Ar_2TBP.

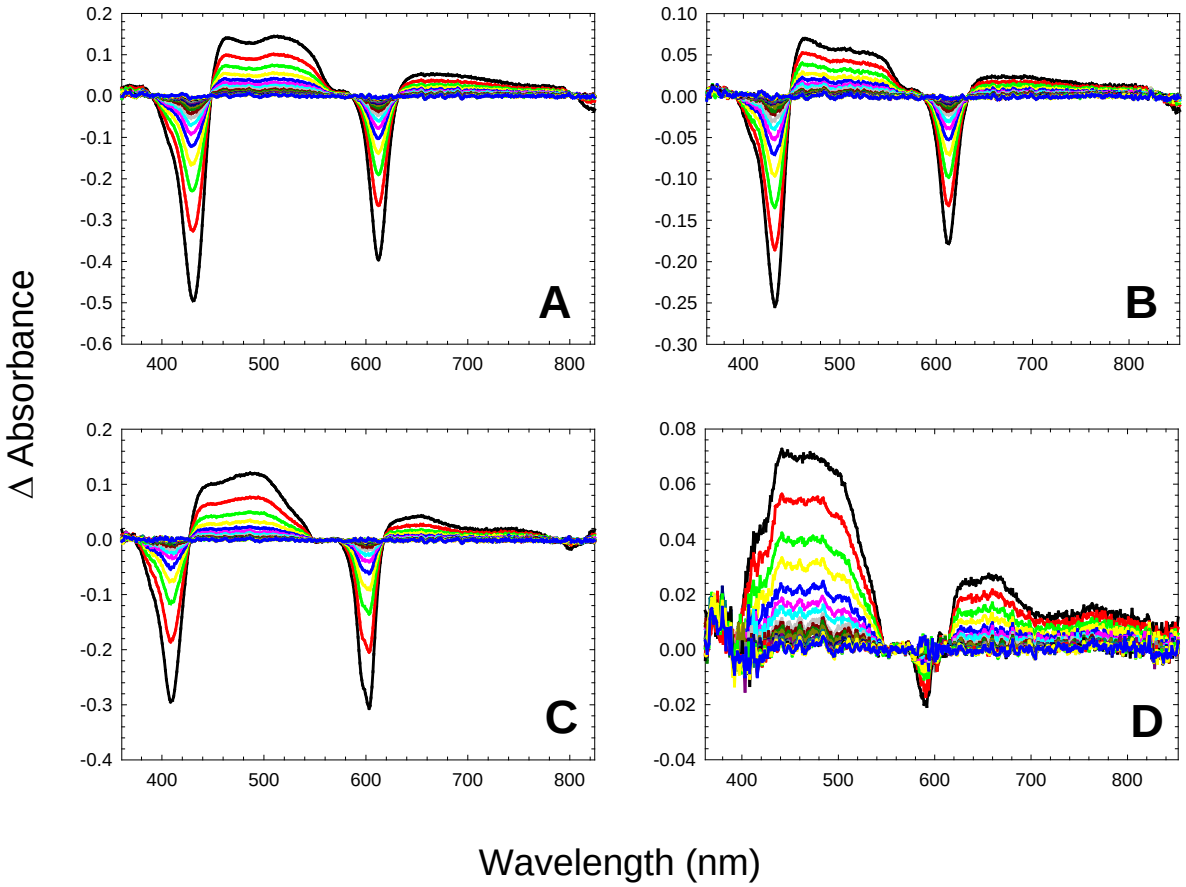

Figure A-4. T_1-T_n absorption data for series 2 π-extended platinum TBPs in deoxygenated toluene: A) Pt-TPTBP, B) Pt-Ar_4TBP, C) Pt-DPTBP, D) Pt-Ar_2TBP.

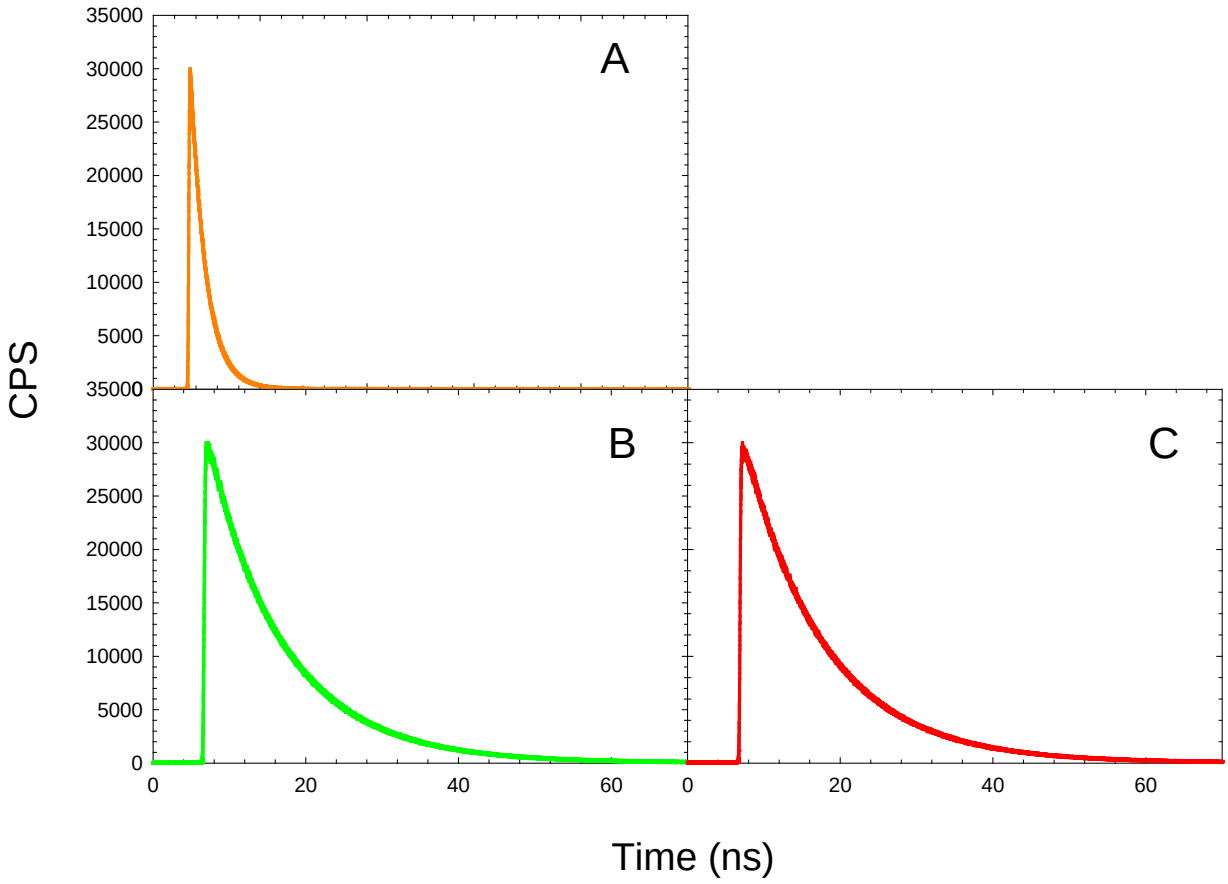

Figure A-5. Fluorescence lifetimes for Series 3 free-base π-extended TBPs in air saturated toluene: A) H_2ArF_4TBP, B) H_2TAr_2TBP, C) $H_2Ar_2OPrTBP$.

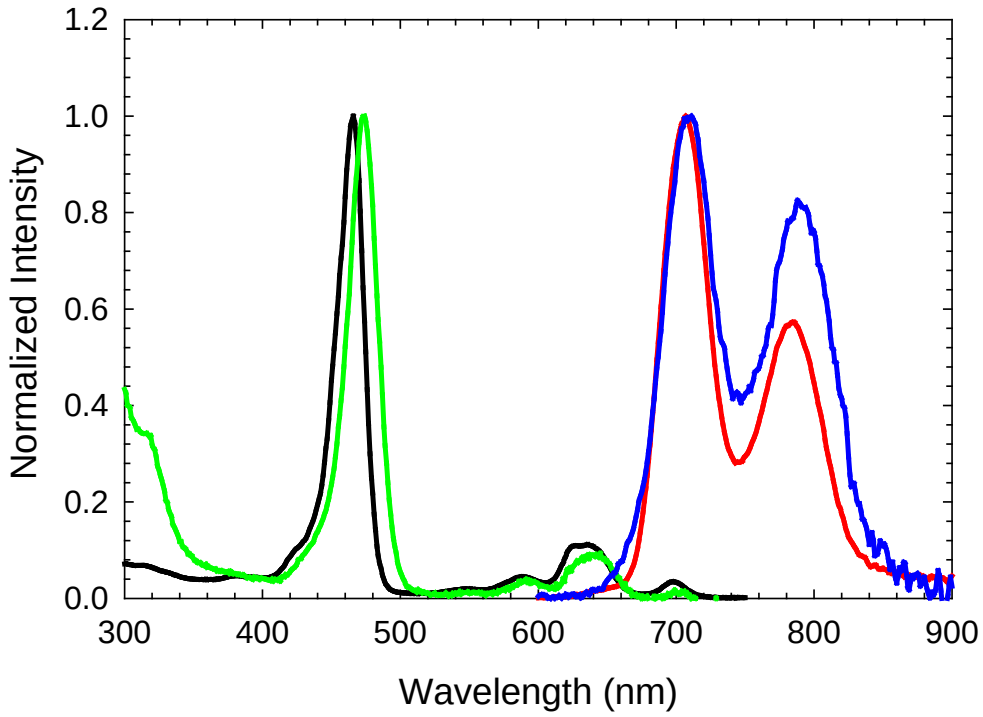

Figure A-6. Normalized absorption and PL of H_2TPTBP (black and red) and H_2ArF_4TBP (green and blue) in air saturated toluene.

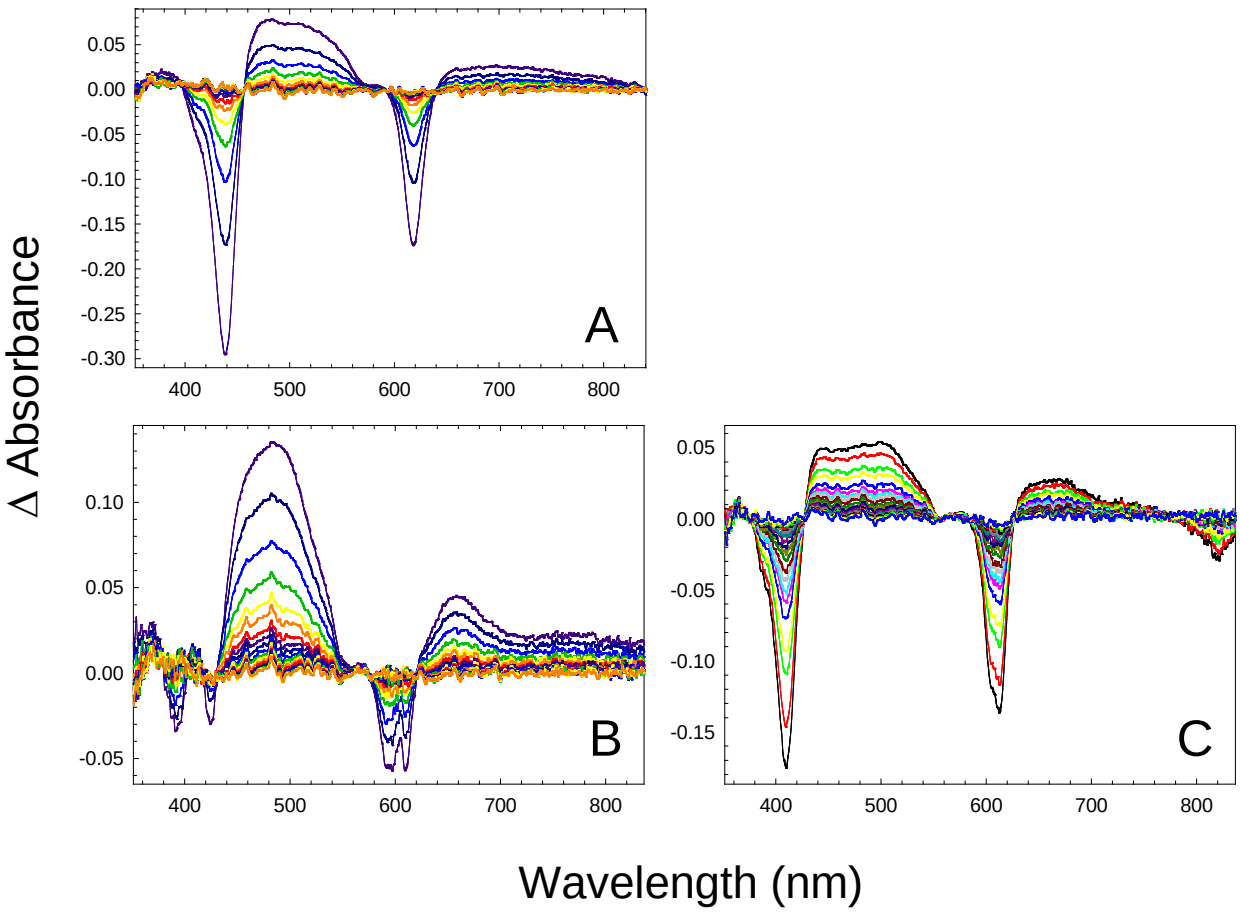

Figure A-7. T_1-T_n absorption data for series 3 π-extended platinum TBPs in deoxygenated toluene: A) Pt-ArF_4TBP, B) Pt-TAr$_2$TBP, C) Pt-Ar$_2$OPrTBP.

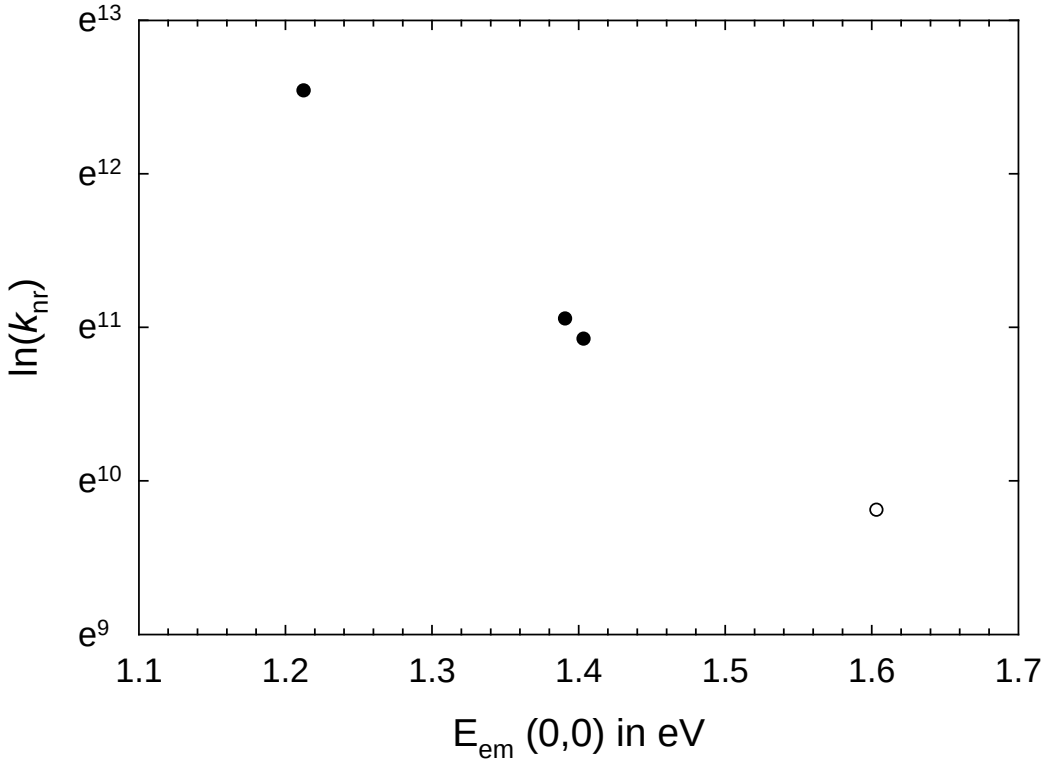

Figure A-8. Plot of the natural log of the non-radiative decay constant (k_{nr}) and the emission maximum in eV (E_{em}) for series 1 π-extended plantium porphyrins.

APPENDIX B
NMR SPECTRA

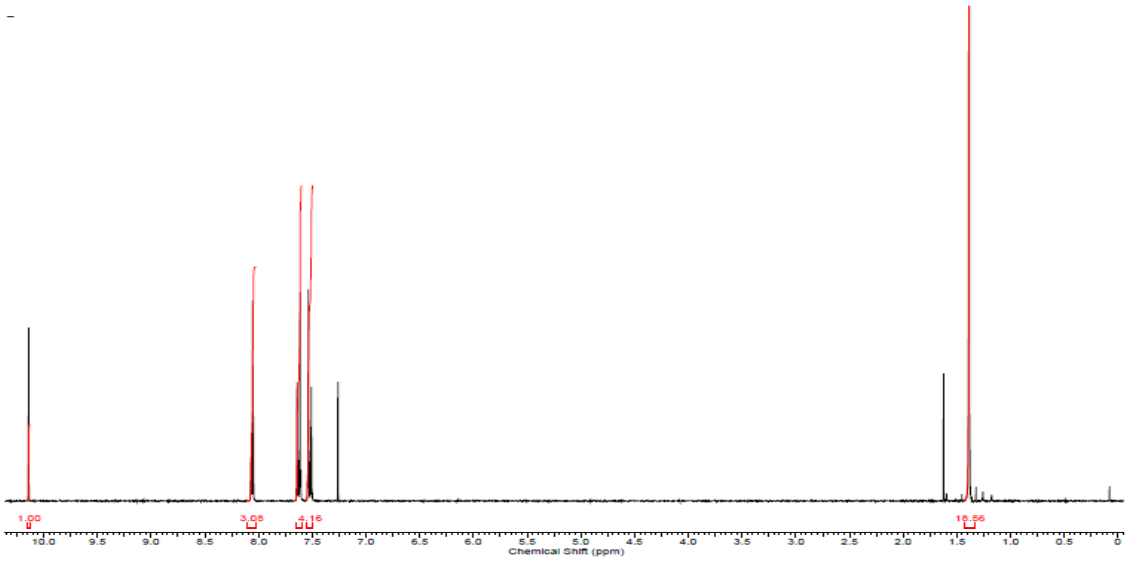

Figure B-1. ^{1}H NMR (300 MHz, $CDCl_3$) spectrum of **6**.

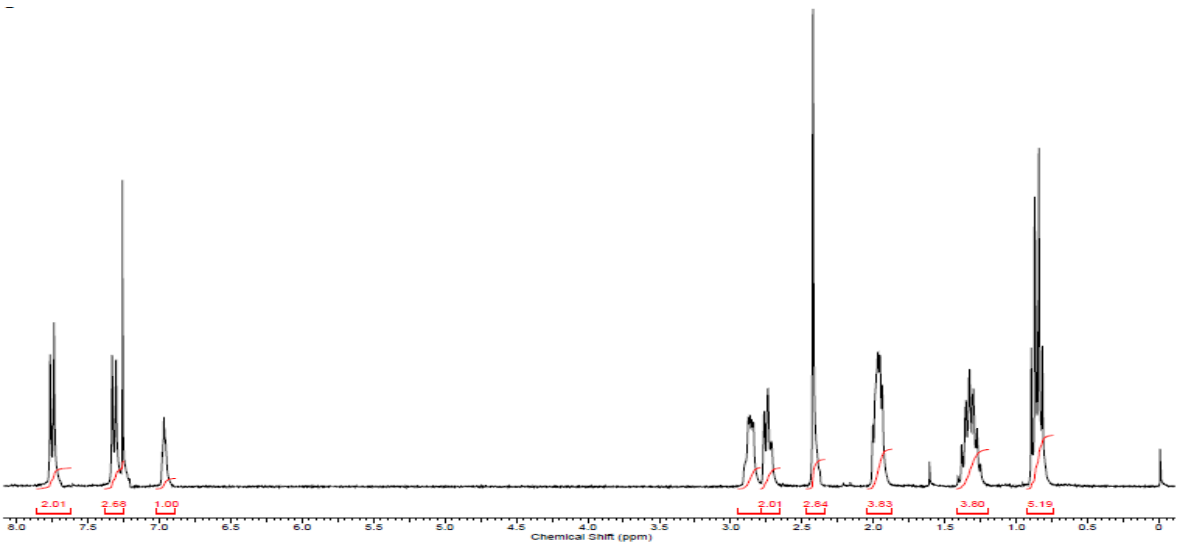

Figure B-2. ^{1}H NMR (300 MHz, $CDCl_3$) spectrum of **17b**.

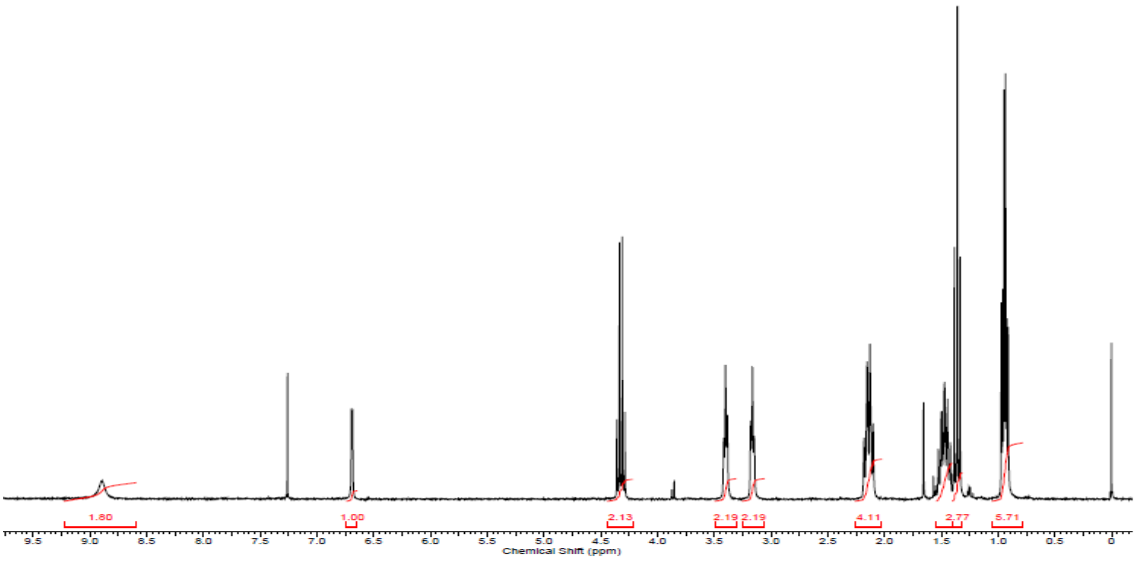

Figure B-3. ^{1}H NMR (300 MHz, $CDCl_3$) spectrum of **18b**.

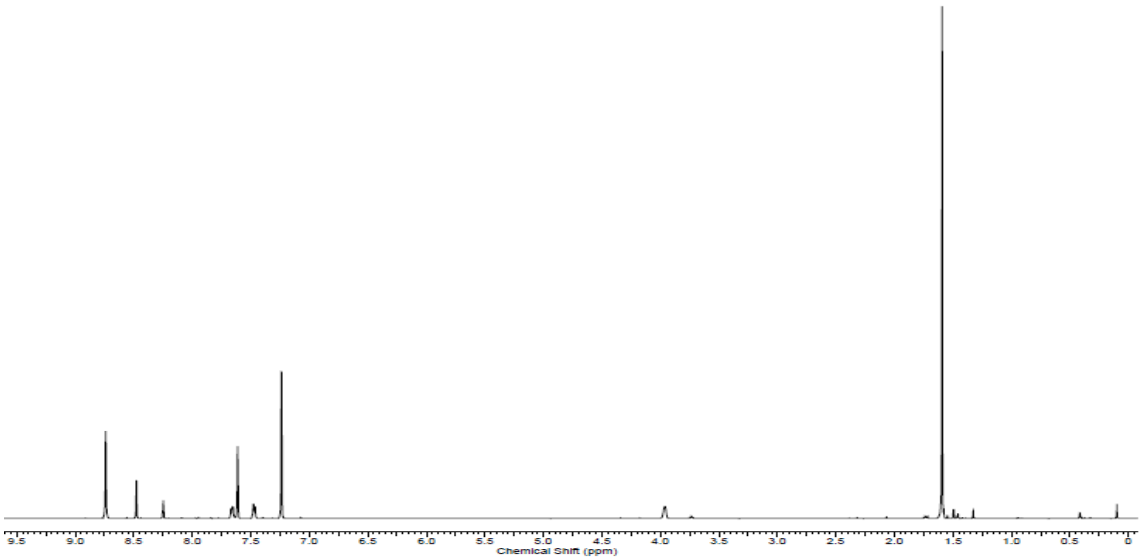

Figure B-4. ^{1}H NMR (300 MHz, pyridine-d_5) spectrum of **39b**.

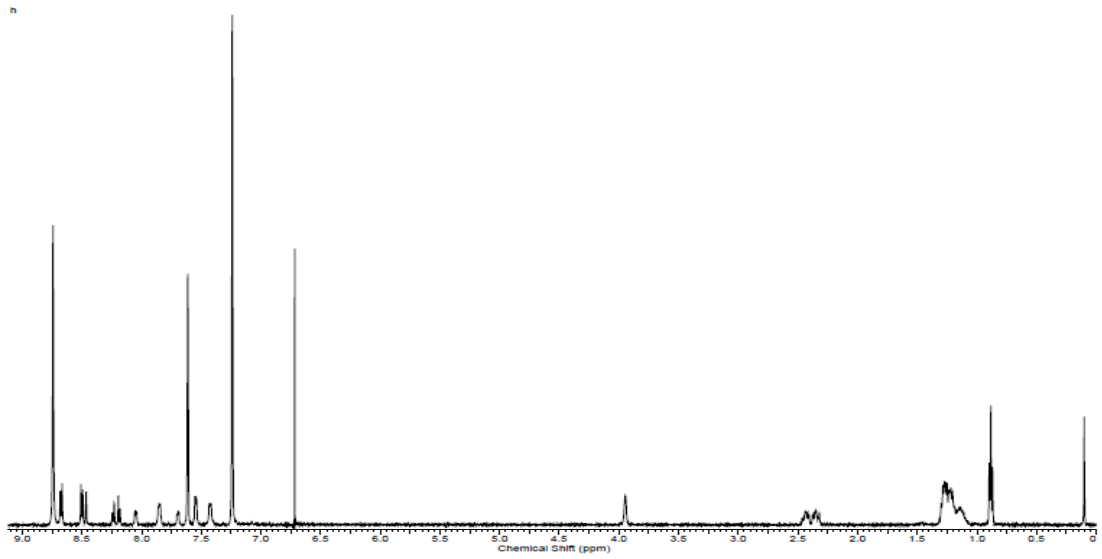

Figure B-5. ^{1}H NMR (500 MHz, pyridine-d_5) spectrum of **39c**.

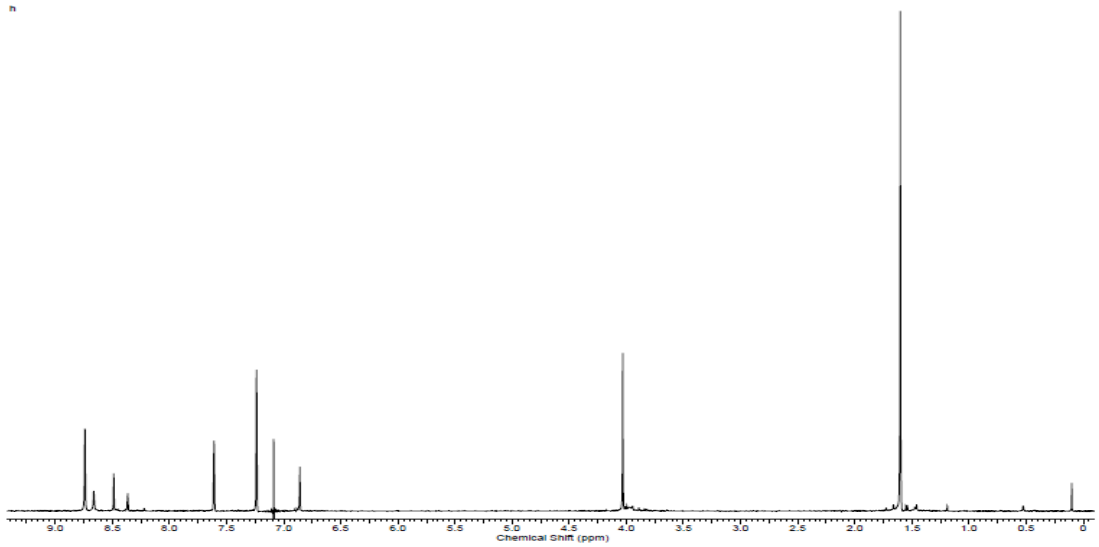

Figure B-6. ^{1}H NMR (500 MHz, pyridine-d_5) spectrum of **40b**.

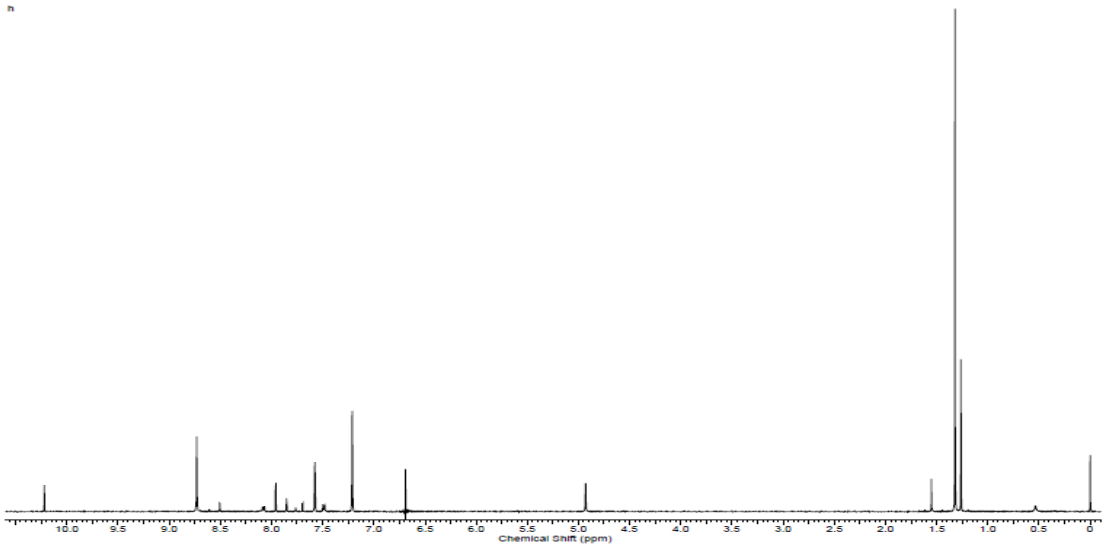

Figure B-7. ^{1}H NMR (500 MHz, pyridine-d_5) spectrum of **42**.

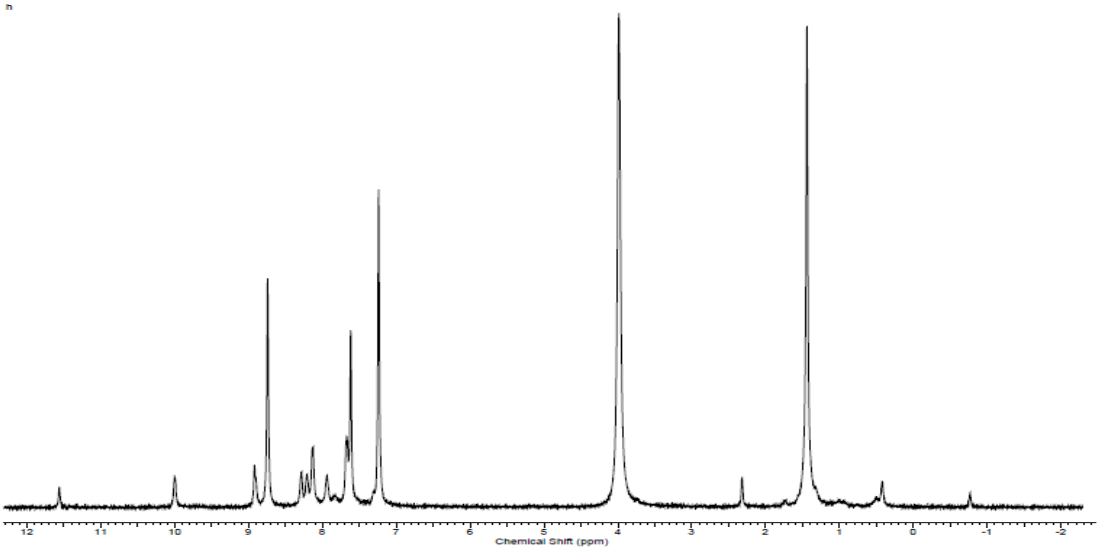

Figure B-8. ^{1}H NMR (500 MHz, pyridine-d_5) spectrum of **45c**.

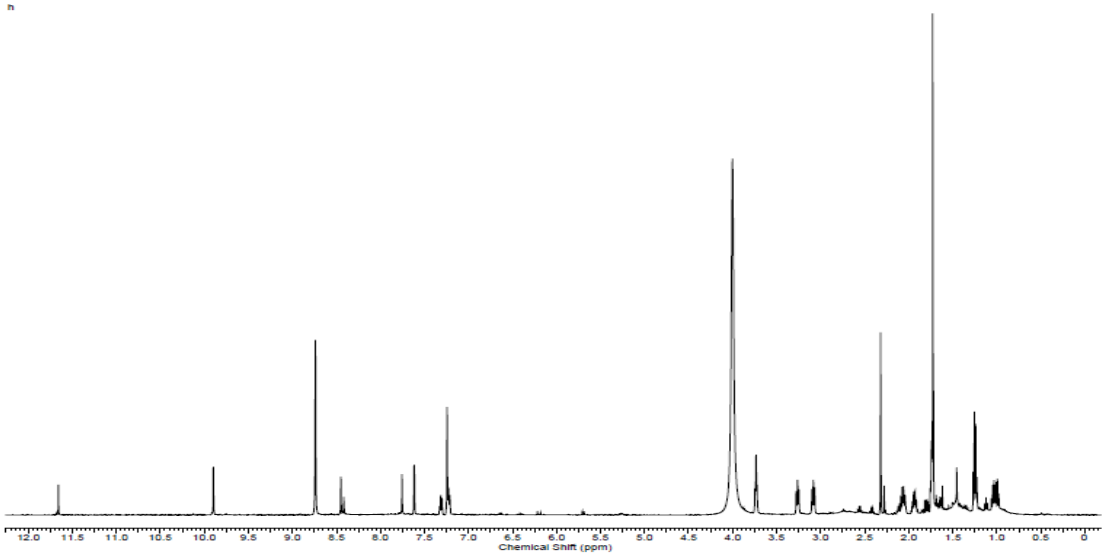

Figure B-9. ^{1}H NMR (500 MHz, pyridine-d_5) spectrum of **45d**.

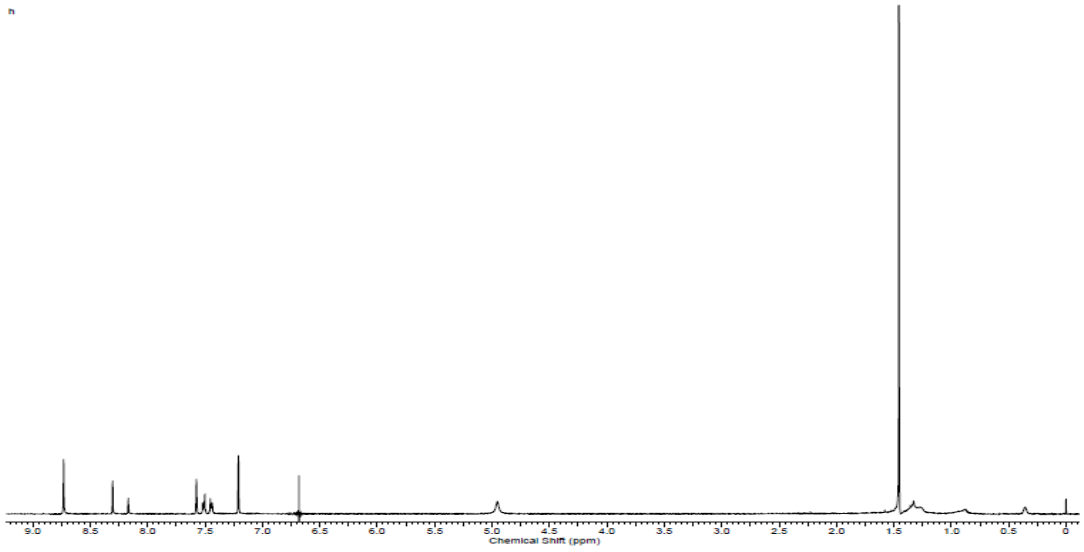

Figure B-10. ^{1}H NMR (500 MHz, pyridine-d_5) spectrum of **Pt-39b**.

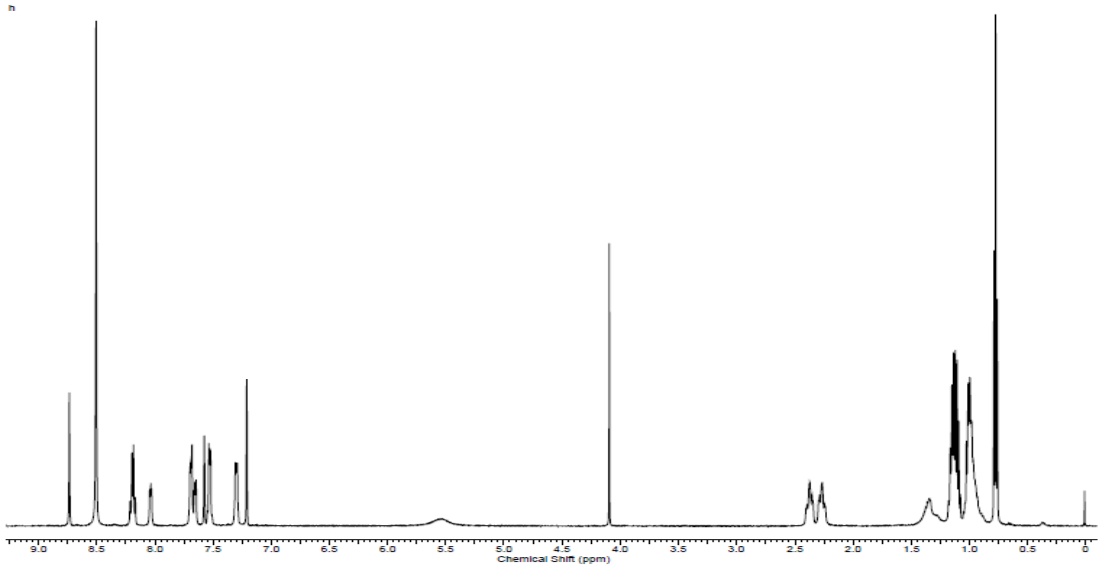

Figure B-11. ^{1}H NMR (500 MHz, pyridine-d_5) spectrum of **Pt-39c**.

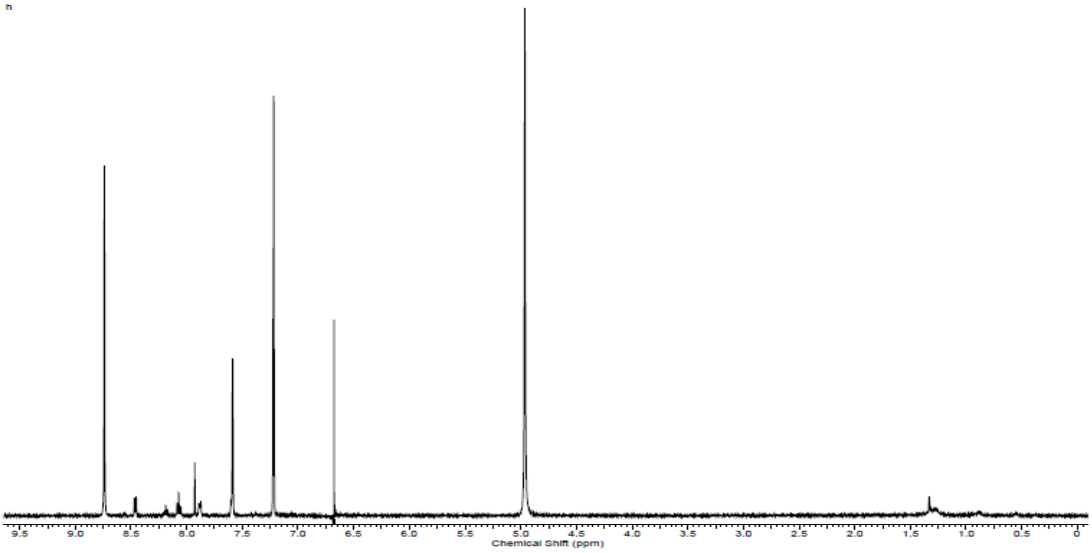

Figure B-12. ^{1}H NMR (500 MHz, pyridine-d_5) spectrum of **Pt-40a**.

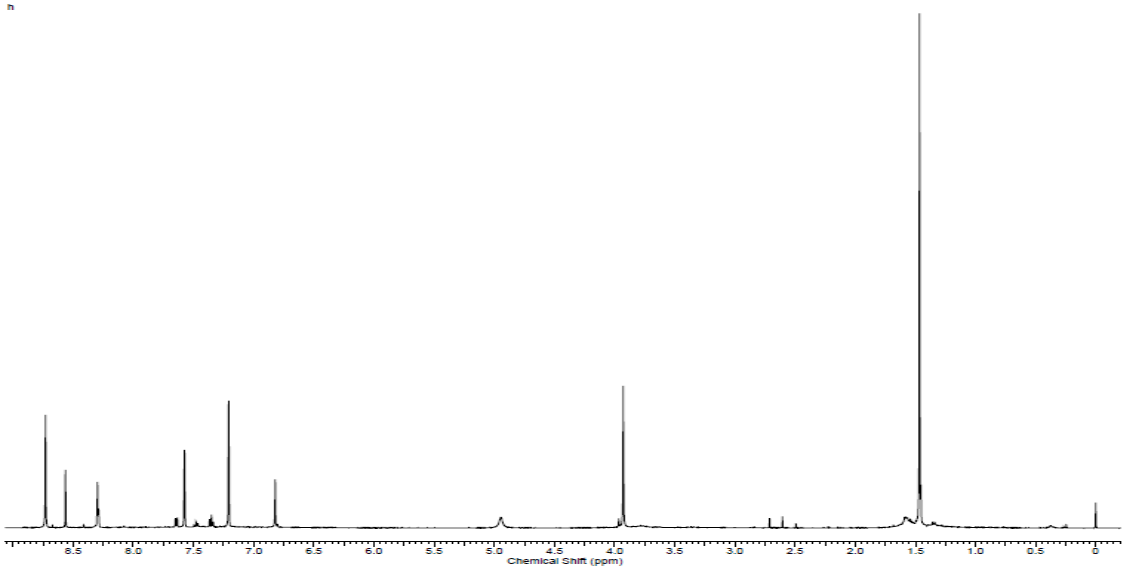

Figure B-13. ^{1}H NMR (500 MHz, pyridine-d_5) spectrum of **Pt-40b**.

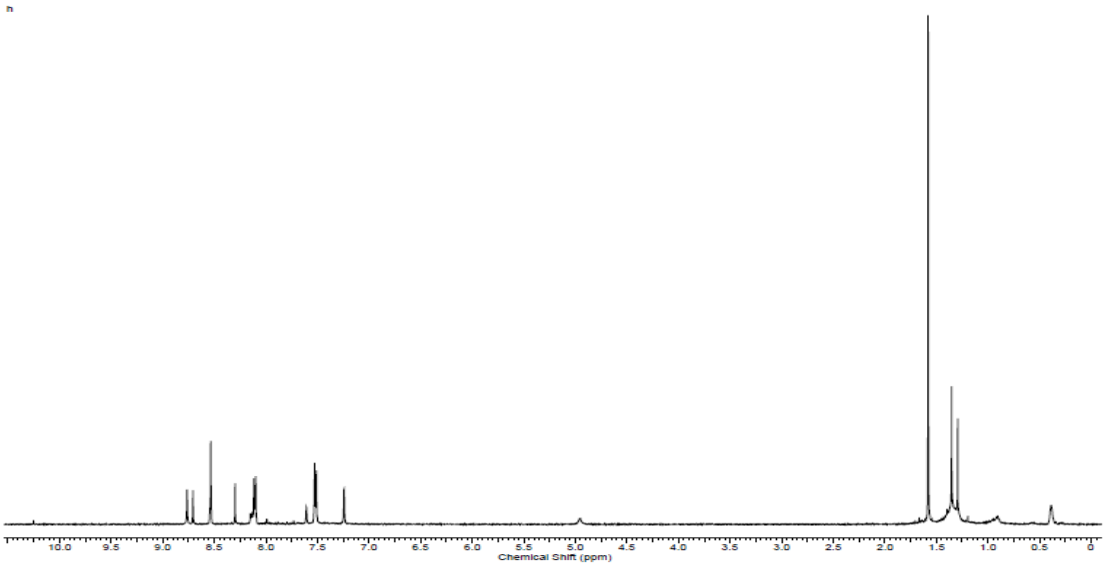

Figure B-14. ^{1}H NMR (500 MHz, pyridine-d_5) spectrum of **Pt-42**.

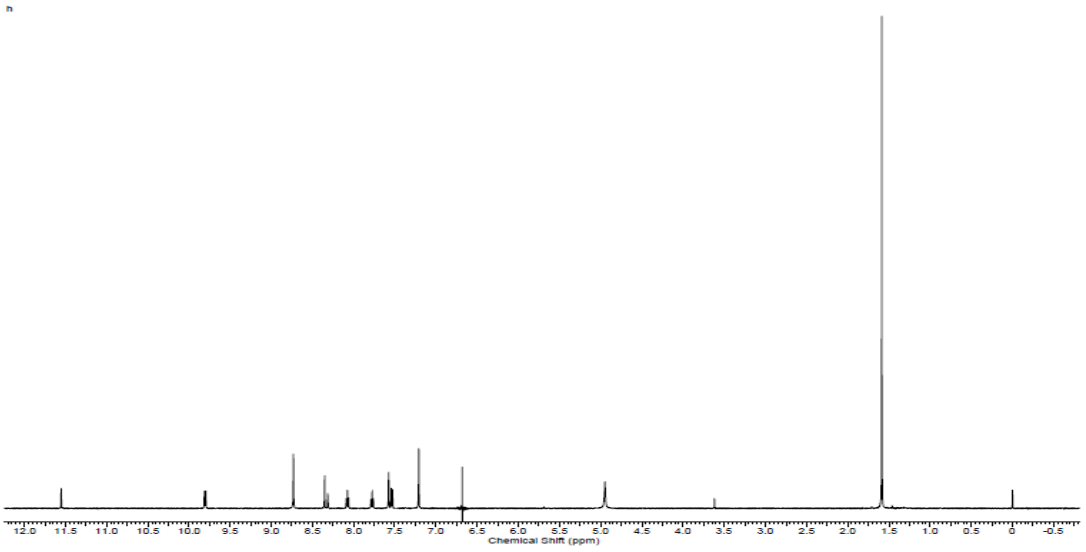

Figure B-15. ^{1}H NMR (500 MHz, pyridine-d_5) spectrum of **Pt-45b**.

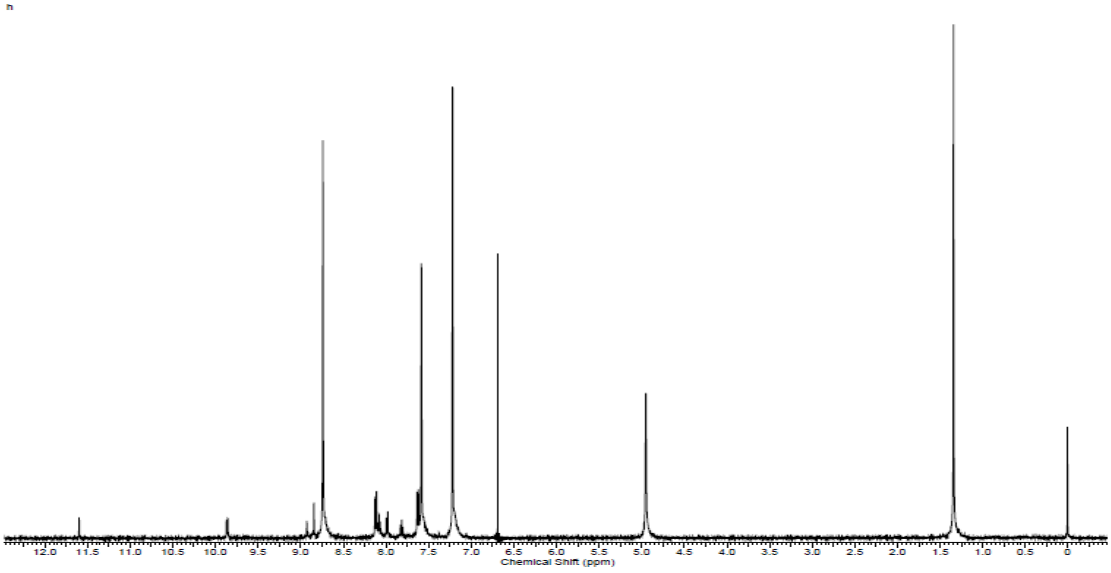

Figure B-16. ^{1}H NMR (500 MHz, pyridine-d_5) spectrum of **Pt-45c**.

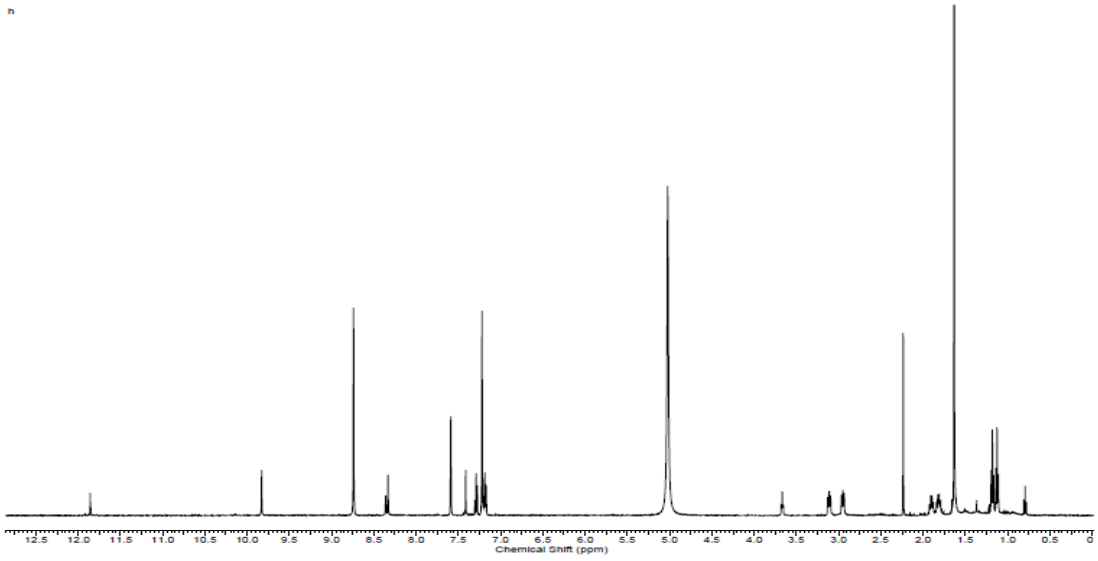

Figure B-17. ^{1}H NMR (500 MHz, pyridine-d_5) spectrum of **Pt-45d**.

LIST OF REFERENCES

1. J. M. Olson, "Photosynthesis in the Archean Era," Photosynth. Res. **88**, 109-117 (2006).

2. R. A. Sheldon, *Metalloporphyrins in Catalytic Oxidations*. (Marcel Dekker, Inc., New York, 1994).

3. J. A. Milroy, "Observations on some metallic compounds of hematoporphyrin," Biochem. J. **12** (1918).

4. H. Fischer and K. Zeile, "Porphyrin syntheses. XXII. Syntheses of hematoporphyrin, protoporphyrin and hemin," Justus Liebigs Ann. Chem. **468**, 98-116 (1929).

5. H. Fischer and H. Orth, *Die Chemie des Pyrrols, Vol. I-III*. (Akademische Verlagsgesellschaft, Leipzig, 1934-1940).

6. H. B. F. Dixon, A. Cornish-Bowden, C. Liebecq, K. L. Loening, G. P. Moss, J. Reedijk, S. F. Velick, P. Venetianer and J. F. G. Vliegenthart, "Nomenclature of tetrapyrroles," Pure Appl. Chem **59**, 779-832 (1987).

7. K. M. Smith, "Strategies for the Synthesis of Octaalkylporphyrin Systems," in *The Porphyrin Handbook*, *Vol. 1,* edited by K. M. Kadish, K. M. Smith and R. Guilard (Academic Press, San Diego, 2000), pp. 2-40.

8. R. B. Woodward, W. A. Ayer, J. M. Beaton, F. Bickelhaupt, R. Bonnett, P. Buchschacher, G. L. Closs, H. Dutler and *et al*, "The total synthesis of chlorophyll," J. Am. Chem. Soc. **82**, 3800-3802 (1960).

9. J. S. Lindsey, "Synthesis of *meso*-Substituted Porphyrins," in *The Porphyrin Handbook*, *Vol. 1,* edited by K. M. Kadish, K. M. Smith and R. Guilard (Academic Press, San Diego, 2000), pp. 46-80.

10. P. Rothemund, "Formation of porphyrins from pyrrole and aldehydes," J. Am. Chem. Soc. **57**, 2010-2011 (1935).

11. P. Rothemund, "New porphyrin synthesis. Synthesis of porphin," J. Am. Chem. Soc. **58**, 625-627 (1936).

12. P. Rothemund and A. R. Menotti, "Porphyrin studies. IV. The synthesis of α,β,γ,δ-tetraphenylporphine," J. Am. Chem. Soc. **63**, 267-270 (1941).

13. A. D. Alder, F. R. Longo and W. Shergalis, "Mechanistic investigation of porphyrin synthesis. I. Preliminary studies on ms-tetraphenylporphyrin," J. Am. Chem. Soc. **86**, 3145-3149 (1964).

14. A. D. Alder, F. R. Longo, J. D. Finarelli, J. Goldmacher, J. Assour and L. Korsakoff, "A simplified synthesis for meso-tetraphenylporphine," J. Org. Chem. **32**, 476 (1967).

15. D. Dolphin, "Porphyrinogens and porphodimethenes, intermediates in the synthesis of m-tetraphenylporphins from pyrroles and benzaldehydes," J. Heterocycl. Chem. **7**, 275-283 (1970).

16. J. S. Lindsey, H. C. Hsu and I. C. Schreiman, "Synthesis of tetraphenylporphyrins under very mild conditions," Tetrahedron Lett. **41**, 4969-4970 (1986).

17. J. S. Lindsey, I. C. Schreiman, H. C. Hsu, P. C. Kearney and A. M. Marguerettaz, "Rothemund and Alder-Long reactions revisited: synthesis of tetraphenylporphyrins under equilibrium conditions," J. Org. Chem. **52**, 827-836 (1987).

18. L. Edwards, M. Gouterman and C. B. Rose, "Synthesis and vapor spectrum of Zinc tetrabenzoporphine," J. Am. Chem. Soc. **98**, 7638-7641 (1976).

19. M. Gouterman, "Spectra of porphyrins," J. Mol. Spectrosc. **6** (1961).

20. L. Bajema, M. Gouterman and C. B. Rose, "Porphyrins. XXIII. Fluorescence of the second excited singlet and quasiline structure of zinc tetrabenzoporphine," J. Mol. Spectrosc. **39**, 421-431 (1971).

21. C. E. Dent, R. P. Linstead and A. R. Lowe, "Phthalocyanines. VI. The structure of the phthalocyanines," J. Am. Chem. Soc., 1033-1039 (1934).

22. P. A. Barrett, R. P. Linstead, F. G. Rundall and G. A. P. Tuey, "Phthalocyanines and related compounds. XIX. Tetrabenzoporphine, tetrabenzomonazaporphine, and their metallic derivatives," J. Am. Chem. Soc. (1940).

23. P. A. Barrett, R. P. Linstead, J. J. Leavitt and G. A. Rowe, "Phthalocyanines and related compounds. XVIII. Intermediates for the preparation of tetrabenzoporphines: the Thorpe reaction with phthalonitrile.," J. Am. Chem. Soc. (1940).

24. A. Vogler and H. Kunkely, "Simple template synthesis of zinc tetrabenzoporphyrin.," Angewandte Chemie **90**, 808 (1978).

25. V. N. Kopranenkov, E. A. Makarova and E. A. Luk'yanets, "New approach to the synthesis of metallic complexes of tetrabenzoporphines," Zh. Obshch. Khim. **51**, 2727-2730 (1981).

26. D. E. Remy, "A versatile synthesis of tetrabenzoporphyrins," Tetrahedron Lett. **24**, 1451-1454 (1983).

27. R. Bonnett and R. F. C. Brown, "Isoindole," J. Chem. Soc., Chem. Commun. **7**, 393-395 (1972).

28. K. Ichimura, M. Sakruagi, H. Morii, M. Yasuike, M. Fukui and O. Ohno, "Reinvestigation of synthetic methods for zinc meso-tetraphenyltetrabenzoporphyrin.," Inorg. Chim. Acta **176**, 31-33 (1990).

29. K. Ichimura, M. Sakruagi, H. Morii, M. Yasuike, M. Fukui and O. Ohno, "Unequivocal synthesis of meso-tetraphenyltetrabenzoporphine," Inorg. Chim. Acta **182**, 83-86 (1991).

30. R. J. Cheng, Y. R. Chen and C. E. Chuang, "Spectroscopic characterizations of meso-phenyl substituted tetrabenzoporphyrin zinc complexes.," Heterocycles **34**, 1-4 (1992).

31. S. Ito, T. Murashima and N. Ono, "A new synthesis of pyrroles fused with polycyclic skeletons," J. Chem. Soc., Perkin Trans. 1 **21**, 3161-3166 (1997).

32. S. Ito, T. Murashima, H. Uno and N. Ono, "A new synthesis of benzoporphyrins using 4,7-dihydro-4,7-ethano-*2H*-isoindole as a synthon of isoindole," Chem. Commun., 1661-1662 (1998).

33. O. S. Finikova, A. Cheprakov, I. P. Beletskaya and S. A. Vinogradov, "An expedient synthesis of substituted tetraaryltetrabenzoporphyrins," Chem. Commun. **2001**, 261-262 (2001).

34. P. B. Hopkins and P. L. Fuchs, "Chlorosulfenylation-Dehydrochlorination Reactions. New and Improved Methodology for the Synthesis of Unsaturated Aryl Sulfides and Aryl Sulfones," J. Org. Chem. **43**, 1208-1217 (1978).

35. P. Carter, S. Fitzjohn, S. Halazy and P. Magnus, "Studies on the synthesis of the antitumor agent CC-1065. Synthesis of PDE I and PDE II, inhibitors of cyclic adenosine-3',5'-monophosphate phosphodiesterase using the 3,3'-bipyrrole strategy," J. Am. Chem. Soc. **109**, 2711-2717 (1987).

36. O. S. Finikova, S. E. Aleshchenkov, R. P. Brinas, A. V. Cheprakov, P. J. Carroll and S. A. Vinogradov, "Synthesis of Symmetrical Tetraaryltetranaphtho[2,3]porphyrins," J. Org. Chem. **70**, 4617-4628 (2005).

37. M. A. Filatov, A. V. Cheprakov and I. P. Beletskaya, "A Facile and Reliable Method for the Synthesis of Tetrabenzoporphyrin from 4,7-Dihydroisoindole," Eur. J. Org. Chem., 3468-3475 (2007).

38. V. Yakutkin, S. Aleshchenkov, S. Chernov, T. Miteva, G. Nelles, A. Cheprakov and S. Baluschev, "Towards the IR Limit of the Triplet-Triplet Annihilation-Supported Up-Conversion: Tetraanthroporphyrin," Chem. Eur. J. **14**, 9846-9850 (2008).

39. A. Gilbert and J. Baggot, *Essentials of Molecular Photochemistry*. (CRC Press, Inc., Boca Raton, 1991).

40. M. Gouterman, P. M. Rentzepis and K. D. Straub, *Porphyrins Exctied States and Dynamics*. (American Chemical Society, Washington, 1986).

41. K. M. Kadish, K. M. Smith and R. Guilard, *The Porphyrin Handbook*. (Academic Press, San Diego, 2000).

42. M. A. Baldo, D. F. O'Brien, Y. You, A. Shoustikov, S. Sibley, M. E. Thompson and S. R. Forrest, "Highly efficient phosphorescent emission from organic electroluminescent devices," Nature **395**, 151-154 (1998).

43. R. C. Kwong, S. Sibley, T. Dubovoy, M. Baldo, S. R. Forrest and M. E. Thompson, "Efficient, Saturated Red Organic Light Emitting Devices Based on Phosphorescent Platinum(II) Porphyrins," Chem. Mater. **11**, 3709-3713 (1999).

44. H. T. Whelan, R. L. Smits, E. V. Buchman, N. T. Whelan, S. G. Turner, D. A. Margolis, V. Cevenini, H. Stinson, R. Ignatius, T. Martin, J. Cwiklinski, A. F. Phillippi, W. R. Graf, B. Hodgson, L. Gould, M. Kane, G. Chen and J. Caviness, "Effect of NASA light-emitting diode irradiation on wound healing " J. Clin. Laser Med. Surg. **19**, 305-314 (2001).

45. T. Karu, *The Science of Low-Power Laser Therapy*. (Gordon and Breach Scientific, New York, 1998).

46. R. Raghavachari, *Near-Infrared Applications in Biotechnology*. (CRC Press Boca Raton, 2001).

47. E. Desurvire, *Erbium-Doped Fiber Amplifiers: Principles and Applications*. (Wiley-Interscience, New York, 1994).

48. B. Harrison, T. J. Foley, M. Bouguettaya, J. M. Boncella, J. R. Reynolds, K. S. Schanze, J. Shim, P. H. Holloway, G. Padmanaban and S. Ramakrishnan, "Near-infrared electroluminescence from conjugated polymer/lanthanide porphyrin blends," Appl. Phys. Lett. **79**, 3770-3772 (2001).

49. J. C. Ostrowski, K. Susumu, M. R. Robinson, M. J. Therien and G. C. Bazan, "Near-Infrared Electroluminescent Light-Emitting Devices Based on Ethyne-Bridged Porphyrin Fluorophores," Adv. Mater. **15**, 1296-1300 (2003).

50. B. C. Thompson, L. G. Madrigal, M. R. Pinto, T. Kang, K. Schanze and J. R. Reynolds, "Donor-acceptor copolymers for red- and near-infrared-emitting polymer light-emitting diodes," J. Polym. Sci. Pol. Chem. **43**, 1417-1431 (2005).

51. X. Li, W. Zeng, Y. Zhang, Q. Hou, W. Yang and Y. Cao, "Synthesis and properties of novel poly(p-phenylenevinylene) copolymers for near-infrared emitting diodes," Eur. Polym. J. **41** (2005).

52. R. Yang, R. Tian, J. Yan, Y. Zhang, J. Yang, Q. Hou, W. Yang, C. Zhang and Y. Cao, "Deep-Red Electroluminescent Polymers: Synthesis and Characterization of New Low-Band-Gap Conjugated Copolymers for Light-Emitting Diodes and Photovoltaic Devices," Macromolecules **38**, 244-253 (2005).

53. C. Borek, K. Hanson, P. I. Djurovich, M. E. Thompson, K. Aznavour, R. Bau, Y. Sun, S. R. Forrest, J. Brooks, L. Michalski and J. Brown, "Highly Efficient, Near-Infrared Electrophosphorescence from a Pt-Metalloporphyrin Complex," Angew. Chem. Int. Ed. **46**, 1109-1112 (2007).

54. T. C. Rosenow, K. Walzer and K. Leo, "Near-infrared organic light emitting diodes based on heavy metal phthalocyanines," J. Appl. Phys. **103**, 043105/043101-043105/043104 (2008).

55. C. W. Tang and S. A. VanSlyke, "Organic electroluminescent diodes," Appl. Phys. Lett. **51**, 913-915 (1987).

56. M. Uchida, Y. Ohmori and K. Yoshino, "Electroluminescence from visible to near-infrared spectral range in buckminsterfullerene diode," Jpn. J. Appl. Phys. 2 **30**, L2104-L2106 (1991).

57. S. M. Borisov, G. Nuss, W. Haas, R. Saf, M. Schmuck and I. Kilmant, "New NIR-emitting complexes of platinum(II) and palladium(II) with fluorinated benzoporphyrins," J. Photoch. Photobio. A. **201**, 128-135 (2009).

58. O. S. Finikova, A. Cheprakov and S. A. Vinogradov, "Synthesis and Luminescence of Solube *meso*-Unsubstituted Tetrabenzo- and Tetranaphtho[2,3]porphyrins," J. Org. Chem. **70**, 9562-9572 (2005).

59. M. A. Filatov, A. Y. Lebedev, S. A. Vinogradov and A. V. Cheprakov, "Synthesis of 5,15-Diaryltetrabenzoporphyrins," J. Org. Chem. **73**, 4175-4185 (2008).

60. O. S. Finikova, A. V. Cheprakov, I. P. Beletskaya, P. J. Carroll and S. A. Vinogradov, "Novel Versatile Synthesis of Substituted Tetrabenzoporphyrins," J. Org. Chem. **69**, 522-535 (2004).

61. A. Y. Lebedev, M. A. Filatov, A. V. Cheprakov and S. A. Vinogradov, "Effects of Structural Deformations on Optical Properties of Tetrabenzoporphyrins: Free-Bases and Pd Complexes," J. Phys. Chem. A **112**, 7723-7733 (2008).

62. M. Giraud-Roux, G. Proni, K. Nakanishi and N. Berova, "Syntheses and Spectroscopic Properties of Methylbenzoate Derivatives of Tetrabenzoporphyrin, Application to Circular Dichroism Studies," Heterocycles **61**, 417-432 (2003).

63. S. Ito, N. Ochi, H. Uno, T. Murashima and N. Ono, "A new synthesis of [2,3]naphthoporphyrins," Chem. Commun., 893-894 (2000).

64. O. S. Finikova, A. V. Cheprakov, P. J. Carroll and S. A. Vinogradov, "Novel Route to Functionalized Tetraaryltetra[2,3]naphthaloporphyrins via Oxidative Aromatization," J. Org. Chem. **68**, 7517-7520 (2003).

65. I. Elghamry and L. Tietze, "Microwave assisted synthesis of novel annealed porphyrins," Tetrahedron Lett **49**, 3972-3975 (2008).

66. H. Yamada, D. Kuzuhara, T. Takahashi, Y. Shimizu, K. Uota, T. Okujima, H. Uno and N. Ono, "Synthesis and Characterization of Tetraanthroporphyrins," Org. Lett. **10**, 2947-2950 (2008).

67. Y. Sun, C. Borek, K. Hanson, P. I. Djurovich, M. E. Thompson, J. Brooks, J. J. Brown and S. R. Forrest, "Photophysics of Pt-porphyrin electrophosphorescent devices emitting in the near infrared," Appl. Phys. Lett. **90**, 213503 (2007).

68. O. S. Finikova, P. Chen, Z. Ou, K. M. Kadish and S. A. Vinogradov, "Dynamic quenching of porphyrin triplet states by two-photon absorbing dyes: Towards two-photon-enhanced oxygen nanosensors," J. Photochem. Photobiol., A **198**, 75-84 (2008).

69. Y. Wang, N. Herron, V. Grushin, D. LeCloux and V. Petrov, "Highly efficient electroluminescent materials based on fluorinated organometallic iridium compounds," Appl. Phys. Lett. **79**, 449-451 (2001).

70. J. Ding, J. Lü, Y. Cheng, Z. Xie, L. Wang, X. Jing and F. Wang, "Solution-Processible Red Iridium Dendrimers based on Oligocarbazole Host Dendrons: Synthesis, Properties, and their Applicaitons in Organic Light-Emitting Diodes," Adv. Funct. Mater. **18**, 2754-2762 (2008).

71. J. Ding, B. Wang, Z. Yue, B. Yao, Z. Xie, Y. Cheng, L. Wang, X. Jing and F. Wang, "Bifunctional Green Iridium Dendrimers with a "Self-Host" Feature for Highly Efficient Nondoped Electrophosphorescent Devices," Angew. Chem. Int. Ed. **48**, 6664-6666 (2009).

72. K. M. Jung, T. W. Lee, K. H. Kim, M. J. Cho, J.-I. Jin and D. H. Choi, "Effect of Charge-transporting Molecules on Electrophosphorescence in a Device Fabricated Using Third-generation Dendrimer Encapsulated Tris[2-benzo[*b*]thiophen-2-ylpyridyl]iridium Complex," Chem. Lett. **38**, 314-315 (2009).

73. K. M. Jung, K. H. Kim, J.-I. Jin, M. J. Cho and D. H. Choi, "Deep-Red Light-Emitting Phosphorescent Dendrimer Encapsulated Tris-[2-benzo[b]thiophen-2-yl-pyridyl] Iridium (III) Core for Light-Emitting Device Applications," J. Polym. Sci., Part A: Polym. Chem. , 7517-7533 (2008).

74. W. Maes and W. Dehaen, "Synthetic Aspects of Porphyrin Dendrimers," Eur. J. Org. Chem., 4719-4752 (2009).

75. K. Albrecht, Y. Kasai and K. Yamamoto, "The Fluorescence and Electromluminescence Properties of the Carbazole-Phenylazomethine Double Layer-Type Dendrimer," J. Inorg. Organomet. Polym. **19**, 118-123 (2009).

76. Y. Li, A. Rizzo, M. Salerno, M. Mazzeo, C. Huo, Y. Wang, K. Li, R. Cingolani and G. Gigli, "Multifunctional platinum porphyrin dendrimers as emitters in undoped phosphorescent based light emitting devices," Appl. Phys. Lett. **89**, 061125/061121-061125/061123 (2006).

77. C. A. Barker, X. Zeng, S. Bettington, A. S. Batsanov, M. R. Bryce and A. Beeby, "Porphyrin, Phthalocyanine and Porphyrazine Derivatives with Multifluorenyl Substituents as Efficient Deep-Red Emitters," Chem. Eur. J. **13**, 6710-6717 (2007).

78. M. Ikai, F. Ishikawa, N. Aratani, A. Osuka, S. Kawabata, T. Kajioka, H. Takeuchi, H. Fujikawa and Y. Taga, "Enhancement of External Quantum Efficiency of Red Phosphorescent Organic Light-Emitting Devices with Facially Encumbered and Bulky Pt^{II} Porphyrin Complexes," Adv. Funct. Mater. **16**, 515-519 (2006).

79. W. Zhuang, Y. Zhang, Q. Hou, L. Wang and Y. Cao, "High-Efficiency, Electrophosphorescent Polymers with Porphyrin-Platinum Complexes in the Conjugated Backbone: Synthesis and Device Performance," J. Polym. Sci., Part A: Polym. Chem. **44**, 4174-4186 (2006).

80. I. Karamé, M. Jahjah, A. Messaoudi, M. L. Tommasino and M. Lemaire, "New ruthenium catalysts containing chiral Schiff bases for the asymmetric hydrogenation of acetophenone," Tetrahedron: Asymmetry **2004**, 1569-1581 (2004).

81. M. Beinhoff, W. Weigel, W. Rettig, I. Bruedgam, H. Hartl and A. D. Schlueter, "Phenylene Alkylene Dendrons with Site-Specific Incorporated Fluorescent Pyrene Probes," J. Org. Chem. **70**, 6583-6591 (2005).

82. Y. Jiang, J.-Y. Wang, Y. Ma, Y.-X. Cui, Q.-F. Zhou and J. Pei, "Large Rigid Blue-Emitting π-Conjugated Stilbenoid-Based Dendrimers: Synthesis and Properties " Org. Lett. **8**, 4287-4290 (2006).

83. C. Li, J.-C. Hsu, K. Sugiyama, A. Hirao, W.-C. Chen and R. Mezzenga, "Synthesis and Self-Assembly Behavior of Poly(fluorenylstyrene)-*block*-poly(2-vinylpyridine)Block Copolymers and Their Blends with Single Wall Carbon Nanotubes (SWCNTs)," Macromolecules **42**, 5793-5801 (2009).

84. J. J. Eisch, B. Shafii, J. D. Odom and A. L. Rheingold, "Aromatic Stabilization of the Triarylborirene Ring System by Tricoordinate Boron and Facile Ring Opening with Tetracoordinate Boron," J. Am. Chem. Soc. **112**, 1847-1853 (1990).

85. L. Waykole, L. A. Paquette, D. A. Heerding and L. E. Overman, "ETHYNL *p*-TOLYL SULFONE [Benzene, 1-(ethynylsulfonyl)-4-methyl-]," Org. Synth. **67**, 149-155 and 1951-1954 (1988).

86. A. Otten, J. C. Namyslo, M. Stoermer and D. E. Kaufmann, "2-(Het)aryl-Substituted 7-Azabicyclo[2.2.1]heptane Systems," Eur. J. Org. Chem., 1997-2001 (1998).

87. G. Tririya and M. Zanger, "Synthesis of Anthracyclinone Precursor: 5,12-Dihydroxy-1,3,4-trihydronaphthacene-2,6,11-quinone," Synth. Commun. **34**, 3047-3059 (2004).

88. L. A. Paquette, F. Bellamy, M. C. Bohm and R. Gleiter, "Electronic Control of Stereoselectivity. 6. Directionality of Singlet Oxygen Addition to 1,4-Dimethoxynaphthalenes Laterally Fused to Bridged Bicyclic Systems," J. Org. Chem. **45**, 4913-4921 (1980).

89. H.-J. Wu, C.-S. Chao and C.-C. Lin, "Synthesis of New Type Diacetal Trioxa-Cage Compounds via an Intramolecular Nucleophilic Addition of the Hydroxy Group to the Carbonyl Oxide Group," J. Org. Chem. **63**, 7687-7693 (1998).

90. A. Menzek and A. Altundas, "Reactions of 3,10-epoxycyclo[10.2.2.$0^{2,11}$.$0^{4,9}$]hexadeca-4,6,8,13-tetrane: a new intramolecular 1,5-oxygen migration," Tetrahedron **62**, 12318-12325 (2006).

91. H. K. Patney, "A general and simple route to the synthesis of triptycenes," Synthesis **9**, 694-696 (1991).

92. S.-C. Chuang, M. Sander, T. Jarrosson, S. James, E. Rozumov, S. I. Khan and Y. Rubin, "Approaches to Open Fullerenes: Synthesis and Kinetic Stability of Diels-Alder Adducts of Substituted Isobenzofurans and C_{60}," J. Org. Chem. **72**, 2716-2723 (2007).

93. T. Nishimura, T. Kawamoto, K. Sasaki, E. Tsurumaki and T. Hayashi, "Rhodium-Catalyzed Asymmetric Cyclodimerization of Oxa- and Azabicyclic Alkenes," J. Am. Chem. Soc. **129**, 1492-1493 (2007).

94. A. Treibs and N. Häberle, "Synthesis and electron spectra of ms-substituted porphines," Justus Liebigs Ann. Chem. **718** (1968).

95. G. P. Arsenault, E. Bullock and S. F. MacDonald, "Pyrromethanes and porphyrins therefrom," J. Am. Chem. Soc. **82**, 4384-4389 (1960).

96. A. Markovac and S. F. MacDonald, "Syntheses with 5-dibromomethyl- and 5-formylpyrromethenes," Can. J. Chem. **43**, 3364-3371 (1965).

97. J. E. Baldwin, M. J. Crossley, T. Klose, E. A. O'Rear, III and M. K. Peters, "Syntheses and oxygenation of iron(II) strapped porphyrin complexes," Tetrahedron **38**, 27-39 (1982).

98. M. Basato, A. Biffis, G. Martinati, C. Tubaro, A. Venzo, P. Ganis and F. Benetollo, "Reaction of platinum acetate with phosphines and molecular structure of *trans*-[$Pt(OAc)_2(PPh_3)_2$]," Inorg. Chim. Acta **355**, 399-403 (2003).

99. P. Sauerberg, J. P. Mogensen, L. Jeppesen, P. S. Bury, J. Fleckner, G. S. Olsen, C. B. Jeppesen, E. M. Wulff, P. Pihera, M. Havranek, Z. Polivka and I. Pettersson, "Design of potent PPARα agonists," Bioorg. Med. Chem. Lett. **17**, 3198-3202 (2007).

100. S. Araki, M. Ohmura and Y. Butsugan, "A facile synthesis of 2,3-dialkyl-1,3-butadienes," Synthesis **10**, 963-964 (1985).

101. T. Okujima, G. Jin, Y. Hashimoto, H. Yamada, H. Uno and N. Ono, "Synthesis of 4,7-dihydro-2H-isoindole derivatives via Diels-Alder reaction of tosylacetylene," Heterocycles **70**, 619-626 (2006).

102. A. V. R. Rao, J. S. Yadav, K. B. Reddy and A. R. Mehendale, "A Stereoconvergent Synthesis of (+)-4-Demethoxydaunomycin," Tetrahedron **40**, 4643-4647 (1984).

103. L. A. Paquette, F. Bellamy, M. C. Böhm and R. Gleiter, "Electronic Control of Stereoselectivity. 6. Directionality of Singlet Oxygen Addition to 1,4-Dimethoxynaphthalenes Laterally Fused to Bridged Bicyclic Systems," J. Org. Chem. **45**, 4913-4921 (1980).

104. J. Mack, M. Bunya, Y. Shimizu, H. Uoyama, N. Komobuchi, T. Okujima, H. Uno, S. Ito, M. J. Stillman, N. Ono and N. Kobayashi, "Application of MCD Spectroscopy and TD-DFT to Nonplanar Core-Modified Tetrabenzoporphyrins: Effect of Reduced Symmetry on Nonplanar Porphyrinoids," Chem. Eur. J. **14**, 5001-5020 (2008).

105. G. Destriau, "The action of an electric field on phosphorescent sulfides " J. Chim. Phys. **33**, 117-124 (1937).

106. G. Destriau and H. F. Ivey, "Electrophotoluminescence and related topics," Proceedings IRE **43**, 1911-1940 (1955).

107. M. Pope, P. Magnante and H. P. Kallmann, "Electroluminescence in Organic Crystals," J. Chem. Phys. **38**, 2042 (1963).

108. W. Helfrich and W. G. Schneider, "Recombination Radiation in Anthracene Crystals," Phys. Rev. Lett. **17**, 229-231 (1965).

109. J. H. Burroughes, D. D. Bradley, A. R. Brown, R. N. Marks, K. Mackay, R. H. Friend, P. L. Burns and A. B. Holmes, "Light-Emitting-Diodes Based on Conjugated Polymers," Nature **347**, 539-541 (1990).

110. D. Braun and A. J. Heeger, "Visible-Light Emission From Semiconduction Polymer Diodes," Appl. Phys. Lett. **58**, 1982-1984 (1991).

111. A. Dodabalapur, "Organic Light Emitting Diodes," Solid State Commun. **102**, 259 (1997).

112. Y. Cao, I. D. Parker, G. Yu, C. Zhang and A. J. Heeger, "Improved Quantum Efficiency for Electroluminescence in Semiconducting Polymers," Nature **397**, 414-417 (1998).

113. R. H. Friend, R. W. Gymer, A. B. Holmes, J. H. Burroughes, R. N. Marks, C. Taliani, D. D. C. Bradley, D. A. Dos Santos, J. L. Bredas, M. Logdlund and W. R. Salaneck, "Electroluminescence in conjugated polymers," Nature **397**, 121-128 (1999).

114. A. Bernanose, M. Comte and P. Vouaux, "A new method of emission of light by certain organic compounds," J. Chim. Phys. **50**, 64-68 (1953).

115. A. Bernanose, "Electroluminescence of organic compounds," Luminescence, 54-56 (1955).

116. K. Kaneto, K. Yoshino, K. Kao and Y. Inuishi, "Electroluminescence in poly(ethylene terephthalate)," Jpn. J. Appl. Phys. **13**, 1023-1024 (1974).

117. D. M. Guldi, C. Luo, M. Prato, E. Dietel and A. Hirsch, "Charge-transfer in a π-stacked fulleren porphyrin dyad: evidence for back electron transfer in the 'Marcus-inverted' region," Chem. Commun. (2000).

118. J. V. Casper and T. J. Meyer, "Application of the Energy Gap Law to Nonradiative, Excited-State Decay," J. Phys. Chem. **87**, 952-957 (1983).

119. J. S. Wilson, N. Chawdhury, M. Al-Mandhary, M. Younus, M. S. Khan, P. R. Raithby, A. Köhler and R. H. Friend, "The Energy Gap Law for Triplet States in Pt-Containing Conugated Polymers and Monomers," J. Am. Chem. Soc. **123**, 9412-9417 (2001).

120. A. Loudet and K. Burgess, "BODIPY Dyes and Their Derivatives: Synthesis and Spectroscopic Properties," Chem. Rev. **107**, 4891-4932 (2007).

121. A. Rosa, G. Ricciardi, E. J. Baerends and S. J. A. van Gisbergen, "The Optical Spectra of NiP, NiPz, NiTBP, and NiPc: Electronic Effects of Meso-tetraaza substitution and Tetrabenzo Annulation," J. Phys. Chem. A **105**, 3311-3327 (2001).

122. K. A. Nguyen and R. Pachter, "Ground state electronic structures and spectra of zinc complexes of porphyrin, tetraazaporphyrin, tetrabenzoporphyrin, and phthalocyanine: A density functional theory study," J. Chem. Phys. **114**, 10757-10767 (2001).

123. A. D. Bond, N. Feeder, J. E. Redmen, S. J. Teat and J. K. M. Sanders, "Molecular Conformations and Intermolecular Interactions in the Crystal Structures of Free-Base 5,15-Diarylporphyrins," Crystal Growth & Design **2**, 27-29 (2002).

124. K. M. Smith, *Porphyrins and Metalloporphyrins*. (Elsevier Press, New York, 1975).

125. A. Antipas and M. Gouterman, "Porphyrins. 44. Electronic states of cobalt, nickel, rhodium, and palladium complexes," J. Am. Chem. Soc. **105**, 4896-48901 (1983).

126. G. A. Crosby and J. N. Demas, "The Measurement of Photoluminescence Quantum Yields. A Review," J. Phys. Chem. **75**, 991-1024 (1971).

127. Y. Wang and K. Schanze, "Photochemical probes of intramolecular electron and energy transfer," Chemical Physics **176**, 305-319 (1993).

128. Y. Zheng, S.-H. Eom, N. Chopra, J. Lee, F. So and J. Xue, "Efficient Deep-Blue Phosphoescent Organic Light-Emitting Device with Improved Electron and Exciton Confinement," J. Appl. Phys. Lett. **92**, 223-301 (2008).

129. S. R. Forrest, D. D. Bradley and M. E. Thompson, "Measuring the Efficiency of Organic Light-Emitting Devices," Adv. Mater. **15**, 1043-1048 (2003).

BIOGRAPHICAL SKETCH

Jonathan R. Sommer was born in Cheboygan, Michigan, and grew up in Orange Park, Florida, a suburb of Jacksonville. He spent the majority of his childhood outside fishing and playing sports such as football and basketball. Jonathan continued playing football while at Orange Park High School growing mentally and physically from the coaching and mentorship of Coach Bill Shields and Roy Clayton. His college career started at Jacksonville University playing football for the Dolphins and studying chemistry. However, his deep affection for the triple-option, which developed during his prep career, led him to transfer to Georgia Southern University to play football under Head Coach Paul Johnson. Here he continued working towards his Bachelor of Science in chemistry. He took a strong interest in both organic chemistry and quantum mechanics from working with his undergraduate research advisors Dr. Kurt Weigel and Dr. James LoBue. He began his graduate studies at the University of Florida under the guidance of Prof. Kirk S. Schanze which provided the opportunity to synthesis advanced materials and study their photophysical properties for materials science applications while pursuing a doctoral degree in organic chemistry.